Departamento de Química Física

Directed Self-Assembly of Janus Nanoparticles For SERS Applications

Memoria que presenta Denis Rodríguez Fernández
para optar al grado de Doctor
Vigo, Febrero de 2015

D. Luis Manuel Liz Marzán, Catedrático del Departamento de Química Física de la Universidad de Vigo y D. Jorge Pérez Juste, Profesor Contratado Doctor en el mismo Departamento

INFORMAN:

Que Denis Rodríguez Fernández, licenciado en Química, ha realizado en el Departamento de Química Física de la Universidad de Vigo y en el Centro de Investigaciones Cooperativas en Biomateriales (CICbiomaGUNE) de San Sebastián bajo su dirección el trabajo descrito en la presente memoria, que lleva por título "Directed Self - Assembly of Janus Nanoparticles for SERS Applications", y que presenta para optar al grado de Doctor por la Universidad de Vigo con Mención Internacional.

Vigo, 3 de Febrero de 2015

Fdo. Luis Manuel Liz Marzán

Fdo. Jorge Pérez Juste

II

Esta tesis se la dedico a todos los que me han apoyado a lo largo de esta aventura

Contents

Thesis Scope

The work presented in this thesis focuses on the preparation of new types of gold Janus nanoparticles using different approaches. The morphological changes induced to the particles were determined using transmission and scanning electron microscopies, and were correlated to changes in their optical properties. Additionally, computer simulations of the optical properties were carried out in order to compare experiments with theory. Directed self-assembly of these particles is also presented, showing some potential applications as surface enhanced Raman scattering (SERS) reporters. The content of each chapter is briefly justified in the following.

The first half of this thesis was carried out in the Colloid Chemistry group (University of Vigo) and the second in the Bionanoplasmonics Laboratory at CIC biomaGUNE (San Sebastián). In fact, both groups were led by the same person and therefore in both places the research activity is mainly focused on the synthesis and assembly of metal nanoparticles (mainly gold and silver) for sensing applications. A broad variety of particles with shape and size control have been developed in these groups, which allowed a fine tuning of the optical properties showed by these colloids in the UV-vis-NIR regions of the electromagnetic spectrum. A literature review reveals the recent interest on Janus particles, exhibiting different properties on each side, with potential applications in self-assembly for preparing new structures, in catalysis, detection, etc. Therefore, taking advantage of groups' experience, gold-silica Janus nanoparticles were prepared during this thesis using colloidal methods in solution. Gold was chosen due to its chemical stability compared to silver, so that the nanoparticles preserve their optical features for longer periods of time, together with silica, mainly to provide electrostatic colloidal stability to the system. The primary objective of this thesis is thus the preparation

of new types of Janus particles and the control of their self-assembly to improve their capabilities for SERS applications.

In Chapter 2, the preparation of gold semishells with a spherical silica core of 495 nm is described. The process is based on the partial functionalization of the silica cores using wax in water Pickering emulsions to mask partially the silica surface. The subsequent seeded growth of attached gold seeds leads to the final gold-silica semishells. On a related work, gold nanowires were grown over silica spheres (Chapter 3), opening the way to adapt the process for obtaining Janus like particles in the near future. For both systems we carried out simulations of their optical properties to correlate experiments with theory.

The preparation of Janus nanoparticles using mesoporous thin films with different pore sizes as templates on gold branching has also been explored (Chapter 4). An extensive characterization of the films is shown, comprising transmission and scanning electron microscopies, TEM and SEM respectively, environmental ellipsometric porosimetry (EEP) and 2D-SAXS.

Janus nanostars were prepared by combining different approaches to synthesize Janus particles in solution: the self-assembly of different ligands over a metallic surface; the growth of a silica mask and the seeded growth of gold branches over the exposed metal surface (Chapter 5). The structure of the resulting Janus nanostars was studied in detail by means of high resolution transmission and scanning transmission electron microscopies, HRTEM and STEM respectively. Chapter 6 describes the self-assembly of gold-silica Janus particles with small gold spheres to form Janus satellites and dimers. Their capabilites as SERS substrates for imaging is also presented.

As a whole, this thesis is expected to represent a significant advancement in the preparation of new Janus metal nanoparticles, regarding the synthetic methods developed, the optical characterization together with the simulations and the final SERS imaging applications derived from their unique self-assembly behaviour. The presented results could have important applications in several fields, such as in catalysis, biosensing or the generation of new self-assembled structures.

Chapter 1

General Introduction

This Introduction section is divided into two different parts. The first part basically comprises the definition of various concepts treated in this PhD thesis like: the directed self - assembly of nanoparticles; the optical properties of metallic particles, the surface enhanced Raman Scattering (SERS) technique and mesoporous thin films. This will be followed by a deeper discussion of the synthesis, properties and applications of metallic Janus nanoparticles.

Prior to starting with the definition of the different concepts mentioned above, the basic materials used during this PhD thesis should be introduced. Gold and silicon oxide have been largely employed for the preparation of a plethora of different nanoparticles. This noble metal has not only been selected due to its exciting optical properties (see Section 1.2), i.e. surface plasmon resonances in the visible - NIR region of the electromagnetic spectrum,[1] but also due to its chemical stability, being difficult to oxidize as compared to other metals like silver or copper. These characteristics have set the focus of scientists on gold nanoparticles synthesis during the past few decades, producing particles of almost any imaginable shape.[2, 3] Considering the properties of gold and that the investigation described in this PhD thesis was developed in a group that is specialized mainly on gold nanoparticles synthesis, assembly and study of its optical properties, gold was chosen to take advantage of the experience of the group and therefore to have a solid base for preparing the more complex structures that will be shown in the following sections. The role of silicon oxide when accompanying gold nanoparticles is mainly to provide electrostatic stability to the colloidal dispersion, avoiding undesired aggregation.

Moreover silicon oxide has been used as a colloidal support when preparing gold semishells, as a planar template with mesoporous films or as a masking group with gold - silica nanostars and hybrid satellites. In addition, silicon oxide has shown chemical stability in organic and aqueous media, as well as biocompatibility for the potential future biological applications of some of these systems.[4]

1.1 Directed Self - Assembly of Nanoparticles

Self - assembly of nanoparticles (also applicable to molecules, polymers or macroscopic particles) is related to the process by which they spontaneously organize through direct interactions or indirectly due to the environment.[5] The forces involved in this process might need some help by means of the rational use of Chemistry, external fields or surfaces, leading to the directed self - assembly of particles.[6] Nanoparticle directed self - assembly and the derived applications will be briefly discussed in this section.

In Fig. 1.1 are summarized some approaches for directing nanoparticle self - assembly using molecular interactions, i.e. Chemistry, on different gold building blocks: spheres, rods and wires. When working with nanoparticles, specially with metallic nanoparticles due to larger attractive forces, one fundamental aspect is the colloidal stabilization to avoid floculation or aggregation. Nevertheless when directing self - assembly the aim is to produce the opposite effect, a controllable bottom - up nanofabrication in which the union of the particles by commonly weak and specific forces is mandatory to obtain the desired structures. This implies the use of stimuli to control the intermolecular interactions of the ligands covering the particles or on top of predefined templates: temperature, pH, redox activity, light or polarity of the solvent.[6] In template - free directed self - assembly temperature - sensitive DNA can induce controlled aggregation into particles clustering [7, 8] or producing two - dimensional superlattices [9] via hydrogen bonding, whereas light - sensitive azobenzens can form colloidal crystals [10] via molecular dipole - dipole forces (Fig. 1.1 A - D). Tuning the volume fraction of different solvents can lead to the assembly of gold nanorods into low symmetry clusters,[11] chains [12] or spherical structures (Fig. 1.1 H - J).[12] Carbon nanotubes can also self - assemble into bundles via H - bonding due to changes in solvent polarity (Fig.1.1 K).[13] A template is thus an object that serves as a scaffold onto which particles can be arranged in a structure

complementary to that of the template, like macromolecules,[14] carbon nanotubes [15] or block - copolymers (Fig. 1.1 E - G).[16]

The use of external fields to direct the self - assembly of particles is a promising tool due to scale - up capabilities in bottom - up fabrication. Nevertheless its greatest power implies the combination of magnetic and electric fields with flows, specially when using particles with asymmetric properties like Janus particles (see Section 1.5).[17, 18] Another route comprises the use of interfaces as templates, based on the reduction of the interfacial energy when particles are there located and where lateral capillary forces control the assembly.[19]

After the main procedures to direct the self - assembly of nanoparticles have been introduced, the next question that shows up is: why is this important? The main goal is to obtain materials with new structures and therefore new properties and applications. For example, Granick's group has shown the preparation of a colloidal crystal with a complex kagome lattice exhibiting both hydrophobic and hydrophilic pores.[20] With metal nanoparticles, showing plasmon resonances (see Section 1.2), when the metal parts are in close proximity there is a huge enhancement of the electric field close to the particles forming the so called hotspots, with potential applications in imaging, sensing (see Section 1.3), catalysis, theranostics or as mirrors, among others.[21, 22]

1.2 Optical Properties of Metal Nanoparticles

Michael Faraday reported in 1857 a systematic study on the synthesis of gold colloids and their respective colors.[23] This opened up the way and has maintained occupied scientists to this day developing a broad variety of synthetic protocols to produce nanoparticles with the desired size, shape and surface properties. The optical properties of metal nanoparticles are strongly affected by their composition, size and shape, but are also sensitive to their aspect ratio,[24] the environment [25] and the distance to other metal particles.[26] For example bulk gold shows a yellow color in reflected light, but in transmission thin films look blue, becoming more reddish as the particle size is reduced to ca. 3 nm.[26] This phenomenon is the result of the interaction of the oscillating electric field of an electromagnetic wave with the metal nanoparticles, which induces a dipole over the metal surface and makes the conduction electrons oscillate to restore the equilibrium electron

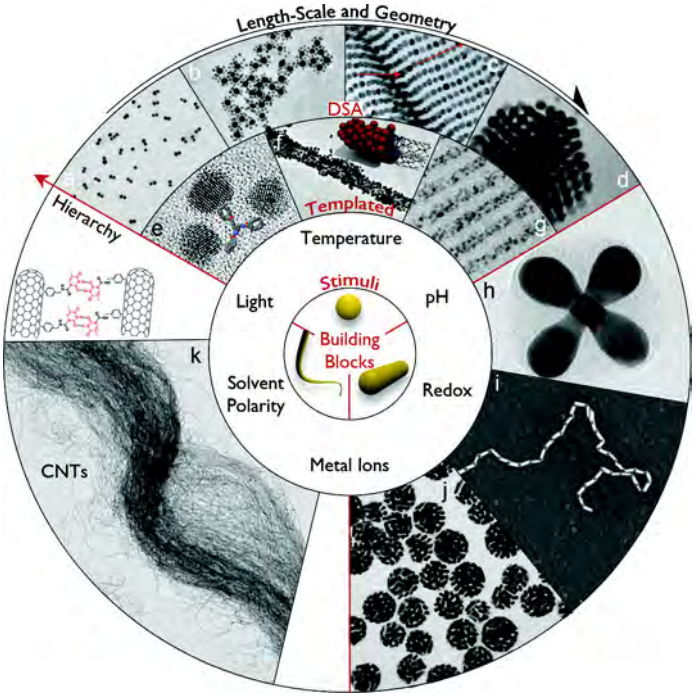

Figure 1.1. Summary of directed self-assembly by molecular interactions. Available building blocks are classified in terms of aspect ratio (AR), ranging from AR = 1 (isotropic, mostly spheres (A-G)) through $1 < AR < 15$ (rodlike (H-J)) to $AR > 15$ (wires (K)). Self-assembly of gold nanoparticles on templates (macromolecules (E); carbon nanotubes (F); block-copolymers (G)) can lead to geometries that are complementary to those of the templates. In template-free self-assembly, stimuli responsive molecules adsorbed on NPs surface induce controlled aggregation. Temperature-sensitive DNA can induce particles clustering (A, B) via H-bonding or induce formation of two-dimensional superlattices (C), whereas light sensitive azobenzenes induce formation of colloidal crystals (D) via molecular dipole-dipole interactions. Hydrophobic interactions can induce assembly of nanorods into low symmetry clusters such as (H) chainlike structures (I) or spherical objects, (J) by tuning the volume fraction of the different solvents. Similarly, highly anisotropic carbon nanotubes undergo assembly into bundles via H-bonding induced changes in the medium polarity (K). Finally, hierarchical self-assembly can be achieved using preformed assemblies as building blocks. Reproduced with permission [6] Copyright 2010, American Chemical Society.

distribution (Fig. 1.2 A). Thus, when resonance is achieved it is known as localized surface plasmon resonance (LSPR).[27] Gold, silver, copper and alkali metals show plasmons in the visible region of the spectrum, giving their intense characteristic colors. This optical phenomenon is not limited only to these metals, since recently has been reported the presence of plasmons in the NIR region on vacancy - doped semiconductor nanocrystals such as copper chalcogenides.[28, 29, 30] It is worth noting that when metal nanoparticles are sufficiently close to each other, a larger enhancement of the electromagnetic field is produced at the interparticle gaps when exposed to an external light, with applications in photonics, photocatalysis or surface enhanced Raman scattering (see Section 1.3).

At the beginning of the 20$^{\text{th}}$ century Gustav Mie found an analytical solution to Maxwell's equations for spheres to explain their optical properties.[31] The extintion cross section C_{ext} for a metal particle, with a wavelength - dependent dielectric function $\epsilon(\lambda) = \epsilon'(\lambda) + i\,\epsilon''(\lambda)$ in a medium of dielectric constant ϵ_m, is given (after some simplifications for very small particles) as: [32]

$$C_{ext} = \frac{24\pi^2 R^3 \epsilon_m^{3/2}}{\lambda} \frac{\epsilon''}{(\epsilon' + 2\epsilon_m)^2 + \epsilon''^2} \tag{1.1}$$

being R de radius of the particle and $\epsilon' - \epsilon''$ the real and imaginary parts of the dielectric constant, respectively. From equation 1.1 it can be predicted that no absorption is produced when $\epsilon'' = 0$ (particles do not absorb) or $\epsilon'' = \infty$ (particles reflect all the radiation); and there is an absorption peak when $\epsilon' = -2\,\epsilon_m$ if ϵ'' is small. A similar expression was derived by Gans for ellipsoids, [33] but for more complicated geometries it is necessary to solve Maxwell's equations using numerical methods like Discrete Dipole Aproximation (DDA), Boundary Element Method (BEM), or the more recent Surface Integral Equation - Method of Moments (SIE - MoM), among others.[34, 35] DDA and BEM give solutions of the electromagnetic field in response to an incident electric field in the frecuency domain. DDA needs the representation of the studied object as a cubic lattice of N polarisable point dipoles occupying a certain position with its characteristic polarizability, with no geometry and composition limitations.[36, 37] Nevertheless, with BEM the object is described as a set of N points at the boundaries.[38] The main advantage of BEM shows up when simulating objects with axial symmetry, reducing the dimensions of the system from the surface boundary to the contour, therefore minimizing the

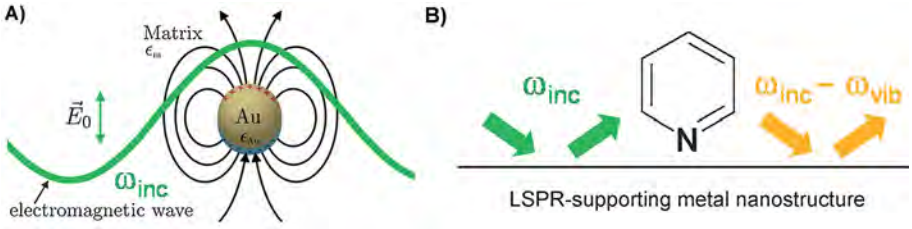

Figure 1.2. Electromagnetic enhancement in SERS. (A) A gold nanoparticle acts as a nanoantenna by excitation of a dipolar localized surface plasmon resonance (LSPR). (B) Both the "incoming" field (ω_{inc}, green) and the "outgoing" field ($\omega_{\mathrm{inc}} - \omega_{\mathrm{vib}}$, orange) are enhanced by elastic light scattering off the LSPR-supporting metal nanostructure (only shown the Stokes Raman Scattering). Adapted with permission from reference.[46] Copyright 2014, John Wiley & Sons.

number of points and the computationl time. With the SIE-MoM method only the boundaries have to be parameterized, like in BEM, but the implementation of the multilevel fast multipole algorithm (MLFMA) combined with the Fast Fourier Transform (FFT) greatly reduces the computational costs allowing the treatment of more complex systems.[35]

1.3 Surface Enhanced Raman Scattering

Surface enhanced Raman scattering (SERS) was first observed in 1974 [39] for pyridine adsorbed over a silver electrode, but the phenomenon was not correctly interpreted until several years later.[40, 41, 42, 43] This technique passed through time without receiving any special interest, however in 1997 two groups presented independently single-molecule SERS detection and since then it has experienced a great development.[44, 45]

The main drawback of "normal" Raman scattering spectroscopy is the low signal intensity obtained. SERS is a type of Raman scattering in which signal intensities are greatly enhanced in the presence of a metal. Two main mechanisms are responsible for this enhancement: the electromagnetic mechanism (EM, Fig. 1.2 B), which can produce an enhancement up to $\sim 10^6$, and the chemical mechanism, that provides up to $\sim 10^2$ enhancement.[27, 47, 46] In Section 1.2 LSPRs were described, showing that this phenomenon produces a dipole over the metal particle and an increse of the local electric field $\mathrm{E}_{\mathrm{loc}}(\omega_{\mathrm{inc}})$, acting the particle as a nanoantenna. This dipole can also induce a dipole μ_{ind} over a molecule close to

the surface, being proportional to the polarizability of the molecule $\alpha_{molecule}$ and the local electric field:

$$\mu_{\mathrm{ind}} = \alpha_{\mathrm{molecule}} \cdot \mathrm{E}_{\mathrm{loc}}(\omega_{\mathrm{inc}}) \tag{1.2}$$

Considering that the Raman intensity can be written as:

$$\mathrm{I} = |\alpha|^2 \left(\frac{|E_{loc}|}{|E_{inc}|}\right)^4 \tag{1.3}$$

a small increase of $\mathrm{E}_{\mathrm{loc}}(\omega_{\mathrm{inc}})$ with respect to the incoming electric field E_{inc} leads to large Raman signal enhancements. This is a brief description of the EM mechanism, which is the main responsible for SERS enhancement. The chemical mechanism also contributes, and it is mainly due to charge transfer between the metal and the molecule. SERS is an exclusively surface effect because the intensity of the electric field decays with the distance as $\mathrm{E}\,(\mathrm{r}) \sim \mathrm{r}^{-3}$, and consequently the Raman intensity decays as $\mathrm{E}_{\mathrm{SERS}}\,(\mathrm{r}) \sim \mathrm{r}^{-12}$. Moreover SERS is sensitive to the spacial orientation of the molecule: flat, tilted and perpendicular orientations with respect to the surface yield different spectra.

The experimental determination of the enhancement factor (EF) can be calculated as the ratio between the SERS intensity I_{SERS} and the Raman intensity I_{RAMAN} of the analyte in solution, normalized to the number of adsorbed molecules (N_{SERS}, SERS) and molecules in solution (N_{RAMAN}, normal Raman):

$$\mathrm{EF} = \frac{\mathrm{I_{SERS}}/\mathrm{N_{SERS}}}{\mathrm{I_{RAMAN}}/\mathrm{N_{RAMAN}}} \tag{1.4}$$

which is often complicated because of the uncertainty in the exact number of adsorbed molecules.

The most employed metals in SERS are gold and silver. The latter is plasmonically more active, thus giving higher EFs, and being preferred for single - molecule detection. On the other hand, gold is chemically more inert, being optimal for applications where chemical stability is important. It has been found that for single silver particles an EF $\leqslant 10^4$ can be obtained,[48] which is however not enough for single molecule detection. So how can it be improved? In Section 1.2 was described that when two or more plasmonic particles are close together, the intensity

of $E_{loc}(\omega_{inc})$ in the gap is extremely enhanced (hotspot), leading to EF $\geq 10^6$. Wustholtz et al. determined the optimal distance as 1 nm for the largest EF, being this extremely dependent on gap distance and independent of the aggregation state.[49]

1.4 Mesoporous Thin Films

Porous materials can be categorized depending on their pore diameter (d) as: microporous ($d < 2$ nm), mesoporous ($2 < d < 50$ nm) and macroporous ($d > 50$ nm). Mesoporous oxides can show highly ordered monodisperse pores with a high surface per weight ratio (100 - 1000 m^2 / g), and can be prepared by combining two processes: sol - gel reactions for the inorganic material and the self - assembly of amphiphilic molecules acting as pore templates. These materials can be applied in catalysis, sensing, optical devices, separation processes, etc.

The sol - gel process implies the hydrolisis of a metal alkoxide (or an anion) to give the intermediate hydroxy compound (equation 1.5), yielding the final material by its condensation (equation 1.6).[50, 51] Hydrolisis of silicon precursors is a slow process, which can be catalysed in acidic or basic media. However, with other transition metals like titanium the process is often too fast, being necessary extremely acidic media or the presence of chelates to make it slower. As a summary, the speed of the process depends on: the metal precursor, the solvent, the pH, the presence of catalysts or chelates and the concentration of all species. By control of the hydrolysis one can tune the size, shape and surface properties of the mesoporous material. On the other hand, the size of the pore is determined by the amphiphilic molecule acting as a template. There are many examples in the literature: cationic, anionic or gemini surfactants, block - copolymers, etc.

$$M-OR + H_2O \rightarrow M-OH + ROH \tag{1.5}$$

$$M-OH + XO-M \rightarrow M-O-M+X-OH \tag{1.6}$$

$$X = H \text{ or } R$$

The first report of the synthesis of a mesoporous material was in 1971.[52] However

until the Mobil Oil Corporation in 1990s showed the preparation of ordered mesoporous silicon oxide materials, there was not a huge development in the field.[53, 54] Barely a few years later studies of the formation mechanism [55, 56, 57] and the first examples of mesoporous materials with different oxides [58, 59] and transition metals [60, 61, 62] were reported.

The preparation of mesoporous thin films (ca. 100 nm) have increased the possible applications of these materials.[63, 64] A wide variety of synthetic approaches have been employed for their preparation, such as spin coating,[65, 66] using interfaces [67, 68] or dip coating,[69, 70] the latter leading to the development of the evaporation - induced self - assembly technique (EISA), which allows the preparation of highly reproducible mesoporous thin films.[71]

1.5 Janus and Patchy Nanoparticles

The tremendous recent development in the production of isotropic nanomaterials has provided access to nanoparticles with pre - selected composition, shape, size and functionality. Beyond the multiple applications found for these nanostructured materials, the early work by Casagrande et al. and subsequently De Gennes' Nobel lecture, opened the way for exploring new types of particles comprising multiple compositions and functionalities.[72, 73] Patchy particles can be defined as particles with one or more well - defined patches, displaying strongly anisotropic and directional interactions.[74] Janus particles, named after the two faced Roman god Janus (Fig. 1.3), can be considered as a special type of patchy particles with only one patch that covers half of the particle. Having different properties at opposite sides enables these particles to mimic the behavior of surfactant molecules, leading to completely new self - assembled structures, with many more possibilities than those found in isotropic particles. Such possibilities rely on a strict control over the balanced forces involved in colloidal stability, to form clusters with predefined size, shape and properties.[75, 20, 76]

In the next sections the general synthetic procedures for the preparation of Janus and patchy particles will be discussed. Although the focus is on metallic Janus particles (containing at least one metal in the zero oxidation state), particularly relevant recent papers on the synthesis of non - metallic particles will be also highlighted. For a deep discussion of this topic, several recent reviews might be

Figure 1.3. Representation of the Janus Roman god as two faces looking at opposite sides (Vatican Museum).

consulted.[77, 78, 79, 80] In general, the preparation of Janus particles can be summarized in (but not limited to) three general approaches: phase separation, masking and self - assembly.[77] The first method mainly involves the preparation of polymeric Janus particles through emulsion polymerization, seeded growth and microfluidics.[81, 82, 83, 84, 85, 86] Masking processes are based on the partial protection of preformed particles by adsorbing them onto either a flat substrate, a larger particle or an emulsion droplet, so that the exposed surface can be further functionalized while maintaining the protected side unchanged.[87, 88, 89, 90] Self - assembly techniques entail the organization of block copolymers in solution or a mixture of incompatible ligands at the particle surface.[91, 92] We finally show an overview of the main properties and applications of metallic Janus particles, derived in most cases from their metallic components, such as: optical response, catalysis, self - assembly, drug delivery, etc.

1.5.1 Preparation of Non - Metallic Janus Particles

The phase separation route has been extensively used for the synthesis of non - metallic Janus particles. For example, Feyen et al. developed a seeded emulsion polymerization method for the preparation of Fe_3O_4 – polystyrene (PS) – SiO_2 hollow mushroom - like nanoparticles (Fig.1.4 A).[81] In this process, magnetite nanoparticles were first partially encapsulated through polymerization of styrene and a silica shell was then grown over the exposed Fe_3O_4 surface, which yielded mushroom - like particles. By subsequently leaching the iron oxide core with hy-

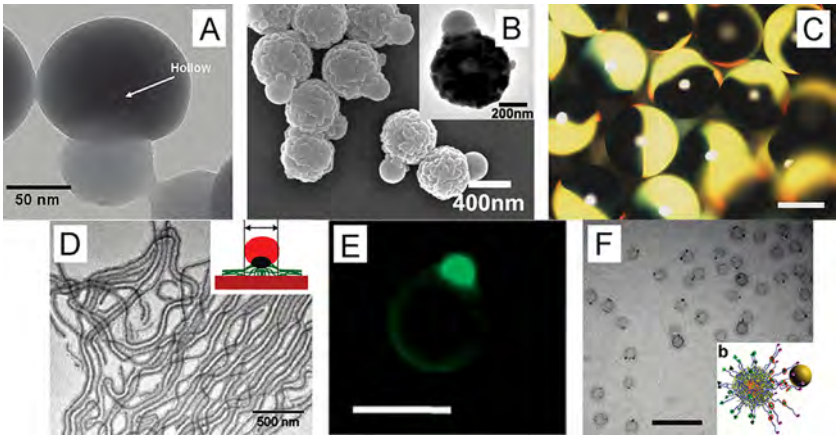

Figure 1.4. (A) TEM image of a Fe_3O_4 − PS − SiO_2 hollow mushroom - like nanoparticle after leaching the 9 nm magnetite core with HCl. (B) SEM and TEM (inset) PS − SiO_2 Janus particle. (C) Optical image of black - green photonic balls; scale bar 200 μm. (D) TEM image of a triblock terpolymer Janus cylinder and schematic representation (inset). (E) Fluorescence microscopy image of a thiolated non - conductive magnetic bead functionalized with fluorescein isocyanate Immunoglobulin G, IgG(FITC); scale bar 5 μm. (F) TEM image of Janus cross - linked knedel - like polymeric shell particles labeled with 2 nm Au nanoparticles, scale bar 100 nm (inset, schematic representation).

drochloric acid, the final hollow structures were formed. Identical results were obtained for $\alpha - Fe_2O_3$ particles, which indicates that the silica shell grows selectively over the exposed oxide surface of the iron oxide particles, even when an excess of reactants is used. Interestingly, similar magnetic PS − SiO_2 Janus particles were also obtained by ultrasound - assisted one - pot dispersion polymerization.[93] Another seeded polymerization approach has been exploited, mainly by the groups of Weitz [82] and Zukoski,[83] where polymer particles were used as seeds and swollen with monomers, which were then polymerized, leading to the formation of a protrusion over the seed. Tang et al. synthesized snowman - like polyacrylonitrile - polystyrene (PAN - PS) particles by growing a PS sphere onto the surface of preformed PAN hollow seeds.[94] They further hydrolyzed the PAN with sodium hydroxide to attach magnetite particles or to grow a TiO_2 or SiO_2 layer (Fig. 1.4 B).

Great effort has been made during the last decade to scale up the phase separation production of Janus particles. Many groups have applied microfluidics to this purpose with remarkable results.[95, 96, 97, 98, 99, 100, 101] Examples include the preparation of colored Janus microspheres with electroresponsive photonic proper-

ties [99] using a microfluidic device with two microcapillaries, containing on one side silica particles dispersed in ethoxylated trimethylolpropane triacrylate resin (ETPTA) and on the other side silica and carbon-black particles dispersed in ETPTA. In the annulus there was a surfactant in water stream to detach the formed droplets from the tips of the inner capillaries and stabilize them. The particles were finally solidified under UV exposure (Fig. 1.4 C). The black color was due to the presence of carbon-black particles, and red or green was formed by the self-assembly of the silica particles into a face-centered cubic (fcc) lattice (a photonic crystal) within the resin, therefore the final color could be tuned through variation of the size and volume fraction of the silica particles. The presence of carbon-black particles additionally provided electrical anisotropy, necessary for application in displays. Another example of biphasic particles is the work of Lahann and co-workers, who used a continuous flow device based on an electrohydrodynamic co-jetting method for continuous production of a variety of morphologies and compositions.[102, 103, 104]

The self-assembly of block copolymers has been largely explored for the preparation of amphiphilic nanostructures. Of particular significance is the work by the Müller group, who recently reported the self-assembly of a triblock terpolymer to obtain Janus spheres, cylinders, ribbons and lamellae.[91] This required the preparation by anionic polymerization of the poly(tert-butoxystyrene)-block-polybutadiene- block-poly(tert-butyl methacrylate), prior to its self-assembly via film casting. Further photo-cross-linking with Lucirin TPO, Janus cylinders were obtained (Fig. 1.4 D). Interestingly, if the film was swollen in acetonitrile and then cross-linked with S_2Cl_2, undulated lamellae were formed, but a mixture of acetonitrile : decane (1:1) allowed them to obtain nonundulated lamellae. Additionally, swelling the films with tertbutanol, which is a bad solvent for polybutadiene but good for the end blocks, led to Janus spheres upon cross-linking.

Masking techniques involve the protection of one part of a preformed particle to selectively functionalize the exposed face. Protection can be carried out by adsorption over flat substrates [105] or particles,[106] by microcontact printing methods [107] and with Pickering emulsions.[108] As an example, Eriksson et al. recently reported the electrochemical oxidation of thiolated non-conductive magnetic beads.[105] These particles were magnetically attracted to the interface between a working electrode and the solution and applied a potential to oxidize the thiol groups close to the electrode into the more reactive thiolsulfinates or thiolsulfonates. The asym-

metry was visualized under a fluorescence microscope, by selective functionalization of the oxidized surface of the beads with fluorescein isocyanate Immunoglobulin G, IgG(FITC) (Fig. 1.4 E). Repeated electrochemical oxidation allowed the authors to obtain particles with additional patches. A cyclic procedure was also applied for the preparation of Janus polymeric spheres using gold particles as templates.[106] Azide - functionalized 22 nm polymeric particles were attached to 46 nm alkyne - modified gold nanoparticles by a click reaction, and Janus polymeric particles with a thiol - end patch were then collected by the addition of excess alkynil thiolended ligands, recovering also the gold templates for additional experiments. Shown in Fig. 1.4 F are images of these Janus polymeric particles, after attachment of 2 nm gold particles on the thiol functional groups.

1.5.2 Preparation of Metallic Janus Particles

Bifunctional Metallic and Metal - Metal Janus Particles

It has been shown that a mixture of ligands can self - assemble in different fashions at the surface of metallic nanoparticles,[109, 110, 111] leading in certain cases to the formation of metallic Janus particles by simply adding suitable competitive ligands to a solution containing the metallic nanoparticles.[112, 113, 114, 115] A recent example is the formation of gold amphiphilic particles.[92] Andala and co - workers used 9.2 nm gold spheres stabilized with dodecylamine (DDA) dispersed in a toluene - water mixture, to which the same amount of hydrophobic dodecanethiol (DDT) and hydrophilic, fully deprotonated mercaptoundecanoic acid (MUA) were simultaneously added, leading to the formation of Janus particles at the interface. The thermodynamic aspects of the process were studied by adding the ligands in different order, which resulted in the same kind of particles (Fig. 1.5 A - C). Contact angle measurements of water droplets at functionalized silicon substrates were carried out to confirm the asymmetric distribution of ligands at the nanoparticles surface (Fig. 1.5 D). A similar approach was used by Sashuk et al. to prepare positively charged gold and negatively charged silver Janus particles.[116] Gold spheres (7.7 nm) were functionalized with N, N, N - trimethyl (11 - mercaptoundecyl) ammonium chloride (TMA) and 1 - undecanethiol (UDT), which are positively charged and neutral, respectively. Silver spheres (6.2 nm) were modified with negatively charged MUA and UDT. When one type of particles was spread at the water - air interface using a Langmuir - Blodgett (LB) trough, ligands self - assembled at the surface of

the metal, and compression led to self-assembled monolayers on functionalized silicon substrates. Other groups have also prepared Janus particles using the LB technique with slight differences. Chen's group obtained gold Janus spheres by spreading thiolated gold particles on the LB trough, compression of the monolayer, followed by injection of an additional thiol in the water subphase to obtain the final asymmetrically modified particles.[117] A modification of this method comprised initial deposition of a monolayer of thiolated gold particles over a glass slide using the LB trough to protect the inner part of the particle against further functionalization, followed by immersion of the glass in a solution of a different thiol, which replaced the external capping molecules.[118, 119] Interestingly, such ligand segregation was recently exploited to prepare bimetallic Janus particles.[120] Chen and co-workers prepared $SiO_2 - Au - Ag$ particles by capping 44 nm Au spheres with 4-mercaptophenylacetic acid and poly-(acrylic acid) as competitive ligands, followed by silica coating to partially encapsulate the gold spheres, and finally these Janus particles were used as seeds to reduce silver nitrate and obtain the final hybrid ternary structure.

Another interesting method is the combined use of microparticle templates and nucleotides to obtain asymmetrically DNA functionalized nanoparticles,[7, 121] which allowed the large-scale preparation of gold dimers or satellite clusters.[8] The use of planar substrates as masks typically involves adsorption of the nanoparticles followed by modification of the exposed surfaces of the particles and their final detachment. For example, Ye et al. prepared silica particles partially covered with gold and platinium by means of electron beam (e-beam) evaporation.[122] Over a monolayer of silica particles adsorbed on a copper substrate, a gold layer was first deposited and then the position of the particles was inverted to evaporate the platinum layer on the opposite side, while an equatorial non-functionalized silica belt remained in the particles. Sardar et al. synthesized chains of gold nanoparticles by thiol modification of previously adsorbed gold particles to an amine-terminated glass substrate.[123] After desorption of the Janus particles by addition of 2-mercaptoethylamine, the coupling reaction between amine groups and the carboxylic acid groups of poly-(acrylic acid) resulted in the final gold particle chains. An interesting approach to prepare gold and recently also Fe_3O_4 Janus particles was developed by Li et al. [124, 125, 126] They first produced single crystals of bifunctionalized polyethylene oxide (PEO) with thiol groups at the surface. Then gold or magnetite particles were covalently adsorbed, and the

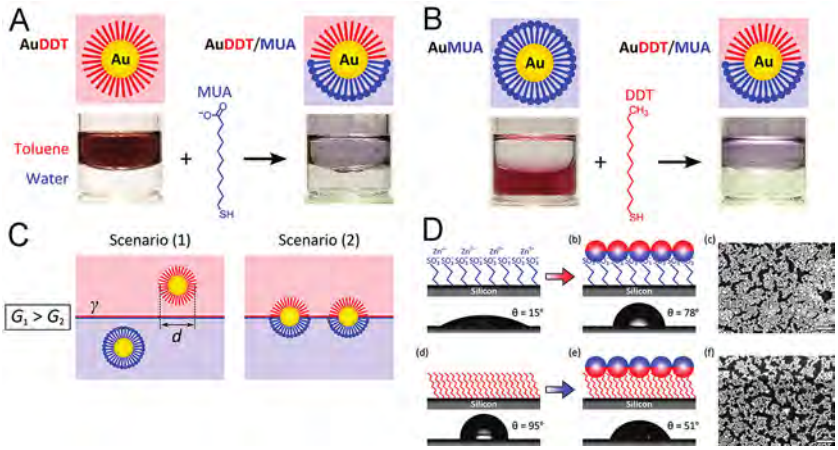

Figure 1.5. Thermodynamic considerations. (A) In one preparation DDT ligands are added first followed by MUA ligands. (B) In another preparation, MUA ligands are added first, followed by DDT ligands. Both preparations yield the same amphiphilic nanoparticles. In (A, B), the initial nanoparticle concentration is 0.2 mM in 4 mL of toluene or 4 mL of water, respectively. (C) Formation of amphiphilic nanoparticles at the liquid - liquid interface is a spontaneous process. (D) Contact angle measurements. On top from left to right: Hydrophilic substrate created by the silanization of an oxidized silicon surface with 3 - (trihydroxysilyl) - 1 - propane sulfonic acid followed by immersion in an aqueous solution of zinc chloride 0.01 M. The measured contact angle (θ) of water in air is $15° \pm 2.3°$ as illustrated in the photograph. Amphiphilic nanoparticle monolayers deposited onto the hydrophilic substrate, $\theta \approx 78° \pm 2.2°$. SEM image of a nanoparticle monolayer deposited onto the hydrophilic substrate via dip coating. In the bottom from left to right: Hydrophobic substrate created by the silanization of an oxidized silicon surface with trimethoxy(octyl)silane, $\theta \approx 95° \pm 2.3°$. Amphiphilic nanoparticle monolayers deposited onto the hydrophobic substrate, $\theta \approx 51° \pm 1.5°$. SEM image of a nanoparticle monolayer deposited onto the hydrophobic substrate. Scale bars are 100 nm.

exposed surface was modified with dodecanethiol, so that Janus particles could be released by simply dissolving the PEO crystal, and subsequently used to fabricate ordered assemblies.

An interesting and flexible approach for the preparation of asymmetric bimetallic particles is the seeded growth method,[84, 127, 128, 129] which has been widely employed to tune the size and shape of metallic nanoparticles.[130] For example, Xing et al. prepared eccentric - (concentric - Au @ Ag) @ PANI (PANI - polyaniline).[128] The reaction mixture was composed of 19 nm citrate stabilized gold spheres, aniline, sodium dodecyl sulfate (SDS) as surfactant, and silver nitrate to initiate the oxidation of aniline and therefore the surface - templated polymerization, so that a silver layer concentric to gold and an eccentric PANI layer were grown at room temperature. In a different approach, Pazos - Pérez et al. applied the seeded growth method to grow gold and silver on magnetic nanoparticles ($CoPt_3$ or FePt).[84] Upon transfer of the magnetic seeds from organic solvents into water using hexadecyltrimethylammonium bromide (CTAB), the reduction of gold or silver salts with a mild reducing agent (ascorbic acid) in the presence of additional CTAB, yielded the final composite particles where the morphology of the metal parts could be tuned through variation of the reduction conditions. It is also interesting to mention the work by Xu et al., who used a gas phase separation process to the one - step preparation of Au - Co and Ag - Fe composite nanoparticles with high quality but limited scalability.[131] Recently the groups of Chen and Nam employed gold nanoparticles as seeds to grow silver in a controlled way leading to either encapsulated or snowman like particles just by varying the concentration of ligands or salt, respectively.[132, 133]

Metal - Dielectric and Metal - Polymeric Janus Particles

The first attempts to obtain asymmetrically functionalized particles implied masking processes on planar substrates. This is a rather simple approach, involving the preparation of a monolayer of particles (metal oxides [87, 134, 135] or polymers [136, 137]) on a substrate to protect one side from any modification and subsequently evaporate a metal onto the exposed surface, forming a layer that covers the upper half of each particle. Several groups developed different techniques to control the amount of surface available to metal deposition in the monolayers, and here are presented some selected cases in what follows. Bao et al. covered with a

silica monolayer a silicon wafer with a photoresist by spin - coating [88] and then removed part of this layer by plasma etching to finally deposit thin titanium and gold layers on the exposed surface. Jang et al. used a monolayer of SiO_2 particles over a polystyrene film,[138] which was then heated to induce the immersion of the particles, thereby controlling the amount of surface to be functionalized. Recently, Zhao et al. developed a mask - unmask method to what they called double - sided etching and modifying, to form asymmetric ternary particles with controllable patchiness.[139] The process is similar to that previously described by Bao et al., who also started by spin - coating a polystyrene film on a silica monolayer formed on a silicon wafer, followed by oxygen plasma etching and then covering the exposed surface with cromium and a gold layer or quantum dots. A polystyrene solution was then drop - casted and the obtained film was peeled off and turned over, so that the process could be repeated on the opposite side and the polystyrene film removed by ultrasonication. Yang et al. prepared PS - Ag particles by forming a monolayer of polystyrene particles, on which a gold layer was evaporated and finally silver nanoparticles were deposited by electrophoresis.[140] Correa - Duarte et al. prepared bifunctional polystyrene or silica spheres by either evaporation of nickel and gold on the opposite sides of 2D colloid monolayers or by layer by layer assembly of gold nanoparticles in solution followed by nickel evaporation. In both cases, functionalization of opposite sides was mediated by PS polymerization and peel - off.[141] A different type of particles that were termed Janus bubbles were synthesized by Brugarolas et al.,[142] using a three fluid system: nitrogen in the inner phase, a suspension of SiO_2 particles in toluene in the middle phase and an aqueous solution of poly(vinyl alcohol) as the outer phase, so that cromium and gold could be deposited over a dried monolayer of bubbles. Microcontact printing [143] and Langmuir - Blodgett [144] methods have also been employed as planar masking processes to obtain ternary silica particles and $Au - TiO_2$ heterodimers, respectively.

The main disadvantage of planar masking processes is the limited amount of Janus particles that can be obtained in one single batch. To overcome this issue, Granick and team developed a Pickering emulsion process that makes use of micrometer - sized quasi - spherical paraffin wax droplets as masks, thereby increasing the available masking surface in several orders of magnitude as compared to planar substrates.[145] Based on this idea Pickering emulsions were also employed to synthesize $Au - SiO_2$,[146] $Fe_3O_4 - Ag$ [147] and Fe_3O_4 hollow $- Ag$

composites,[148] Au − SiO_2 and Ag − SiO_2 [149] or Au − PNIPAm Janus particles. [150]

Soft interfaces have also been employed for the preparation of Janus metallic particles. Wang et al. managed to assemble positively charged SiO_2 particles in water with negatively charged gold nanoparticles from an organic phase, at the interface between the two liquids.[151] Perro et al. have reported the preparation of SiO_2@Au particles [90] by protecting one side of the silica surface with polystyrene, so that a dumbbell - like particle was obtained and the exposed face of the silica particle could be functionalized with a silane, followed by removal of the polymer. The unmodified silica surface was then covered with gold spheres. Polymer - fibers were used in the group of Kuo as substrates to form Janus and also ternary silica nanoparticles with a variety of functionalities and degrees of coverage, as shown in Fig. 1.6.[152, 153] Silica particles were adsorbed to previously prepared polymer - fibers, so that the immersion of the particles in the fiber was controlled through temperature, due to the presence of two glass transitions in the polymer at 120 °C and 140 °C, which led to changes in the surface tension between the particles and the fiber and therefore in the degree of immersion. Hence, isothermal treatment at 120 °C, 135 °C and 150 °C yielded immersion of one - third, one - half and two - thirds of the silica particles. The exposed faces of the nanoparticles could then be modified with an aminosilane and covered with gold particles as described in Fabrication Path I (Fig. 1.6). Adjustment of the immersion after covering one - third of the particles with gold nanoparticles, so that the silica is immersed two - thirds allows etching (with 5 wt% NaOH) of the exposed upper part and formation of ternary particles (Fabrication Path II, Fig. 1.6). Applying the same procedure but etching half of the surface, the formed Janus particles can be further functionalized with Fe_3O_4 spheres (Fabrication Path III, Fig. 1.6). SEM microscopy images of the as synthesized particles are shown in Fig. 1.6. On a different strategy, McConnell et al. proposed a method to prepare Janus SiO_2@Au spheres and a process to convert them into patchy Janus particles or even multi - region particles.[154] The covalent attachment of amino modified silica particles to styrene - acrylic acid copolymer films produces the immersion of the particles in the fiber, allowing electrostatic assembly of gold nanoparticles on the upper surfaces of the modified silica particles. Reshaping of the deposited gold particles at moderate temperatures allowed them to obtain different morphologies upon annealing. By coating the Janus particles with an Au : Pd alloy prior to annealing, multiregion particles could be obtained

since dewetting was prevented.

It is worth mentioning the one-step approach developed at the Chen's group to synthesize eccentric Au-polymer [155] and Au − SiO_2 [120] nanocomposites. The process is based on the competition between two incompatible ligands to self-assemble over the metal surface and then grow the polymer or the eccentric silica particle. Apart from hydrophobic and hydrophilic ligands, a block-copolymer (PS-b-PAA) was also added to the citrate stabilized gold spheres, to yield the final Janus particles after heating at 110 °C. This process can be applied to other nanoparticle geometries like rods and cubes, and the corresponding nanocavities are also obtained upon metal removal.[156]

Phase separation methods have been strongly developed to prepare metallic heterodimers comprising metal oxides or polymers. The main advantages of these procedures rely on their ability to produce Janus particles in one step and in large amounts. Polymeric-metallic Janus particles have been prepared by using interfacial reactions,[157, 158] electrifying co-jetting methods,[159] precipitation polymerization [160] or employing micelles or vesicles as templates.[161, 162, 163] A method based on interfacial reactions was recently reported by He et al.,[158] involving a water-oil interface with gold salt dissolved in water and 2-ethoxyaniline (EOA) in the oil phase. EOA could reduce tetrachloroauric acid ($HAuCl_4$) into Au(0) while the oxidative polymerization of EOA yielded poly-(2-ethoxyaniline) particles attached to gold seeds, which subsequently migrated into the water phase to continue gold growth, forming patches over the polymer surface. Similarly, the precipitation polymerization method developed by Ohnuma et al. permits the synthesis of metal-PS (metal = Au, Ag, Pt, Pd) particles.[160] The preparation comprises the polymerization of polystyrene in a water / ethanol mixture at 70 °C in the presence of 4-styrenesulfonic acid sodium salt and potassium persulfate as stabilizers. Metal colloids were then added to the solution to produce dimers, but the timing of colloid addition was found to be crucial, since addition before polymerization led to aggregation, whereas late addition resulted in a drastic reduction in the yield of Janus particles. Kang et al. recently employed these particles as seeds to obtain Au-PS semishells using hydroxylamine hydrochloride as reducing agent to grow the gold part over the polymer surface.[164]

A common method to obtain dielectric-metallic particles is the seeded growth over metal or dielectric particles (similar to above described for bimetallic particles). Yu et al. prepared Au − Fe_3O_4 dumbbells by thermal decomposition of

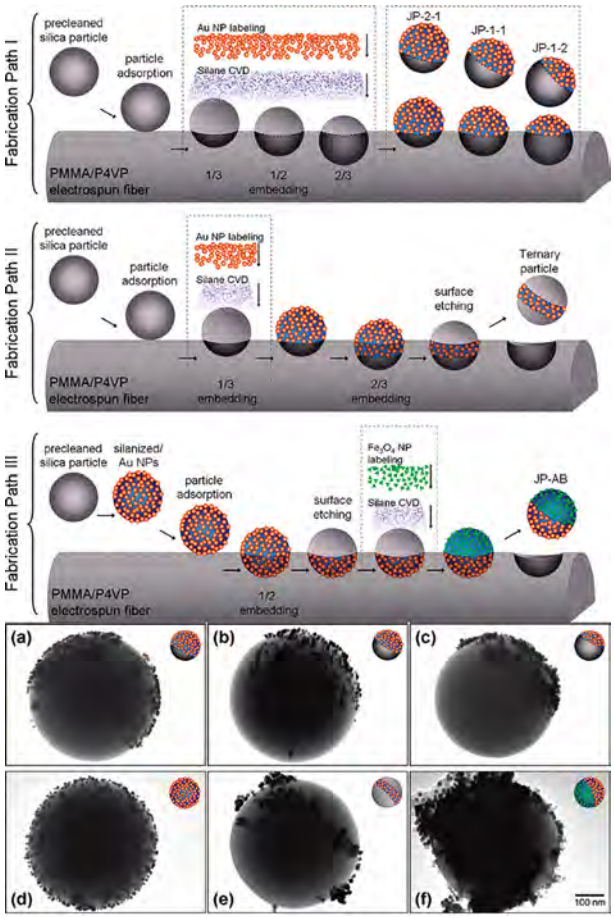

Figure 1.6. On top: 3 synthetic routes to obtain SiO_2@Au Janus particles, SiO_2@Au ternary particles and SiO_2@Au − Fe_3O_4 Janus particles. In the bottom: SEM images of a SiO_2@Au Janus particle with decreasing grade of coverage (A - C), SiO_2 particle fully covered with gold seeds (D), SiO_2@Au ternary particle (E) and SiO_2@Au − Fe_3O_4 Janus particle (F).

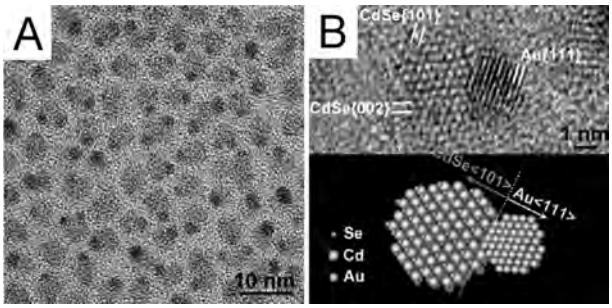

Figure 1.7. (A) TEM image of CdSe - Au hybrid nanocrystals with a CdSe size of 3.4 nm. (B) HRTEM image and a schematic representation of a CdSe - Au nanocrystal.

$Fe(CO)_5$ on gold seeds, in the presence of oleic acid and oleylamine, followed by room - temperature oxidation.[165] Gold particle size could be tuned by controlling the temperature of $HAuCl_4$ injection or modulating the $HAuCl_4$ / oleylamine ratio. The use of non - polar solvents was found to be critical in order to obtain dumbbell - like instead of patchy structures. When magnetite starts to nucleate, free electrons from the gold seed compensate the charge induced by the polarized plane at the metal - oxide interface, inducing electron deficiency on the exposed facets that inhibits further nucleation, thus resulting only in dumbbell particles. Oppositely, when the slightly polar diphenyl ether was used as solvent, flower - like structures were obtained. The same method was applied with $X - Fe_3O_4$ and $X - CoO$ heterodimers (X = Au, Ag, AuAg, Pt).[86] Similar approaches were employed to obtain $Ag - Fe_3O_4$ particles,[166, 167] Ag - Se,[168] PbS - Au,[169] Ag - AgBr,[170] $Ag - SiO_2$ [171] or $Au - TiO_2$,[172] while Shi et al. described the preparation of different hybrid structures: $XFe_2O_4 - Au$ (X = Fe, Mn, Co), PbS - Au, PbSe - Au, $PbS - Fe_3O_4$, $Fe_3O_4 - Au - PbS$ and $Fe_3O_4 - Au - PbSe$.[173] Schaak et al. demonstrated the synthesis of $M - Pt - Fe_3O_4$ (M = Au, Ag, Ni, Pd) heterotrimers and went one step further obtaining $M_xS - Au - Pt - Fe_3O_4$ (M = Pb, Cu) heterotetramers.[174]

Diffusion of metals in semiconductors is a well - known process in bulk materials and its application to nanostructured materials has recently been started. Yang et al. prepared core shell $Au - Ag_2S$ particles and observed that within 72 h gold ions migrated from the interior to the surface, forming heterodimers.[175] The same procedure was applied to $Pt@Ag_2S - Au$ by first preparing core - shell Pt @ Au and then coating with Ag_2S, followed by diffusion of gold ions to the surface. Zeng

et al. reported the synthesis of CdSe - Au, PbSe - Au, FePt - Au, Cu_2O – AuAg, and FePt - CdS - Au.[176] CdSe - Au was obtained by reduction of Au(I) - alkanethiol (SR) with ethylene glycol over the surface of CdSe nanocrystals at 30 °C (Fig. 1.7). The process started with the reduction of the Au(I) - SR complex by polyethylene glycol at the CdSe surface. No gold reduction was observed without the presence of semiconductor nanocrystals, which acted as a heterogeneous nucleation point for gold ions. Sotiriou et al. described a gas phase separation approach with flame spray pyrolysis to obtain Ag – Fe_2O_3 nanocomposites.[177] The feeding solutions containing iron (III) acetylacetonate and silver acetate dissolved in organic solvents were fed into a reaction chamber, where the spray was ignited to yield the final dimers. This process is suitable for scalability but it probably lacks quality in the size distribution of the final particles.

Non Spherical Janus Particles

The preparation methods for spherical Janus particles have substantially evolved through progress in tuning the composition and properties by applying the knowledge achieved in the synthesis of symmetric nanoparticles. However, tuning anisotropy has been demonstrated to play a major role in the manipulation of the properties of nanomaterials, so the preparation of non - spherical Janus particles has also become an attractive playground for the design of novel nanoparticle systems. The widely employed seeded growth method is usually the basis for obtaining non - spherical Janus particles. Here are highlighted some of the most recent articles describing the preparation of Janus nanorods with a variety of compositions: CdSe / CdS - Au,[178, 179, 180] CdSe / CdS - Co,[181] CdS - Au,[178, 179] CdSe - Au,[182] CdSe - Co,[183] Co - Au,[184] Te - Au,[185, 186] Pd - Au,[187] Au – TiO_2,[173] ZnO - Ag,[188] TiO_2 – Co,[189] Au - Ni and Au - (Ni - Pd).[190] Deka et al. described the preparation of semiconductor - magnetic Janus (CdSe / CdS - Co) nanorods,[181] using CdSe @ CdS as seeds during decomposition of $Co_2(CO)_8$ under inert atmosphere at high temperature. It was found that the growth mechanism involved the nucleation of cobalt at the opposite edge to where the CdSe seed was located, followed by selective autocatalytic growth. This directional growth was driven by the semiconductor tips due to the hexagonal close - packed (hcp) structure of cobalt obtained in the Janus nanorods, compared to the cubic ϵ - phase obtained under the same conditions without seeds. It should be noted that only the

matchstick structure was obtained, with no other intermediate particles that could evolve to the final geometry by ripening processes. Chakrabortty et al. reported the growth of gold particles over one tip of preformed CdSe@CdS nanorods under ambient light conditions.[180] CdS rods were grown on CdSe spherical seeds and then the CdSe@CdS nanoparticles where dispersed in a mixture of toluene and n-octadecylphosphonic acid, where the gold particles were grown by injection of $HAuCl_4$, tetraoctylammonium bromide and dodecylamine in toluene. The growth of the gold particle at either one or both tips, or at rod sides was found to depend on the amount of gold added, which was related to differences in the reactivity of the different facets. In fact, when a sufficiently low amount of gold precursor was used, growth occurred only at the rod tip that was farther away from the CdSe seed, but gold would grow at both tips and at the sides when the amount of gold salt was increased. In a related work, Maynadié et al. grew cobalt over the tips of preformed CdSe nanorods,[183] finding that the ligands added to stabilize the dumbbells played a significant role in directing cobalt growth. By varying the reaction temperature, they were also able to grow a full cobalt rod over the CdSe rod seeds. In addition, a masking process has also been applied for the preparation of $SiO_2 - Au$ matchsticks.[191] The process implied the synthesis of silica nanorods followed by alignment along their long axis over a substrate, assisted by an alternating current (AC) electric field. In a third step titanium and gold layers were evaporated over the rods. To mitigate the presence of imperfections, the end-functionalized region was protected with a PDMS stamp and a gold etching process was carried out. After removing the stamp, the matchsticks were released by ultrasonication.

Besides Janus gold nanorods, other structures have been obtained. He et al. reported lollipop-, dumbbell- and frogegg-like PANI-Au shapes by using interfacial reactions,[158] while Xing et al. applied the procedure to prepare eccentric-(concentric-Au@Ag)@PANI nanoparticles with gold nanorods,[128] and Choi et al. synthesized $Cu_2S - In_2S_3$ heterostructured materials with acorn, bottle or larva shapes by the decomposition of copper and indium oleates at different temperatures.[192] Other examples involve the growth of cobalt spheres over iron oxide tetrapods,[193] the formation of $Pt - Au_n$ ($n = 1, 2, 4$) by controlling the gold nucleation spots on platinum seeds,[194] or the synthesis of $Cu - Cu_3P$ nanocrystals [195] by Trizio et al. Controlling the amounts of CuCl and trioctylphosphine, copper nanocrystals were prepared, which evolved into Cu_3P nanocrystals

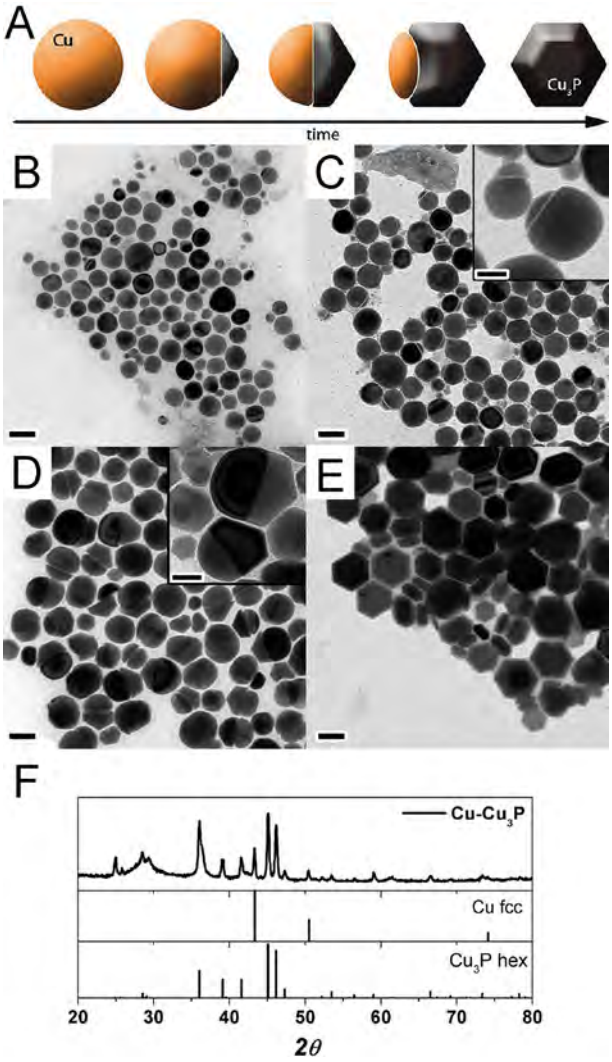

Figure 1.8. (A) Scheme of synthesis: first Cu particles are grown, and then they are progressively phosphorized to Cu_3P Janus - like particles in which the volume fraction of the truncated bipiramidal Cu_3P domain increases over time. (B - E) TEM images of Cu nanoparticles and their conversion to Janus - like and Cu_3P particles. Aliquots were collected at: (B) 4 min, (C) 10 min, (D) 25 min and (E) 45 min. Scale bar is 50 nm for the panels and 20 nm for the insets. (F) XRD pattern of the powder sample of Janus - like particles shown in panel (D).

through Janus Cu − Cu_3P intermediates (Fig. 1.8). X-ray powder diffraction (XRD), high resolution transmission electron microscopy (HRTEM) and energy filtered TEM (EFTEM) confirmed the presence of the two components in the structure. Copper crystals were formed by annealing Cu_3P nanocrystals at 400-500 °C, which produced the dephosphorization by phosphorus evaporation. Both kinetic (as the inhomogeneous coverage of surfactants), and thermodynamic aspects (as the presence of epitaxial interfaces between copper and Cu_3P domains that would minimize the energy) could explain the formation of Janus instead of the expected centrosymmetric particles. Ag_2S − Ag dumbbells and $(Ag_2S)_2$ − Ag or even $(Ag_2S)_3$ − Ag structures were prepared by Pang et al. by the assembly of dimers with ethylenediamine.[196] Finally, it is worth to mention the formation of different structures like Janus carbon nanotubes,[197] pyramids,[198] and Pd-Ag nanocubes.[199]

1.5.3 Applications of Janus Particles

The multiple combinations of properties that Janus particles can exhibit, including hydrophobicity-hydrophilicity, plasmonic, magnetic, catalytic, etc. open a wide variety of potential applications. In the specific case of metallic Janus particles, their use has been reported in drug delivery for cancer treatment,[200] as bactericides,[196] biomarkers including magnetic manipulation,[167, 177] or as functional elements at liquid-liquid interfaces,[201, 202] among others.

Application of Janus particles in drug delivery has been demonstrated with cisplatin, a well-known antitumor agent. This type of complexes can be hydrolyzed to the active molecule cis − $[Pt(NH_3)_2(H_2O)_2]^{2+}$, which is responsible of cell death. The nonspecificity of this anticancer treatment produces the destruction not only of tumor cells but also of healthy cells, resulting in undesirable side-effects. Sun and co-workers used Au − Fe_3O_4 heterodimers as carriers for delivering cisplatin molecules specifically into breast tumor cells.[200] Considering that the fast growing tumor cells often have antigens overexpressed on their surface, these can be used as specific binding targets for monoclonal antibodies. Au − Fe_3O_4 nanoparticles were used as nanocarriers, binding the platin complex to the gold side and the monoclonal antibody to the oxide surface. Plasmonic and magnetic properties of gold and magnetite respectively make these particles suitable as magnetic imaging probes for tracking the delivery of platin into the cells. The therapeutic

effect experiments showed that non-modified Au − Fe_3O_4 dimers did not affect cell growth, whereas platin − Au − Fe_3O_4 − antibody nanoparticles showed lower half-maximal inhibitory concentration (IC 50) than bare cisplatin, 1.76 vs. 3.5 μg of Pt/mL, and platin − Au − Fe_3O_4 were less toxic than cisplatin molecule, which was related to the non-specificity of the complex and to the slow hydrolysis rate of platin in the nanoconjugate. Therefore, these Janus dumbbells have demonstrated great potential as nanocarriers for diagnosis and therapeutic applications.

Pang et al. showed the antibacterial properties of Ag_2S − Ag dumbbells under UV irradiation against E. coli. [196] The bactericidal properties of silver containing materials are known but the mechanism underlying this property is not completely understood. Cell viability experiments have shown that under UV light alone and with the only presence of the heterodimers (0.10 mg/mL) there are no significant bactericidal effects. The non-toxic effects of the dumbbells can be explained by the large size of the silver particles (50-75 nm), as has been reported that bactericidal properties of silver are enhanced as the size decreases. However, combination of UV irradiation with Ag_2S − Ag particles (0.01 mg/mL) leads to significant enhancement of the antibacterial capability, and increasing the concentration to 0.10 mg/mL, E. coli was found to be completely inactivated within 50 min.

Optical Properties

The synthesis of new types of materials such as metallic Janus particles requires in turn the development of theoretical models and simulations to explain their properties. In this respect gold semishells, composed of a spherical polymeric or dielectric core partially covered with a gold layer have become the system of choice. Interestingly, all theoretical studies try to compare their results with experimental measurements, for which planar masking processes are consistently employed to fabricate the gold semishells, since they offer a high degree of control as compared to colloidal methods. Of particular significance is the work by Nordlander and Halas, which provided an explanation for the observed optical properties of both complete nanoshells and semishells.[203, 204, 205] In 2009, Mirin et al. prepared gold semishells with a polymer core by a planar masking process (core $\approx$ 80 nm, shell $\approx$ 20 nm), and carried out optical measurements varying the angle of incidence of light and comparing their results with simulations based on finite element modeling (FEM). [204] These authors found that gold semicapsules display two main

plasmon modes, one axial and one transverse, due to their asymmetry. The weak axial mode around 600 nm corresponds to a dipole-driven electroinductive plasmon response of the particle and its scattering pattern is determined by the angle of irradiation.[205] The stronger transverse mode is located around 800 nm and under p-polarization the semicapsule orientation is responsible for the scattering direction and amplitude instead of the direction of the light. The axial and transverse modes were observed when the electric field is parallel to the cup rotational axis and when it was normal to the rotational axis, respectively. Ye et al. reported the preparation of gold semishells by first synthesizing complete SiO_2@Au shells in a colloidal process, and then using a planar masking process to etch a selected part of the exposed gold layer to yield the final structures.[206] They studied the evolution of the optical spectra as the gold layer was removed in a 224 nm silica core with 17 nm shell thickness and also with 87 nm silica and 30 nm gold. The explanation of the spectral changes was based on the plasmon hybridization model, which treats interactions between plasmons as hybridized bonding and antibonding states.[207, 208] In a subsequent study they also fabricated silver, copper, gold and aluminium semishells in PDMS films.[209] The evolution of the optical spectra as a function of the cut-off parameter (δ), the fractional height compared to the full nanoshell geometry, was studied by Cortie et al. for 70 nm core and 30 nm gold shell diameter (Fig. 1.9).[210] When $1.0 < \delta < 0.85$ (no hole yet), the optical properties remained as those of complete nanoshells ($\alpha = 610$ nm), but below 0.85, as soon as the hole appears, a strong resonance was observed at 690 nm (β). They showed that α became weak, blue-shifted and finally disappeared as δ decreased. There was also a third band, γ, at 580 nm. The main parameters affecting the LSPRs in these structures are the core size, shell thickness, degree of coverage or the as above mentioned cut-off parameter, but also the surface roughness.[211] Unfortunately, although many recent publications deal with the optical properties of gold semishells and semicapsules, a systematic study of this system is still missing. The variety of parameters affecting the optical response of the system make it difficult to compare the results provided by the different groups to fully understand the effect of every parameter, and then to be able to synthesize particles with preselected plasmon properties.

Recent simulations by Shaviv et al. for CdS-Au matchstick and CdSe-Au dumbbell-shaped nanoparticles [212] show that the optical properties of these hybrid structures arise from both components. In the UV-Vis region, the optical ab-

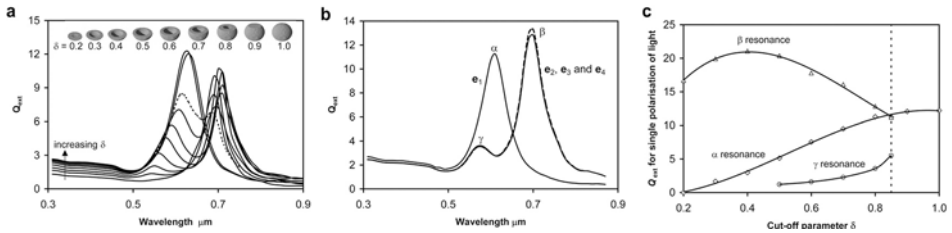

Figure 1.9. Conversion of a nanoshell into a semishell and the effect on the calculated optical extinction spectra. (A) Average cross section (Q_{ext}) for δ from 0.2 to 1.0, also showing the shapes simulated. Data for $\delta = 0.85$ is shown as a dotted line. (B) Separation of effects due to orientation of light for $\delta = 0.8$. (C) Peak Q_{ext} values of main resonances as a function of δ for this series of semishells, extracted for a single but appropriate orientation of the light. The wavelengths at which the three resonances occur converge near $\delta = 0.85$ (dotted line) and they cannot be distinguished from one another when $0.85 < \delta < 1.0$. Adapted from reference [210].

sorption is due to the plasmon band of the gold part and to the exciton band of the semiconductor, while in the NIR region an absorption tail is also observed. It should be noticed that the fluorescence from the semiconductor is quenched by the rapid electron transfer from the semiconductor to the metal. Discrete dipole approximation (DDA) simulations showed that the optical features of the hybrid particle strongly depend on small variations at the gold domain.

An interesting property of metallic Janus particles was exploited by Jiang et al. to promote the movement of these nano particles by applying a defocused laser beam over them.[213] Using 1 μm silica - gold semishells in a solution sandwiched between two cover slides, a Nd : YAG laser operating at 1064 nm was defocused over the sample and one particle was pushed up into the chamber, recording then the 2D movement with a high speed camera. They found that the movement of the particle under the laser beam was faster than in normal diffusion and the direction followed the Janus polarity. They proposed that this movement was due to three kinds of motions: Brownian motion, movement induced by the laser and the optical trapping confinement. They proposed that the movement induced by the laser was due to the temperature gradient generated when the metal was heated by the radiation. It was also possible to produce the rotation of the particles, which might find application in micromachines design.

Self - Assembly

During the self - assembly (See Section 1.1), Janus and patchy particles may play an important role by inducing directionality, being this property responsible for obtaining new kinds of structures that are not observed with symmetric nanoparticles. [75, 20, 76, 214, 215]

Regarding field - induced self - assembly, it is necessary that Janus nanoparticles exhibit surface charge or magnetic properties. Velev's group has carried out assembly experiments assisted by electric or magnetic fields that yielded structures in agreement with simulated phase diagrams.[216, 217] The application of a magnetic and / or electric field on 4.0 μm PS Janus particles partially covered with an iron layer, the particles assembled into chain structures in the direction of the applied field. When using magnetic fields, two kinds of configurations were observed, "staggered chains" and double - chains with metal - metal parts in contact. These structures do not disassemble upon application of the magnetic field because of the remnant magnetization in the metal semishells, unlike the case of electric fields, where the particles separate after field removal due to Brownian motion. Certain long - range lateral repulsion forces exist between the chains that lead to only end - to - end rather than side - to - side chain assembly. This self - assembly process is reversible, allowing recycling of the building blocks.

The addition of additives such as salt to increase the ionic strength of the dispersing medium and induce colloidal aggregation has been widely used to produce the assembly of symmetric particles. Recently, the group of Granick reported a kinetic study of the assembly of Janus particles [76] and the directed self - assembly into a kagome lattice [20] by control of the interparticle forces through variation of the salt concentration. This kinetic study was carried out using Janus particles that display hydrophobic and negatively charged components, thereby showing short range and reversible interparticle interactions. At very low salt concentrations the particles repel each other, whereas at high concentrations the double layer repulsion is screened, van der Waals attraction forces becoming more important and leading to assembly of the particles. With Janus particles, the maximum number of neighbors was six for each particle, and the authors showed that the different combination of particles or clusters determine the visualized structures. At very high salt concentration, long helical structures were also observed.

The presence of ligand molecules can direct the assembly of Janus particles with

specific interactions using DNA moieties,[218, 219] polymers [114, 115, 123, 220, 12] or controlling the binding preference using masking ligands.[221] In an interesting work, Xing et al. prepared 160 nm PS Janus gold semishells.[218] Upon functionalization of the metal with a thiolated DNA linker, they attached 15 nm gold nanospheres modified with the complementary DNA chain to the metal part of the Janus particles. The assembly showed its reversibility by the addition of a complementary DNA moiety that produces a more stable hybridization. They prepared different reversible asymmetric assemblies by modifying the Janus particles with two different DNA chains and selectively attaching gold particles with the complementary DNA functionalization (Fig. 1.10). Wang et al. reported the formation of homoparticle clusters made of Janus particles with PEO and PMMA patches and heteroparticle clusters with PEO - modified magnetite particles.[221] Worm - like structures made of Janus particles were obtained when a poor solvent for PEO as dioxane was added to the particles, assembling into structures with the collapsed PEO chains away from the solvent. Applying the same procedure to a mixture of Janus and magnetite particles, satellite structures with a magnetite particle surrounded by Janus particles that behave as the PMMA brushes in contact with the solvent were obtained. All these assemblies could also be reversed by simply adding a good solvent for the PEO fragment. Sahoo et al. have reported the controlled assembly of snowman - like $Pt - Fe_3O_4$ particles over WS_2 nanotubes.[222] In the absence of additional ligands, $Pt - Fe_3O_4$ particles assemble with the platinium part in contact with the nanotubes, but by masking the platinium with a thiol molecule the assembly takes place with the magnetite part in contact with the WS_2 nanotubes.

In addition to their ability to organize into new types of structures, the self - assembly of Janus particles may have promising applications on surface enhanced Raman scattering (SERS) spectroscopy in the near future. The key aspect here is the ability to organize the particles in such a way that the production of hotspots can be optimized, which will in turn strongly enhance the sensitivity in detection applications.[223, 224] In this respect, Chen et al. prepared eccentrically encapsulated gold spheres and nanorods covered with a polymer only on their sides.[155, 156] The exposed gold surface was available to binding by SERS active ligands, and the enhancement factor obtained for partially covered rods was 3.65×10^4, compared to fully functionalized gold nanorods (1.35×10^4), suggesting a strong electric field magnification at the tips. However, no enhancement was ob-

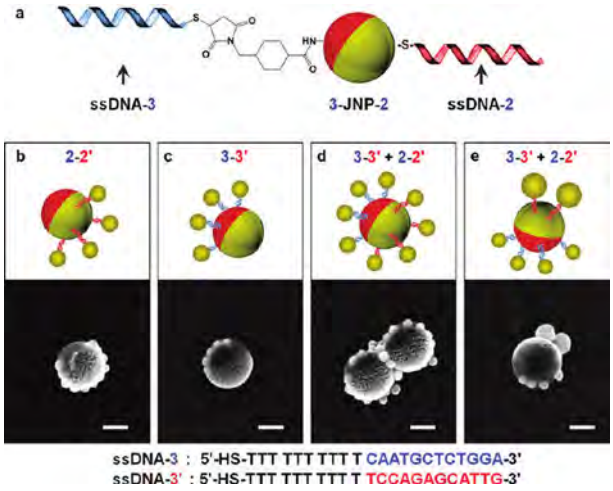

Figure 1.10. (A) Schematic view of two different coupling chemistries on the surface of an amine-modified 200 nm polystirene Janus nanoparticle. (B-E) Schematic views and SEM images of representative asymmetric nanoclusters formed by dual DNA-functionalized JNP and different DNA encoded AuNSs: (B) 40 nm AuNS-2´, (C) 40 nm AuNS-3´, and (D) equal mixture of 40 nm AuNS-2´ and AuNS-3´; and (E) equal mixture of 80 nm AuNS-2´ and 40 nm AuNS-3´ (scale bar = 100 nm). Reproduced with permission [218] Copyright 2012, American Chemical Society.

served when the same procedure was applied to gold spheres. Janus gold semishells were used by He et al. to detect 4-mercaptopyridine with a concentration as low as 100 nM, for which an enhancement factor of 4.1×10^8 was quoted.[158]

Catalysis and Nanoengines

Many applications can be foreseen in the field of catalysis and other active nanostructures when several functionalities can be combined within the same nanosized unit. For example, metal oxide nanoparticles have been largely used as photocatalysts, though their efficiency has been found rather poor. An effective way to enhance their activity is by coupling metal to metal oxide nanoparticles. Pradhan et al. have shown the catalytic activity of $Au - TiO_2$ heterodimers in the oxidation of methanol to formaldehyde triggered by light, [144] where the proposed mechanism involves the promotion of electrons into the conduction band of the metal oxide, leaving a hole in the valence band that reacts with adsorbed water to form hydroxyl radicals. These radicals react with adsorbed methanol to form α-hydroxymethyl radicals which in turn react with dissolved oxygen to yield

formaldehyde, which was detected by a colorimetric reaction. This process was facilitated by the presence of gold acting as an electron sink to maintain the separation between electrons and holes. Wang et al. used Au − Fe_3O_4 and Pt − Fe_3O_4 particles to oxidize CO from a feeding gas, with implications in cleaning and energy conversion reactions.[86] This was usually carried out by platinium - based catalysts at high temperatures and comparison of the activity of both catalysts with their commercial counterparts showed higher activity, particularly at low temperatures. More recently, Seh et al. reported the use of Au − TiO_2 particles as photocatalysts for H_2 generation from an isopropyl alcohol / aqueous solution under visible light irradiation.[225] The photocatalytic activities of bare gold and titanium oxide were very low under light irradiation. On the other hand, the production of hydrogen was largely increased using Janus and also with core - shell particles (Fig. 1.11 A), indicating a synergistic effect between both components. The authors found a magnification in the electric near field intensity for both Janus and centrosymmetric particles, which was larger for Janus, with a localization of the plasmonic properties at the Au − TiO_2 interface (Fig. 1.11 B - D). Considering that amorphous materials possess electronic states in the band gap that are susceptible for electronic transitions, the localization of the electric field at the interface between both materials leads to an increase in the optical absorption and is consequently responsible for the photocatalytic enhancement. Employing heterodimers with larger gold spheres, the catalytic properties were found to be higher because of the more intense electric near fields generated.

The catalytic activity of metallic Janus particles has also been recently used by several groups for different purposes, including the design of swimmers or nanoengines and nanotransporters.[226] A nanoengine is a nanoparticle that makes use of a chemical reaction,[227, 228, 229, 230, 231, 190, 232] an external field [190] or ultrasounds [233, 234] to obtain the necessary self - propulsion to overcome Brownian motion, while a nanotransporter is a swimmer that additionally loads a cargo.[235] Two mechanisms have been proposed to explain the motion of these particles in solution using H_2O_2 as fuel, generating H_2O and O_2. The first model proposes that oxygen nanobubbles detach from the surface of the catalyst due to the amount of liberated oxygen, which makes it impossible to be dissolved and thus provides the device with a momentum. These bubbles have been observed with large catalysts, but it is unclear whether they are responsible for the motion of smaller swimmers. The second mechanism suggests that the motion is caused by the concentration gra-

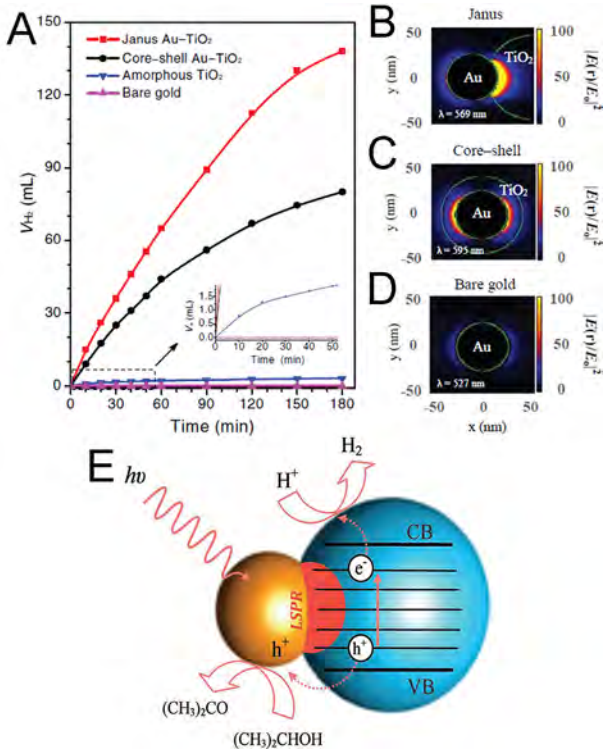

Figure 1.11. (A) Volume of hydrogen generated V_{H_2} under visible-light irradiation from a tungsten halogen lamp using Janus and core-shell $Au_{50nm} - TiO_2$ nanostructures, as well as amorphous TiO_2 and bare gold nanoparticles (50 nm). (B-D) Plasmonic near-field maps (cross-section view at z = 0) simulated using DDA for Janus $Au_{50nm} - TiO_2$ (B), core-shell $Au_{50nm} - TiO_2$ (C) and bare gold nanoparticles (50 nm) (D). The maps show the electric near-field intensity enhancements $|E(r)/E_0|^2$ of the nanostructures at their LSPR wavelengths (indicated on each map) with the incident polarization along the x-axis. (E) Proposed photocatalytic process for efficient hydrogen generation using the Janus $Au - TiO_2$ nanostructures, based on excitation of the LSPR under visible-light irradiation.

dient generated during the reaction, called diffusiophoresis. The first model only explains the movement in the direction opposite to the metal, whereas in the second the direction depends on the interactions between the solvent and the catalytic and non-catalytic parts of the particle.[231] Actually, there is no single mechanism explaining the behavior of swimmers in all systems, and other aspects like geometry of nanoengines do affect the propulsion.[236] An important contribution was provided by Howse et al., who observed that Pt-PS semishells only display Brownian motion in the absence of fuel, but when fuel is added the particles self-propel and if the concentration is increased the velocity of the particles also became higher.[227] The aim of these devices involves the transport of a cargo within a liquid medium, with potential applications in drug-delivery or biosensing.[235]

Chapter 2

Colloidal Synthesis of Gold Semishells

Abstract

A novel and scalable colloidal strategy is presented to fabricate gold semishells based on the selective growth of gold onto Janus silica particles (500 nm in diameter) with amino functionality on one side. The modulation of the Janus silica particles geometry allows us to tune the final morphology of the gold semishells. Besides, this method provides a new route to fabricate hollow gold semishells through etching of the silica core with hydrofluoric acid. The optical properties were characterized by visible - NIR spectroscopy. Comparison with simulations performed using the boundary element method, BEM, reveals that the main optical features are located beyond the NIR region because of the large core size.

2.1 Introduction

The recent advances in the fabrication of colloidal particles comprising different properties (such as chemistry, polarity, optical and magnetic properties) at opposite sides, commonly known as Janus particles,[237] have opened new avenues toward the development of advanced materials. The reduced symmetry in these materials provides them with fascinating properties and therefore with potential applications in various fields including electronic paper,[96] photonic materials,[99] imaging probes,[102] and sensors.[99] Exciting future applications are expected in connection with their interesting self-assembly behavior, since the presence of distinct areas within Janus particles renders them as powerful building blocks for the fabrication of novel structures.[20, 238, 76]

Janus particles comprising a dielectric / polymeric core partially covered with a metallic shell are commonly referred to as semishells, but different terms have been used such as half-shells or nanocups depending on the extent of metal surface coverage. More recently, the expression "plasmonic patchy particles with reduced symmetry" has been used for particles with a more heterogeneous metal distribution on the core.[239] It has been demonstrated that plasmonic semishells present unusual and unique optical properties due to their reduced symmetry.[240] The inherent asymmetry of these systems leads to the presence of two types of dipolar surface plasmon modes: a blue-shifted axial mode and a red-shifted transverse mode. While the blue-shifted axial mode is purely electric, calculations predict that there is also a significant magnetic component in the red-shifted transverse mode.[210, 205, 204] These dipolar resonances display different light-scattering characteristics that are strongly influenced by the angle of incidence and polarization of the incident light and by variations in the dielectric environment. Moreover the optical response can be easily modulated from the visible through the near-infrared (NIR) by tuning the core radius, metal thickness and surface coverage. Altogether, plasmonic semishells offer a variety of new possibilities for the fabrication of metamaterials with negative refractive index at NIR and visible frequencies[241] or for the fabrication of surface enhanced Raman scattering (SERS) probes.[242]

On the basis of the above-described properties, there is a need to develop novel and efficient synthetic methods that allow us to control the compositional and morphological parameters of semishells. Two fundamentally different approaches have been applied so far to prepare plasmonic nanostructures with reduced symmetry:

the deposition of a metal onto a close-packed colloid monolayer, using electroless plating, e-beam evaporation or sputtering; or anisotropic etching via ion milling, argon-ion plasma or electron-beam-induced ablation of full nanoshells previously deposited on a substrate.[240] However, the application of colloidal synthesis to plasmonic semishell synthesis has been far less explored. Probably the closer example is the work by Klupp Taylor et al., who have reported the fabrication of silver patchy particles with tunable optical properties via electroless deposition onto nonfunctionalized colloidal silica spheres.[239, 171] Although this method shows a certain degree of control on metal coverage, it has not demonstrated to wark for the formation of solid semishells. We present in this chapter an alternative method for the design and fabrication of gold semishells using a colloid chemistry route, based on the use of preformed Janus silica particles as templates where the selective growth of gold can only take place on the functionalized areas. A similar approach was employed by Perro et al. for the production of large quantities of Janus particles but they did not complete the process for the synthesis of gold semishells.[146] The growth of the gold semishells is carried out by means of the well-known method developed by Halas et al.[243] for gold nanoshell synthesis, however, partial coverage is achieved by selective partial functionalization of the silica particles with amino groups on one side. Such Janus silica particles were synthesized by a masking process based on Pickering emulsions recently reported by Granick et al.[108] The final morphology of the gold semishells can thus be tuned through the geometry of the Janus silica template. We additionally demonstrate the fabrication of hollow gold semishells by simply etching the silica cores with a hydrofluoric acid solution. The optical response of the resulting semishells was characterized by vis-NIR spectroscopy and compared to calculations of the extinction cross section using the boundary element method (BEM).[244, 38] This allows the analysis of the effect of gold surface coverage, shell thickness and core diameter.

2.2 Experimental Section

Chemicals

Tetrachloroauric acid ($HAuCl_4 \cdot 3H_2O$, 99%) and didodecyldimethylammonium bromide (DDAB, 98%) were supplied by Sigma. Ammonium hydroxide (NH_4OH, 28%) and tetraethylorthosilicate (TEOS, 98%), (3 - ethoxydimethylsilyl) propylamine - (APDMES), paraffin wax (melting point ranging from 58 to 62 °C), potassium carbonate (K_2CO_3, 99%), chloroform, tetrakis (hydroxymethyl) phosphonium chloride (THPC, 80%), sodium hydroxide, sodium chloride and formaldehyde (H_2CO, 37%) were supplied by Aldrich. Hydrofluoric acid (HF, 40%) was procured from Panreac. Absolute ethanol (Scharlau) and Milli - Q water were used as solvents. All the chemicals were used as received from the supplier.

Synthesis of Janus Silica Particles

The first step comprised the preparation of 495 nm silica particles as described elsewhere, using a variation of the Stöber method.[245] All glassware was cleaned with an HF 2% solution before starting. To 250 mL of an ethanolic solution containing 7 M H_2O and 2 M ammonium hydroxide a certain amount of TEOS ($[TEOS]_{final} = 0.3$ M) was added under vigorous stirring. When the solution became turbid, slow stirring was applied for 8 h. Then, the formed silica particles were washed by 4 cycles of centrifugation (3400 RCF, 20 min) and redispersion with ethanol. The nanoparticles were finally dried under vacuum and stored.

Pickering emulsions were subsequently prepared according to Jiang et al.[108] with some modifications. 20 mL of a freshly prepared DDAB aqueous solution (15 - 90 mg/L) containing 0.4 g of silica (495 nm) was heated up to 70 - 75 °C and then added to molten paraffin wax (5 g) also at 70 - 75 °C. The mixture was maintained at that temperature with refrigeration for 1 h to reach equilibrium, and then cooled down to room temperature. The resulting colloidosomes, wax solid droplets with adsorbed silica particles, are visible with a naked eye. The removal of unattached and weakly attached silica particles was performed by adding 40 mL of water to the colloidosomes and then stirred manually for a few seconds. The process was repeated multiple times till observing a colorless solution. Colloidosomes were then filtered and dried under vacuum (30 °C and 300 mbar) for 2 days.

Figure 2.1. Experimental setup employed for the gas - phase silane deposition.

The surface functionalization was carried out using a gas phase method also reported by Jiang et al.[108] Briefly, a silane vapor, produced by bubbling dry nitrogen (at 0.25 bar) through 500 μL of APDMES, is allowed to react with colloidosomes (ca. 0.5 g) deposited onto a filter funnel for 30 min (Fig. 2.1). Every 5 min colloidosomes were moved around by rolling the filter in order to obtain a homogeneous surface functionalization. Finally a dry nitrogen flow was passed through the particles for 30 min to remove the silane in excess.

To release the Janus silica particles from the wax surface, paraffin wax was dissolved by adding chloroform (2 x 30 mL) and then particles were further washed with ethanol (30 mL) by two cycles of centrifugation (2300 RCF, 20 min) and redispersion. Finally, Janus particles were stored dry until use.

Fabrication of Gold Semishells

Gold semishells were prepared by a sequential growth method according to the process described by Halas group,[243] with slight modifications. First 200 mL of THPC gold seeds (1 - 2 nm) were prepared as described by Duff et al.:[246] 180 mL

of water were mixed and vigorously stirred with 1.2 mL of 1 M NaOH and 4 mL of $6.8 \cdot 10^{-2}$M THPC solution in water. After 5 min, 1.53 mL of 0.13 M $HAuCl_4$ solution in water was added in one quick motion. The solution changed instantly from colorless to deep brown. This solution was stored in the refrigerator and used when it was 2 to 8 weeks old.

Then 500 mL of aqueous gold plating solution containing 1.8 mM K_2CO_3 and 44 μM $HAuCl_4$ was prepared and stored in the fridge for 24 h prior to use. More homogeneous shells were obtained when the plating solution was aged between 24 and 48 h.

The as prepared gold seeds were attached onto the Janus silica particles to form the precursor particles as follows: to 40 mL of gold seeds (previously sonicated for 1 min) 4 mL of 1 M NaCl and 300 μL of ethanol (containing 5 - 10 mg of Janus silica particles) were added. The mixture was sonicated for 2 min and allowed to reach equilibrium for 12 - 24 h. Then, the particles were centrifuged (20 min at 850 RCF) and washed 3 times with water. Finally, precursor particles were dispersed in water ($7 \cdot 10^9$ particles / mL) and stored in the fridge. These particles can be used for at least 48 h to obtain complete gold semishells.

The growth of the gold semishells was carried out as follows: all solutions were maintained at 25 °C for 30 min before use. First, 96.4 mL of plating solution was mixed with 3.6 mL of the precursor particles dispersion ($7 \cdot 10^9$ particles / mL). The ratio between gold ions and precursor particles was 10^8. Subsequently, 500 μL of H_2CO was added to the mixture under vigorous stirring. After 15 seconds stirring was slowed down and it was allowed to react for 10 - 15 min. Before starting the second growth step, particles were centrifuged (850 RCF, 30 min) and redispersed in 3.6 mL of water. After 5 growth steps, the resulting gold semishells were washed by four cycles of centrifugation (850 RCF, 30 min) and redispersion in water to ensure the complete removal of K_2CO_3 and H_2CO in excess. Gold semishells were kept in water and stored at room temperature.

Finally, hollow plasmonic structures were obtained by exposure of gold semishells to 10% hydrofluoric acid for 6 h. The particles were finally washed by three cycles of centrifugation (850 RCF, 30 min) and redispersion in water.

Instrumentation

Visible - NIR spectra were measured in 1 cm path length quartz cuvettes using a Cary 5000 UV - visible - NIR spectrophotometer. A JEOL JEM 1010 transmission electron microscope operating at an acceleration voltage of 100 kV was used for particle characterization. SEM images were obtained using a JEOL JSM - 6700F FEG scanning electron microscope.

Optical Modeling

Simulations of optical spectra for complete shells and gold semishells with a silica core and water as solvent were performed using the boundary element method (BEM).[244, 38] The edge of the semishell was described as an arc to avoid sharp corners that can cause numerical problems. The dielectric data for gold and silica were taken from Johnson and Christy [247] and Palik,[248] respectively. Convergence has been achieved with 200 (140) parameterization points for the 500 (100) nm core and 160 (120), 220 (160), 160 (160) points for 50%, 75% and 100% surface coverage, respectively.

2.3 Results and Discussion

A schematic representation of the general strategy used for the fabrication of gold semishells is shown in Fig. 2.2. The process involves two main steps: the preparation of Janus silica particles partially functionalized with amine groups and the seeded growth to obtain gold semishells. Initially, Janus particles were synthesized following the toposelective modification method.[108, 89] More specifically, 495 nm Stöber silica spheres were adsorbed onto the liquid - liquid interface of an emulsion formed by molten paraffin wax and water.[89] Once the emulsion cooled, the silica particles were locked at the interface, forming stable colloidosomes (Fig. 2.3), so that the silica surface embedded into the wax was protected from further chemical modification. The following step was the silanization of the available silica surface (Fig. 2.2, step 1), using the more volatile (3 - ethoxydimethylsilyl) propylamine, APDMES, rather than other common aminosilanes, such as (3 - aminopropyl) triethoxysilane (APTES), in order to achieve self - assembled monolayers of higher quality.[249] The silane grafting was carried out

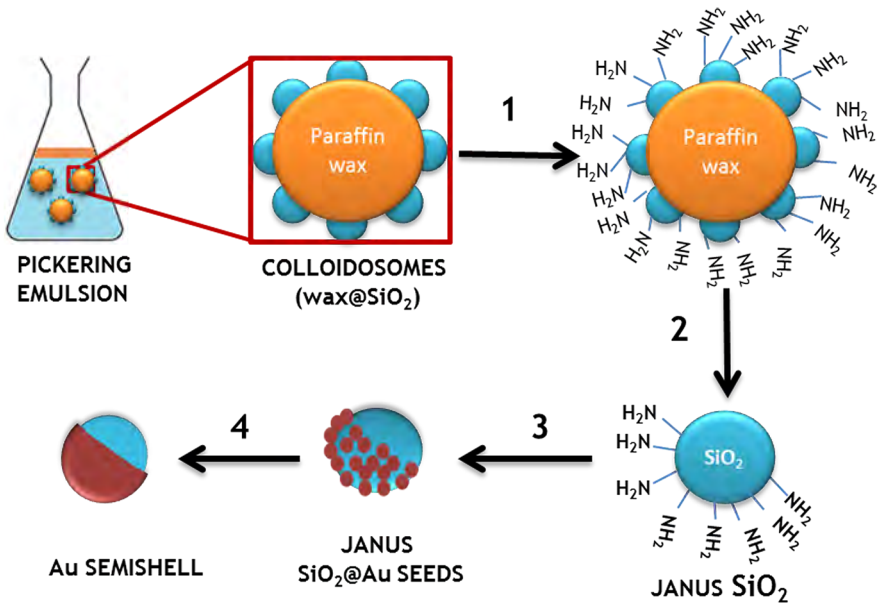

Figure 2.2. Schematic representation of the synthetic route to form gold semishells. (1) gas phase amine modification of silica particles attached to wax colloidosomes (2) dissolution of the wax and release of the Janus silica particles, (3) adsorption of gold seeds through amine groups and (4) formation of gold semishells through seeded growth.

using a solvent - free method at room temperature[108] comprising the volatilization of APDMES with bubbling N_2 and the reaction of the produced silane vapor with the dried colloidosomes deposited on a filter funnel (Fig. 2.1). This route was preferred over solution - phase silanization since it proved to have no effect on either the adhesion of the silica particles or the stability of colloidosomes, while additionally improving the efficiency of silane grafting (Fig. 2.3 E). Different chemical modification routes in solution where tested prior to selecting the gas - phase silanization. With organic solvents such as methanol, paraffin wax started melting within a few minutes, being totally dissolved in 24 h (Fig. 2.3 B - C). This process was minimized when the surface modification was carried out in an ice bath, nevertheless the quality of the functionalization was not good enough for the subsequent steps (Fig. 2.3 D). After APDMES deposition, the silica particles can be easily released by dissolving the paraffin wax with chloroform (Fig. 2.2, step 2), resulting in the formation of Janus silica particles with toposelective amine functionality.

Interestingly, the surface composition of the Janus silica particles can be tuned by adding small amounts of didodecyldimethylammonium bromide (DDAB) during the preparation of the Pickering emulsion (Fig. 2.4).[89] The cationic surfactant adsorbs strongly onto the negatively charged silica particles surface, changing the effective surface hydrophobicity and producing a deeper immersion of the silica into the wax and, therefore, increasing the three-phase contact angle of the particles at the emulsion interface. The SEM micrographs in Fig. 2.4 show selected areas on wax-silica colloidosomes synthesized in the presence of different amounts of DDAB (15-90 mg/L). It can be observed that silica particles are more deeply embedded into the wax phase at increasing DDAB concentrations. An accurate characterization would require the measurement of the contact angle of the particles at the water-wax interface. This can be indirectly performed by measuring the size of the voids that are left on the wax when the silica particles are detached during the washing step.[89] Experimentally, this measurement is not trivial, since at room temperature the samples might be affected by the electron beam and therefore the use of cryo-SEM is required. In this case, the process was even more complicated due to the small dimensions (<500 nm) of the silica particles, resulting in the formation of rather small voids. Fig. 2.3 F shows a representative cryo-SEM image from a sample obtained with a DDAB concentration of 60 mg/L. The average contact angle measured for this sample was approximately 68°, which is in agreement with the values reported by Granick et al.[89]

The preparation of gold semishells templated by Janus silica particles with toposelective amine functionality is represented in Fig. 2.2, steps 3 and 4. This approach is based on the well-known method for the growth of gold nanoshells developed at Halas' group.[243, 250] Initially, gold nanoparticles smaller than 3 nm in size were adsorbed onto the functionalized side of the Janus silica particles through a weak covalent bond with the amino groups of the aminosilane.[251] Subsequently, a continuous gold semishell was grown on the gold seeds in a multistep process through the further catalytic reduction of hydrogen tetracholoraurate $HAuCl_4$ by formaldehyde (Fig. 2.5). It was found that the sequential growth of the gold semishell was required to obtain uniform and smooth gold surfaces. Another important parameter that should be taken into account to fabricate homogeneous gold semishells was the ratio between Au^{3+} ions and Janus silica particles in each growth step. While ratios below 10^8 : 1 led to uniform gold semishells (Fig. 2.5), a greater excess of Au^{3+} ions resulted in the metal surface of the semishell being uneven and spiked,

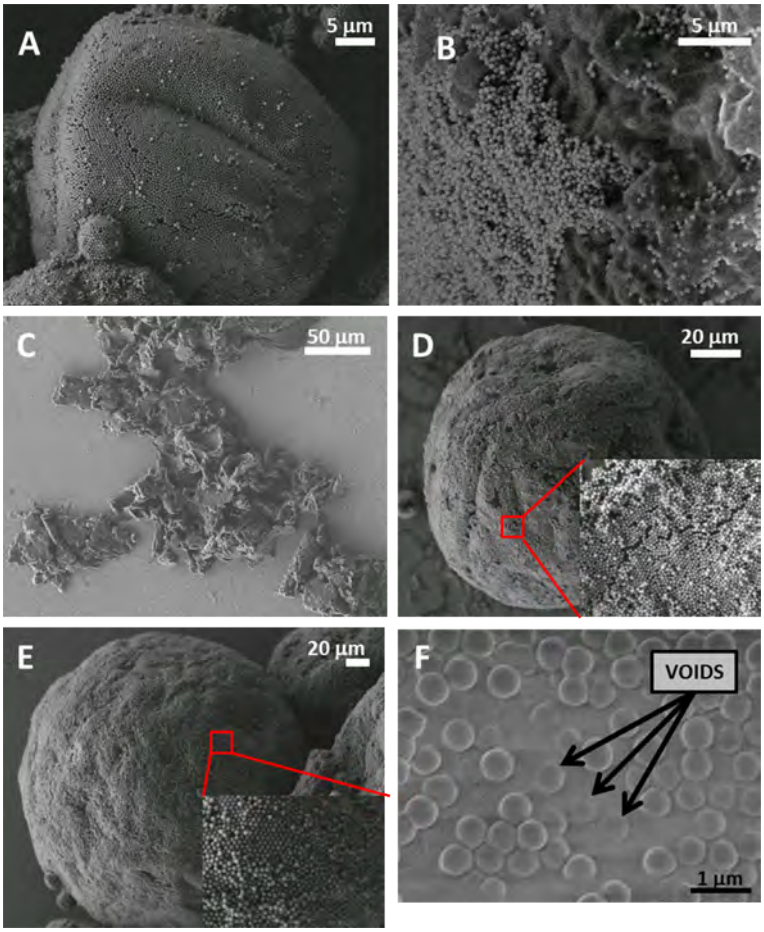

Figure 2.3. SEM micrographs of as prepared colloidosomes (A) and after silanization processes (B - E). (B and C) Chemical modification in MeOH with 3 - aminopropyltrimethoxysilane (APTMS) at room temperature for 20 min and 24 h, respectively. (D) equal to B but an ice bath. (E) Gas - phase silanization. (F) Cryo - SEM micrograph of 495 nm silica colloidosomes prepared using 60 mg/L DDAB concentration. Some voids left by the silica particles during the washing steps are indicated with arrows.

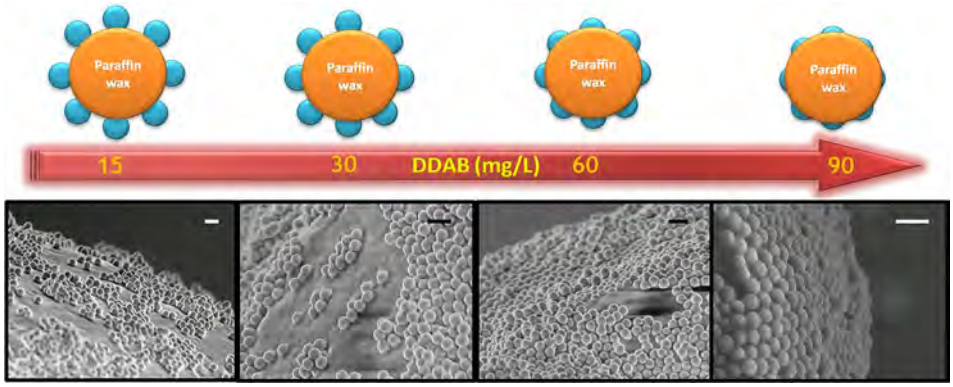

Figure 2.4. Upper panel: schematic representation of the effect of DDAB concentration on the immersion of silica particles into the wax phase. Lower panel: SEM images of the surface of colloidosomes fabricated with ca. 495 nm SiO_2 particles and different DDAB concentration: 15, 30, 60 and 90 mg/L, from left to right. All scale bars correspond to 1 μm.

and gold debris and bare silica particles were also observed, probably due to the fast reduction of the gold salt. These gold semishells sediment after a few minutes, but applying weak sonication redisperse again. The random orientation of the gold semishells on the substrate makes the morphological characterization rather difficult. In order to demonstrate the anisotropy of these plasmonic nanostructures, the silica core was dissolved using hydrofluoric acid (Section 2.2). As clearly shown in Fig. 2.5 E and F, the removal of the dielectric cores led to the formation of hollow metallic semishells. Apart from the possibility of synthesizing hollow nanostructures, another advantage of this colloidal synthetic route is that the gold semishell geometry can be controlled by tuning the concentration of DDAB and, thus, the coverage of amine functionality in the Janus silica particles, as discussed above. This is exemplified in Fig. 2.5, where SEM images are shown of gold semishells fabricated from Janus silica particles obtained with different DDAB concentrations (60 and 90 mg/L). Although the random orientation of the gold nanoshells makes comparison rather difficult, it is possible to observe that the particles fabricated using 60 mg/L DDAB (Fig. 2.5 A and B) present a higher metal coverage than those obtained using 90 mg/L DDAB (Fig. 2.5 C and D).

The mechanism of gold semishell growth is similar to that observed by Halas et al. for gold nanoshells.[250] In this multistep process, the small gold particle seeds initially attached onto the Janus silica particles grow larger and ultimately merge

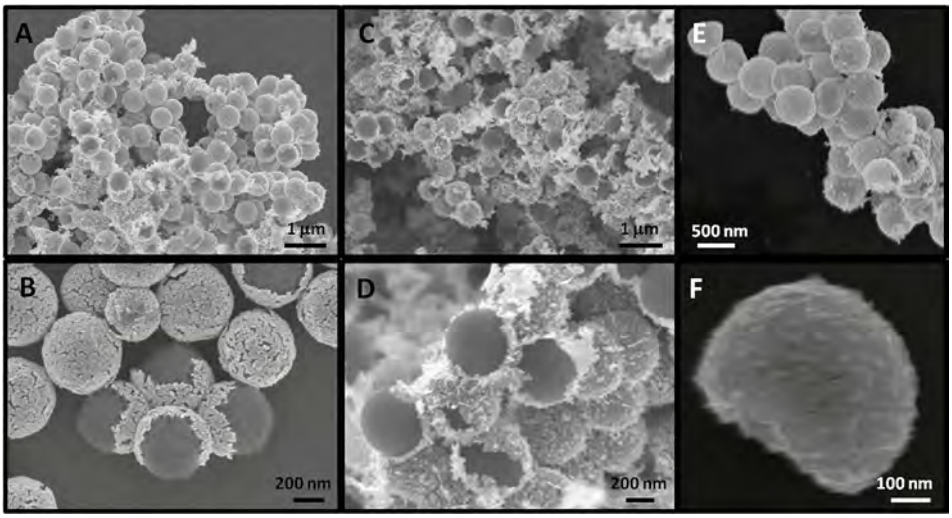

Figure 2.5. (A - D) SEM images of gold semishells obtained after six growth steps and using Janus silica particles prepared with DDAB concentrations of 60 mg / L (A, B) and 90 mg / L (C, D). (E, F) SEM images of hollow gold semishells upon etching of the silica cores (prepared with a DDAB concentration of 60 mg/L).

to form a continuous and polycrystalline gold semishell, getting darker in TEM micrographs (Fig. 2.6 A - C). This process can be monitored through vis - NIR absorption spectra measured during gold semishell growth (in six steps) as shown in Fig. 2.6 D. Initially, the surface plasmon resonance band shifts to longer wavelengths and broadens due to the growth of the gold seeds and also to the plasmon coupling that arises when the distance between metal particles on the silica surface decreases. Further reduction leads to the formation of a continuous shell and results in a shift of the surface plasmon resonance band beyond the NIR. However, these main features cannot be resolved experimentally, since the optical characterization is limited to the vis - NIR range (up to about 1400 nm) and in this region just a broad continuum band is observed. The experimental spectra of gold semishells made with 60 or 90 mg/L of DDAB are similar in that a broad plasmon band in the analyzed region is observed (vis - NIR).

The optical properties of the obtained gold semishells were analyzed through simulations based on the boundary element method (BEM) for numerical resolution of Maxwell's equations.[244, 38] Since the core size and shell thickness are the main parameters affecting the surface plasmon energies of gold nanoshells,[252, 206, 211]

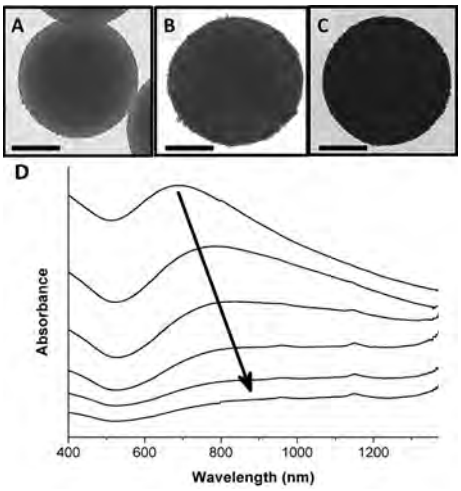

Figure 2.6. (A - C) TEM images of Janus silica particles after the first, third and fifth growth step, showing increased gold surface coverage. D) Evolution of the vis - NIR spectra during sequential growth (in six steps) of gold seeds attached to 495 nm Janus silica particles (60 mg / L DDAB) to obtain gold semishells. The spectra were shifted to facilitate comparison. All scale bars correspond to 200 nm.

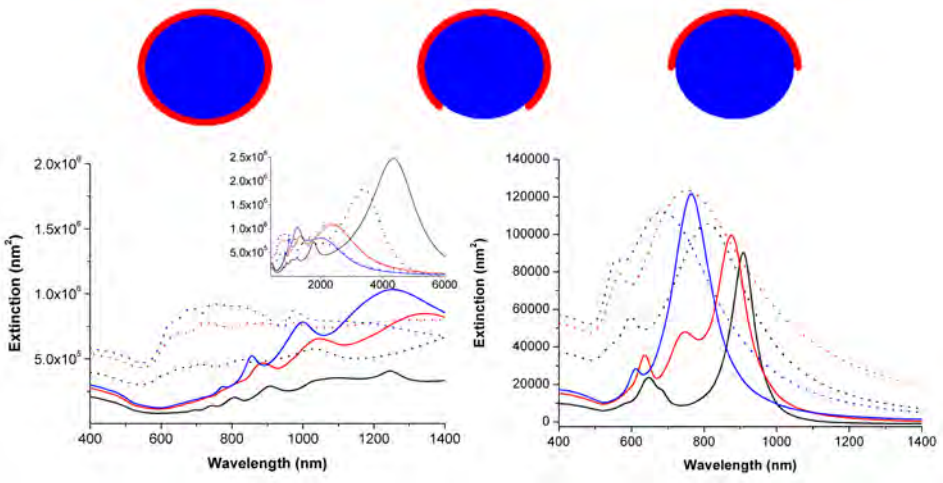

Figure 2.7. Calculated extinction spectra for Au semishells with 50% (black) and 75% (red) metal coverage, and nanoshells (complete shell, blue). The thickness of the gold shells was 10 nm (solid lines) and 30 nm (dotted lines). The inset shows the same spectra for an extended wavelength range, up to 6000 nm. The diameter of the silica cores was 500 nm (on the left) and 100 nm (on the right). On top the geometrical models employed in the simulations.

different morphologies were modeled varying these parameters as well as surface coverage. The geometrical models used for the simulations are shown in Fig. 2.7. The extinction cross sections obtained for gold semishells with silica cores of 500 nm in diameter, metal surface coverage of 50% and 75% and gold - shell thicknesses of 10 and 30 nm are plotted in Fig. 2.7, left spectra. For comparison, the calculated spectra for gold nanoshells (100% surface coverage) are also included. The most important point to note is that the loss of symmetry (from nanoshell to semishell) produces a strong red - shift of the main plasmon bands, this effect being stronger for lower metal surface coverage. Due to the relatively large dimension of the silica core (500 nm) and the thin gold shell, the main plasmon band in the semishell, arising from transverse dipolar resonances (perpendicular to the axis of symmetry, Fig. 2.8), is located beyond the NIR (in the far IR region for 50% coverage). The optical features observed in the vis - NIR region (broad band) seem to correspond to a less intense axial dipolar mode (resonances parallel to the axis of symmetry and located around 1100 nm, Fig. 2.8) and several multipolar plasmon modes. These simulations are in good agreement with the broad bands obtained experimentally (Fig. 2.6) and show that the main plasmon band could be shifted within the NIR (region of interest for biomedical applications) by using smaller Janus silica particles as templates. This was confirmed by calculations for shells and semishells comprising 100 nm silica cores (Fig. 2.7, right panel), which showed that the tranverse dipolar modes are located in that case between 750 and 950 nm, depending on surface coverage and gold shell thickness.

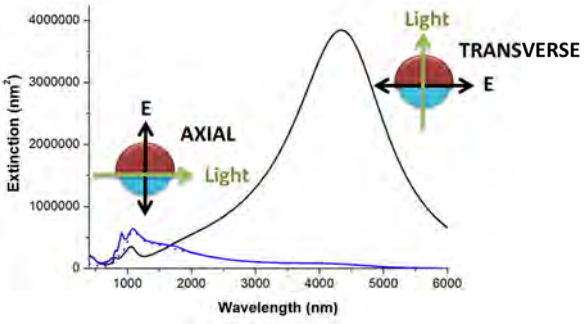

Figure 2.8. BEM simulations for 500 nm gold semishells with a metal layer of 10 nm. (black) Extinction spectrum calculated with the incident light polarized parallel to the axis of symmetry showing the transverse modes. (blue) Extinction spectrum calculated with the incident light polarized perpendicular to the axis of symmetry showing the axial modes. Full line was calculated with multipoles up to $l = 5$, whereas dashed line correspond to $l = 1$ (only dipoles).

2.4 Conclusions

A versatile and easily scalable colloidal strategy for the synthesis of gold semishells, based on using Janus silica particles as templates to grow uniform metallic shells has been developed. Preliminary results show that this method enables to control the geometry of the plasmonic structures by tuning the Janus silica particle composition through variation of the concentration of the surfactant didodecyldimethylammonium bromide (DDAB), which modulates the penetration of the silica particles at the wax - water interface. Additionally, the silica cores can be readily etched away, leading to the fabrication of hollow gold semishells. The simulation of the optical properties using the boundary element method (BEM) has shown that the main optical features in the case of gold semishells with 500 nm silica cores are located beyond the NIR range and therefore cannot be observed experimentally. Additionally their Janus behaviour might be exploited to form monolayers of particles using a Langmuir - Blodgett trough, with the gold parts close together, thus with potential applications on surface enhanced Raman scattering (SERS) detection. Simulations also predict that it is possible to fabricate gold semishells with optical properties in the NIR region by simply decreasing the core size to 100 nm, nevertheless the method described here gives not such high quality semishells with this small core size.

Chapter 3

Radial Growth of Plasmon Coupled Gold Nanowires on Colloidal Templates

Abstract

The library of plasmonic nanosystems keeps expanding with novel structures with the potential to provide new solutions to old problems in science and technology. Here is reported the synthesis of a novel plasmonic system based on the growth of gold nanowires radially branching from the surface of silica particles. The nanowires length could be controlled by tuning the molar ratio between metal salt and surface - grafted seeds. Electron microscopy characterization revealed that the obtained one - dimensional nanoparticles are polycrystalline but uniformly distributed on the spherical template. The length of the nanowires in turn determines the optical response of the metallodielectric particles, so that longer wires display red - shifted longitudinal plasmon bands. Accurate theoretical modeling of these complex objects revealed that the densely organized nanowires display intrinsically coupled plasmon modes that can be selectively decoupled upon detachment of the nanowires from the surface of the colloidal silica template.

3.1 Introduction

The research on the optical properties of plasmonic nanoparticles is progressively shifting from individual particles to ensembles.[253, 254] The plasmon hybridization model to explain optical interactions between metallic nanoparticles,[207] opened new possibilities not only at the level of theoretical understanding of complex optical phenomena, but also as a guide in the rapidly developing field of applied plasmonics.[255] Plasmon coupling is especially interesting in anisotropic nanoparticles. Gold nanorods, for example, support longitudinal and transverse plasmon resonances, which shift depending on mutual orientation of the nanoparticles.[256] Thus, tip - to - tip arrangements lead to red shifts of the longitudinal surface plasmon band whereas side - to - side assembly induces blue shifts. Geometry - dependent plasmon modulation is in fact an interesting property in the design of platforms for optical biosensing.[223, 257]

Large electromagnetic field localization is the main prerequisite for surface enhanced Raman scattering (SERS) spectroscopy, and this is typically achievable on plasmonic supercrystals composed of anisotropic nanoparticles.[258, 259, 260] Although, extended supercrystals of anisotropic nanoparticles will find application in chip - based, point - of - care devices, they are not suitable for use in complex biological media in suspension (e.g. in vivo). Thus, a large scientific and technological effort goes into the production of 3D platforms based on standing nanorod arrays that are stable in colloidal phase.[21] Naturally, the most attractive strategy in achieving such a system is the use of pre - made colloidal particles as building blocks for bottom - up self - assembly into complex 3D clusters with controlled size, shape and even interparticle distance.[261] Although progress has been made toward this, the self - assembly approach for standing rods arrays on 3D clusters remains a challenging task.

To overcome the inherent difficulties in controlled self - assembly we developed an alternative strategy for the synthesis of anisotropic nanoparticles in the side - to - side mode, directly on colloidal templates. Recent work by Chen and co - workers make such strategy feasible.[262] These authors demonstrated a relatively simple protocol for the synthesis of forest - like assemblies of gold nanowires on glass substrates. Our research group recently showed that such gold nanowire forests constitute a promising architecture as SERS substrate.[263]

We propose here a novel type of plasmonic architecture consisting of a dielectric core covered with radially distributed gold nanorods / nanowires branching out from the silica surface. The radial growth of nanoparticles is based on one - directional seeded growth from covalently attached gold seeds (Fig. 3.1). The molar ratio between seeds and metal precursor determines the length of the nanoparticles, which in turn affects the plasmon response. Theoretical modeling of this multi - particle system points toward strong plasmon coupling between arrayed wires.

3.2 Experimental Section

Chemicals

Ammonium hydroxide (NH_4OH, 28%), tetraethylorthosilicate (TEOS, 98%), 3 - aminopropyl (triethoxysilane) (APTES), sodium citrate tribasic dihydrate, tetrachloroauric acid ($HAuCl_4 \cdot 3H_2O$, 99%), sodium borohydride ($NaBH_4$), 4 - mercaptobenzoic acid (4 - MBA, 99%), and L - ascorbic acid were purchased from Sigma Aldrich. Absolute ethanol (Scharlab) and Milli - Q water were used as solvents. All the chemicals were used as received from the supplier.

Synthesis of gold seeds

To an aqueous solution (20 mL) containing $HAuCl_4$ (0.125 mM) and sodium citrate (0.25 mM), $NaBH_4$ (0.3 mL, 10 mM) was added under vigorous stirring.[264] The solution was further gently stirred to decompose remaining borohydride. The as prepared gold spheres have an average diameter of 4.3 ± 0.9 nm.

Synthesis of silica spheres

Silica nanoparticles were prepared following the Stöber method.[265] Briefly, TEOS (0.75 mL, 3.35 mmol) was added dropwise to 25 mL of absolute ethanol containing ammonia solution (2.0 mL, 30 wt%) and Milli - Q water (1.13 mL) under vigorous stirring. After 1 h the solution turned from colorless to opaque white and then it was gently stirred overnight. Silica spheres were collected by centrifugation and directly used in subsequent steps. The average diameter of the silica particles was 264 ± 9 nm.

Functionalization of silica spheres with APTES

Silica particles were redispersed in a mixture containing ethanol (25 mL) and Milli-Q water (1.3 mL). To this solution was added in turn NH_4OH (0.125 mL) and APTES (0.02 mL). The solution was vigorously stirred for 2 h at room temperature and subsequently for 1 h at 70 °C to complete the covalent bonding of the organosilane molecules to the silica surface. The particles were finally centrifuged three times (2000 rpm, 8 min) and redispersed in ethanol (10 mL). The final concentration of silica was estimated to be $9.4 \cdot 10^{11}$ particles / mL.

Attachment of gold seeds on the silica spheres

Amino-functionalized silica nanoparticles (0.346 mL) were added to the solution of as-prepared gold seeds (10 mL). The solution was stirred for 2 h at room temperature. The particles were centrifuged three times (2000 rpm, 10 min) to remove excess of gold seeds. The pinkish precipitate was redispersed in Milli-Q water (1.2 mL).

Growth of gold nanowires on silica spheres

Different amounts of Au-primed silica particles (0.60, 0.55, 0.50 mL) were added to an ethanol / water solution (10 mL, 3 : 1 V / V) containing 4-MBA (0.275 mM) and $HAuCl_4$ (0.825 mM). After 15 s of gently stirring, L-ascorbic acid (0.488 mL, 42 mM) was added and the reaction mixture was gently stirred for 5 s. The solution was left undisturbed for 10 min, as the color of the solution changed from yellowish to colorless and further to bluish. The particles were centrifuged three times (2000 rpm, 8 min) redispersed in ethanol (2 mL) and further characterized.

Instrumentation

UV / Vis / NIR spectra were collected using a scanning spectrophotometer Varian, Cary 5000. Transmission electron microscopy (TEM) images were collected with a JEOL JEM-1400PLUS, operating at 120 kV. HRTEM images were collected with a JEOL JEM 2100F field emission gun electron microscope, operating at 200 kV. Scanning electron microscopy (SEM) images were obtained with a Helios NanoLab 600i Dual Beam FIB / FE-SEM (FEI, USA), operating at 10 kV.

Optical Modeling

Spectral and near field enhancement simulations were carried out in colaboration with *Departamento de Teoría de la Señal y Comunicaciones* (University of Vigo), using a numerical method based on the surface integral equation - method of moments (SIE - MoM) formulation (M3 solver).[35] With this methodology, the metallic nanostructures are replaced by equivalent electric and magnetic currents placed over the particle boundary surfaces and interfaces. Through the integro - differential Stratton - Chu representation formulas and the boundary conditions for the total fields are derived a set of SIEs for the unknown equivalent currents. These SIEs are subsequently discretized by applying a Galerkin MoM procedure in terms of a set of basis and testing functions, leading to a dense $N \times N$ matrix system of linear equations (being N the number of basis functions used to expand the unknown equivalent currents). For the realistic simulation of the large - scale plasmonic systems considered here, SIE - MoM was expedited via the multilevel fast multipole algorithm - fast Fourier transform (MLFMA - FFT),[266] providing a high algorithmic efficiency – computational cost of O (NlogN) – along with high - scalability via parallelization using multicore computer clusters. The simulations were carried out on a workstation with four 8 - core Intel Xeon E7 - 4820 18 MB L3 cache processors at 2 GHz. A high surface mesh density was considered using 855,600 basis functions both for the radially distributed and the randomly distributed nanowire systems, with an edge size ranging from 1 / 96 wavelengths for the shortest simulated wavelength to 1 / 311 for the longest. Otherwise, a relative error norm of 10^{-5} was considered to halt the Krylov iterative solver. Considering the above, the computation times per wavelength ranged from 145 to 617 seconds, while the memory use ranged from 5.3 to 21.4 GB.

3.3 Results and Discussion

3.3.1 Growth of nanowires on silica beads

Silica particles with an average diameter of 264 ± 9 nm were prepared according to the well-established Stöber method.[265] This process allows the production of large quantities of monodisperse silica spheres with a wide range of particle sizes. It is based on the hydrolysis of an alkyl silicate such as TEOS and the subsequent condensation of the silicic acid in alcoholic solutions, catalysed in the presence of a base such as ammonia. The silica spheres were functionalized with the aminosilane APTES using a variation of the method developed at Halas' group.[250, 243] Citrate-stabilized gold nanoparticles [264] with an average diameter of 4.3 ± 0.9 nm (Fig. 3.2 A) were then adsorbed onto the amine functional groups at the silica surface. The role of APTES as a linker is thus a crucial ingredient to achieve a homogenous distribution of the gold seeds. In all experiments were used excess of gold seeds to ensure maximal surface coverage; unattached gold seeds were removed by centrifugation.

Figure 3.1. Schematic representation of the experimental strategy for radial growth of gold nanowires on a silica template. Gold seeds are first attached to amine functionalized silica particles SiO_2 @ NH_2. Metal nanowires grow from the seeds via reduction with L-ascorbic acid (AA) in the presence of 4-mercaptobenzoic acid (4-MBA) as a stabilizer.

The synthetic methodology described here presents two major challenges: (1) the formation of gold nanowires on spherical substrates in a colloidal phase and (2) tuning the length of the resulting nanowires. As reported by He et al. when explaining the growth mechanism of gold nanowires over macroscopic susbstrates [262], one-dimensional nanowire growth is strongly affected by the interaction of 4-MBA with the growing gold surface, such that it is favored by a higher deposition rate of the metal and lower diffusion rate of the ligand. As these two factors correlate with the respective concentrations, the molar ratio between $AuCl_4^-$ and 4-MBA should be sufficiently high $\left(AuCl_4^- / 4-\mathrm{MBA} = 3\right)$ to ensure anisotropic

growth. It has been reported that the final length of the nanowires grown on the macroscopic surface can be readily controlled by simply tuning the reduction time. Thus, removal of the substrate from the growth solution, typically 15 min after reduction commenced, produced 1 μm long nanowires.[262, 263] In the present system however, the substrate is not a macroscopic glass, but a colloid which therefore cannot be abruptly removed from the growth solution. Thus, the length of the nanowires was controlled in a similar fashion to the well-known seeded-growth method, by simply tuning the molar ratio between gold salt and gold seed-coated silica particles, while keeping a large excess of 4-MBA to ensure anisotropic growth and nanowire formation. A systematic study was carried out in which was varied the concentration of the gold-primed SiO_2 (0.095, 0.086, 0.078 nM) but maintained the concentration of $HAuCl_4$ (0.825 mM), 4-MBA (0.275 mM) and L-ascorbic acid (2 mM) constant. Upon extended storage of the samples at 4 °C, no sign was observed of wire detachment from the silica surface.

3.3.2 Morphological Characterization

With increasing the ratio between metal salt and silica-supported seeds, the nanowires were found to grow progressively longer, while their width remained constant (6.1 ± 0.8 nm). The length of the resulting nanowires was estimated by analysis of TEM images as: 38 ± 11 nm, 114 ± 20 nm, 207 ± 9 nm, (hereafter named as short, intermediate and long nanowires), for gold-primed SiO_2 concentrations of 0.095, 0.086, and 0.078 nM, respectively (Fig. 3.2 B-D). The capping molecules (4-MBA) form a compact layer on the metal surface during nanowire growth, thereby ensuring the separation between the nanowires.[263] It is therefore reasonable to assume that 4-MBA acts as a shape-directing agent, inducing anisotropic growth in radial fashion.

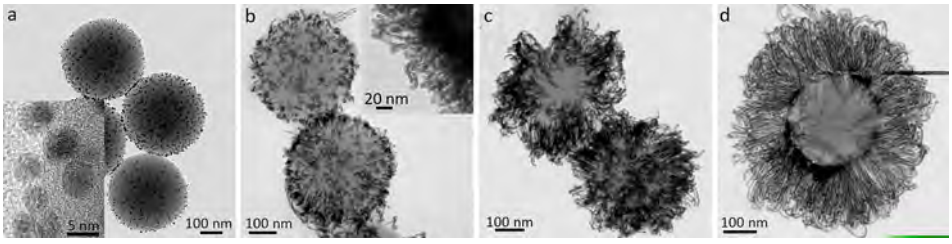

Figure 3.2. TEM characterization of silica-gold metallodielectric colloids. Silica particles coated with gold seeds (A) and short (B), intermediate (C), and long (D) nanowires.

Interestingly, for long nanowires the TEM images seem to indicate that the central part of the silica particles remains partly uncovered (Fig. 3.2 D). This is likely to be an artifact derived from collapse of the nanowires upon drying. The short and intermediate wires not only distribute homogenously but also form a shell where such a collapsing effect is not observed, due to optimal surface coverage. To further visualize full coverage of the silica nanoparticles SEM characterization was carried out, which confirms uniform coverage and radial distribution of the nanowires (Fig. 3.3 A), which stand on the spherical substrate even after solvent evaporation. It is however interesting to note that in all cases the nanowires display a certain degree of twisting, i.e. they are not perfectly straight.

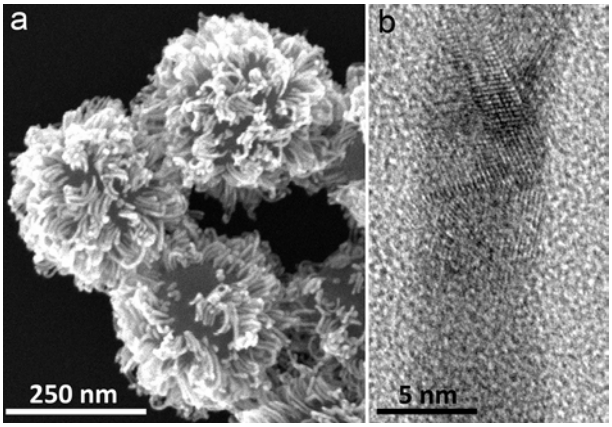

Figure 3.3. (A) SEM image of intermediate nanowires homogenously distributed on silica beads, with radial orientation but twisted morphology. (B) HRTEM image of a single nanowire showing multiple twin planes and a polycrystalline structure.

This particular growth mechanism is based on the relatively fast kinetics of metal reduction. In the conventional methodologies the degree of anisotropy has been reported to increase with decreasing the rate of metal reduction.[267] For example, the growth of single crystal gold nanorods is completed within 3 hours,[268] whereas over 5 hours are needed to complete the formation of oleylamine - capped nanowires.[269] In contrast, in the present system the reaction is completed within only 10 minutes. Fast kinetics is most likely an essential factor in determining the polycrystalline nature of the obtained nanowires. Multiple twin planes with random lattice orientations can be observed in Fig 3.3 B, which ultimately lead to the above mentioned twisted morphologies. More accurate control of the growth process would be required to obtain single crystal nanowires, which would not

only form more uniform composite structures but are also relevant in the design of optoelectronic devices.[270]

3.3.3 Optical Characterization

The high aspect ratio and the side-to-side mutual orientation of the nanowires determine the overall optical response of the composite colloids. The colloidal dispersion of silica particles covered with gold seeds exhibits a weak plasmon band centered at 506 nm, with enhanced Rayleigh scattering due to the silica spheres (Fig. 3.4 A, grey line). In contrast, broad plasmon bands emerge at 740 and 960 nm upon growth of short and intermediate nanowires, respectively (Fig. 3.4 A, blue and red lines). For long nanowires (Fig. 3.4 A, black line) the plasmon band splits to produce two modes at 545 nm (transverse) and at >1300 nm (longitudinal). This trend of red-shifting plasmon band with increasing nanowire length is in accordance with the usual observations in gold nanorods, but in this system the overall optical properties are dominated by the radial distribution of the nanowires in side-to-side orientation, leading to much broader plasmon bands. The forest-like growth of the nanowires leads to strong coupling of the plasmon bands and therefore it is expected that they should differ from those of the free nanowires in solution. To qualitatively verify this assumption, the wires were detached from the surface of the silica particles through a short sonication process (5 min), and redispersed them in pure ethanol. As shown in Fig. 3.4 B, in the long nanowires the transverse plasmon band blue-shifted (from 545 to 507 nm) and sharpened, while the longitudinal plasmon band seems to further shift toward the near-IR, as indicated by a valley at 700 nm. TEM characterization of the samples after detachment revealed randomly distributed nanowires (Fig. 3.4-3). In the case of intermediate nanowires two bands are clearly visible, at 507 and ~ 1300 nm (Fig. 3.4 B-red), again indicating redispersion of individual nanowires. For the short nanowires however, the spectrum did not change significantly suggesting that the side-to-side orientation is somehow preserved after detachment. TEM characterization confirms the presence of nanowire bundles, more frequently for the shorter nanowires, in agreement with the optical measurements. Presumably the strong interaction between the small wires via stabilizing agent does not allow them to fully disperse. Longer nanowires, however, disperse better in ethanol since exhibit many surface defects facilitating solvation by the solvent molecules.[271]

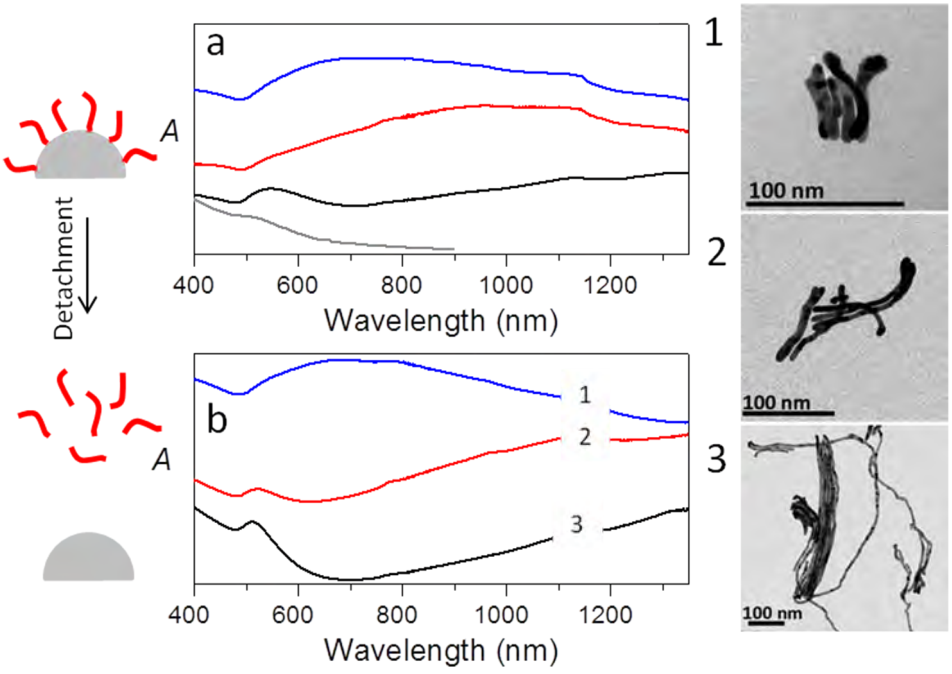

Figure 3.4. Optical properties of the radially distributed gold nanowires and randomly distributed in solution. (A) UV - Vis - NIR spectra of silica nanoparticles coated with gold seeds (grey), short (blue), intermediate (red) and long nanowires (black). (B) UV - Vis - NIR spectra of the samples detached from the silica substrate. (Right) TEM images of the wires after detachment for short (1), intermediate (2), and long (3) nanowires.

3.3.4 Theoretical modeling

To further correlate the structural complexity of these systems with their optical properties, the extinction spectra of the composite particles comprising intermediate nanowires radially distributed on the surface of silica spheres were simulated. Although conventional simulation approaches (e.g. FDTD, DDA, BEM) require large calculation costs to provide reliable optical information about such complex objects, a recently reported methodology was employed, which implements accelerated calculations based on surface integral equations with the method of moments formulation and the multilevel fast multipole algorithm.[35] The SIE - MoM methodology brings about important advantages with respect to volumetric approaches, namely, a significantly smaller computational cost (as only the particle boundaries and interfaces must be parameterized) and larger stability, particularly when dealing with resonant metallic response (as the singular behavior of fields is analytically handled by the Green's function and its derivatives.) The computational power of this approach allows to model the particles in their full complexity. These simulations are focused on the intermediate nanowires, since their dimensions estimated from TEM analysis in dried state better represent real dimensions in the solution as compared to short and long wires. The input width, length and the silica core diameter were 6, 100 and 260 nm, respectively. A certain degree of twisting was implemented to better represent the real system and a certain degree of polydispersity in size (± 1 nm in diameter and ± 19 nm in length) as well as in shape (four different nanowire models) was also considered. Over 1000 nanowires were used both in the radially and the randomly distributed systems. Otherwise, a large number of different orientations were simulated and averaged for the radially distributed system in order to increase the polydispersity effect. The silica sphere was not parameterized, as it was found through simulation that its contribution to the spectra is negligible compared to that of the nanowires. The so - calculated extinction spectra of radially distributed nanowires on silica exhibited two plasmon bands at 516 and 900 nm, closely resembling the experimental spectrum (cf. Figs. 3.5 A and 3.4 A - red). On the other hand, the spectrum of free nanowires exhibits a transverse plasmon band at 520 nm and a longitudinal plasmon band significantly red - shifted (> 1300 nm) as compared to radially - distributed nanowires.

These results are in strikingly good agreement with the experimental observations and again point toward strong plasmon coupling in the dense radial nanowire ar-

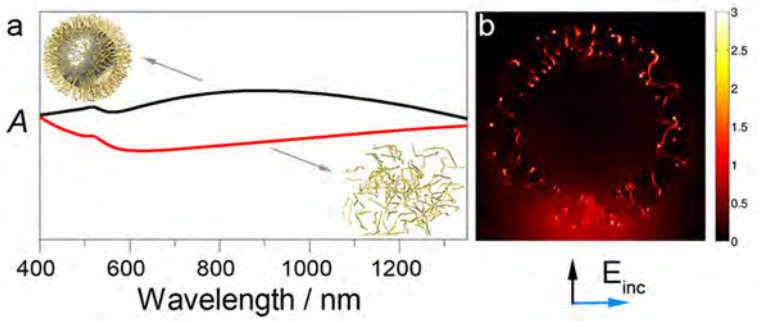

Figure 3.5. Optical modeling of gold nanowires. (A) Simulated extinction spectra of gold nanowires radially distributed on the silica surface (black) and randomly distributed in water (red). The insets show the 3D models used for the simulations, in both cases containing ca. 1000 nanowires. (B) Calculated near field enhancement map ($\lambda = 785$ nm) of the radially distributed nanowires, showing the presence of numerous hot spots.

rays. To further visualize the presence of plasmon coupling and hot spot formation, the electric near field enhancement was calculated (Fig. 3.5 B), which indeed shows a large number of hot spots randomly distributed in the region occupied by the nanowires, around the silica template colloid. Although large near field enhancements up to 100 were found in selected spots, Fig. 3.5 B shows the distribution of more moderate field enhancements for better visualization. Overall, the combination of the optical features and hair - like morphology provides an exciting scenario for the development of new materials with potential in biosensing.

3.4 Conclusions

A new type of plasmonic metallodielectric nanoparticles, comprising radially distributed gold nanowires branching out from a colloidal template have been developed. The length of the nanowires, ranging from 40 to 200 nm, was controlled by simply changing the molar ratio between seeds (gold - primed silica nanoparticles) and metal salt. The optical properties show significant differences between nanowires that are radially distributed and those free in solution, indicating strong plasmon coupling, which was confirmed by theoretical modeling. This method opens up a new synthetic pathway in colloidal nanofabrication. Here is shown that growth of plasmonic nanowire forests is not limited to solid substrates,[262, 263] but can also be grown on amino - functionalized colloidal particles. These particles offer

new opportunities toward applications in fields such as (photo) catalysis.[272] From a general perspective, radially distributed anisotropic nanoparticles are also highly appealing materials for the development of a new class of conductive substrates or biosensors with intriguing optical properties.[273] An interesting extension of this work would comprise the synthesis of Janus like silica particles, half covered with gold nanowire forests, to take advantage of the Janus geometry and be able to control their self - assembly over surfaces [19] and improve their SERS capabilities (work in progress).

Chapter 4

Mesoporous Thin Film Sandwiches as Templates for Branching in Gold Nanoparticles

Abstract

The preparation of new composite materials by combination of different components is a popular strategy that leads to either multifunctionality or even to novel properties in one single structure. An attractive combination comprises mesoporous thin films and metal nanoparticles, which has raised interest in various fields such as catalysis, sensing or optics. We introduce in this chapter a composite material comprising gold nanospheres located at the interface between two mesoporous films with different pore sizes. This configuration allows us to grow spikes on the metal particles, using the mesopore network as a template. The resulting nanostructures were characterized by TEM, SEM, environmental ellipsometric porosimetry (EEP) and two - dimensional small angle X - ray scattering (2D - SAXS).

4.1 Introduction

Oxide mesoporous materials have experienced a great development since their discovery in the 1990s. Advances in colloid chemistry and evaporation - induced self - assembly (EISA)[71] allow the production of a wide variety of mesoporous oxide structures with tunable pore size and organization.[274, 275, 276, 64] In particular, the preparation of mesoporous materials as thin films (mesoporous thin films or MTFs), opens up the possibility to create novel systems with not only the usual advantages of these materials (controlled pore size, shape, composition, high surface area or surface modification), but also special optical properties and a substrate as support.[276] The presence of a substrate facilitates real world applications as catalysts, in solar cells, insulators, batteries, sensors or photonics among others.[64]

Composite materials made of MTFs containing metallic nanoparticles, specially gold and silver, are of high interest due to the combination of the structural properties of the thin films with the optical properties of the metal particles, namely localized surface plasmon resonances (LSPRs) and high electric field enhancement at the nanoparticle surface under illumination. Examples include a SERS - selective sensor for the detection of the dye rhodamine 6G, comprising a mesoporous silica film containing 5 nm silver nanoparticles patterned by hard X - rays, which induced at the same time formation of the particles and removal of the organic template.[277] More recently, our group reported a SERS sensor based on gold nanoparticles deposited under a mesoporous film, so that the pore structure could be used as a molecular sieve.[278]

The system described here is the continuation of the project started by Dr. Angelomé in our group.[279, 280] Basically it consisted in the preparation of composite materials containing a sub - monolayer of gold particles with different shapes, covered with a MTF, to grow then gold branches over these nanoparticles through a seeded growth process. The aim of the work described in this chapter, in colaboration with Dr. Angelomé, is the preparation of Janus nanoparticles within a mesoporous film sandwich with different pore sizes acting as planar masks (Section 1.5). The system comprises two dissimilar films, made of silica and titania and fabricated using different templates (CTAB, Brij58, F127). During the fabrication, 60 nm gold spheres were loaded in between both MTFs and subsequently gold spikes were grown from these metal nanoparticles through the big F127 pores under different conditions. Characterization of the system demonstrates a high

porosity, so we expect that these structures can be used as SERS sensors as well as catalysts with higher activity than composite materials where nanoparticles are directly attached to the substrate.

4.2 Experimental Section

Chemicals

All reactants were supplied by Sigma and used without further purification unless otherwise indicated. Tetrachloroauric acid ($HAuCl_4 \cdot 3H_2O$, 99%), sodium citrate tribasic dihydrate (98%), hexadecyltrimethylammonium bromide (CTAB), poly (vinylpyrrolidone) (PVP, $M_w = 40$ kg / mol) L - Ascorbic acid (L - AA, 99%), tetraethylorthosilicate (TEOS, 98%), titanium tetrachloride (Merck), F127, Brij58 (Merck), silver nitrate (99%), hydrochloric acid (Panreac, 37%). Absolute ethanol (Scharlab) and Milli - Q water were used as solvents.

Preparation of 60 nm gold spheres

Gold seeds of 15 nm were synthesized by means of the well - known Turkevich method and were used without further purification.[281] Using a seeded growth process, these particles were grown up to ca. 60 nm, in the presence of cetyltrimethylammonium bromide (CTAB).[282] The resulting spheres were transferred to ethanol using PVP[283] by centrifuging 50 mL of CTAB particles at 4000 rpm for 25 min and redispersion in 40 mL of water. Then 10 mL of the PVP solution (60 molecules / nm^2) were added dropwise, stirring the mixture overnight. The modified particles were centrifuged at 4000 rpm for 25 min, and redispersed in 25 mL of ethanol. Then the particles were centrifuged under the same conditions and redispersed in 5 mL of supernatant.

Preparation of mesoporous thin films

Silica and titania mesoporous thin films were prepared by spin - coating on top of glass slides or silicon wafers. Silicon oxide films templated with CTAB (SC), Brij58 (SB) or F127 (SF) were spinned at 4000 rpm using 125 μL of solution (see below); whereas titania films templated with Brij58 (TB) or F127 (TF) were prepared at

6000 rpm using 50μL of solution (diluted 2 : 1 in ethanol at 40 °C for decreasing its viscosity). The detailed composition of film precursor solutions was previously reported.[284] For silica films, solutions comprised of TEOS : EtOH : template : H_2O: HCl with a 1 : 20 : 0.1 : 5 : 0.004 molar ratio for CTAB, 1 : 40 :0.05 : 10 : 0.008 for Brij58, and 1 : 40 : 0.005 : 10 : 0.008 for F127 were prepared. These solutions were aged for 72 hours at room temperature prior to use. For titania films, solutions containing $TiCl_4$: EtOH : template : H_2O, with a 1 : 40 : 0.05 : 10 molar ratio for Brij58, and 1 : 40 : 0.005 : 10 for F127 were employed with no aging. After spin - coating the films were stored in 50% relative humidity containers (prepared with $Ca(NO_3)_2$ water saturated solutions) for 30 min. The films were thermally treated for 30 min at 60 °C, then the same time at 120 °C, followed by a final step of 2 h at 200 °C.

Then the films were covered with particles, *vide infra*, and a second mesoporous film was spin - coated. After thermal treatment, the template was removed by immersing the films in ethanol for 3 days.

Attachment of the particles

100 μL of the 60 nm gold spheres dispersed in ethanol ([Au] $\sim$ 2.5 mM) were spin - coated over the films at 6000 rpm for $\sim$ 1 second. The process was repeated one more time, with no aparent aggregation.

Growth of gold branches

Two different approaches were employed to grow spikes on the gold particles. The first conditions (named as *P*) comprised the immersion for 2 h (3 times) of the glasses with deposited mesoporous films inside plastic tubes containing 5 mL of growth solution $\big([\mathrm{Au}] = 6.25 \cdot 10^{-5}\,\mathrm{M}$, $[\mathrm{CTAB}] = 30\,[\mathrm{Au}]$, $[\mathrm{AA}] = 16\,[\mathrm{Au}]\big)$. L - ascorbic acid (AA) was added after aging the Au : CTAB mixture for 1 h, prior to introducing the glasses. The second conditions (named as *R*) implied one growth step of 2 h using the following growth solution: [Au] = 0.5 mM, [CTAB] = 0.1 M, [HCl] = 19 mM, [$AgNO_3$] = 0.12mM, and[AA] = 0.8 mM.

TEM grid preparation

Tthe TEM grid was first placed over a silicon oxide substrate. Then a drop of ethanol was casted over the grid, covering it totally. Thereafter the film was

scratched with a blade and put in contact with the ethanol drop to be finally deposited on the grid.

Instrumentation

A JEOL JEM 1400F transmission electron microscope operating at an acceleration voltage of 120 kV and a Zeiss Supra 40 scanning electron microscope operating at 3.0 kV were used for particle characterization.

UV - vis spectra were measured with a HP 8453 UV - vis diode - array spectrophotometer.

The mesostructure of the films was characterized using 2D - SAXS at the D11A - SAXS line at the Laboratório Nacional de Luz Síncrotron (LNLS), Campinas, SP, Brazil, using $\lambda = 1.608$ Å and a sample - detector distance of 650 mm. Image plates were used as detectors (4 or 90° incidence).

The optical properties of SiO_2 and TiO_2 thin films were measured in ambient conditions (RH $\sim 50\%$; $\sim 25°C$) using a Spectroscopic Ellipsometer (SE SOPRA GES5A). From the ellipsometric parameters Ψ and Δ the film thickness and the refractive index were deduced.[285]

Water adsorption - desorption isotherms (at 25 °C) of a nitrogen flux containing variable water vapor quantities (P/P^0, P^0 being the saturation water vapor pressure at 25 °C) were measured by Environmental Ellipsometric Porosimetry (EEP SOPRA GES5A). The experimental device is based on coupling a pressure controlled chamber and a spectroscopic ellipsometer. The volume of water adsorbed at each P/P^0 value is determined by modeling the obtained refractive index according to a three - component (water - air - oxide) effective medium approximation, from which the porosity of the film can be estimated. From the adsorption and desorption isotherms, we can determine the diameter of the pore and the diameter of the neck, respectively.

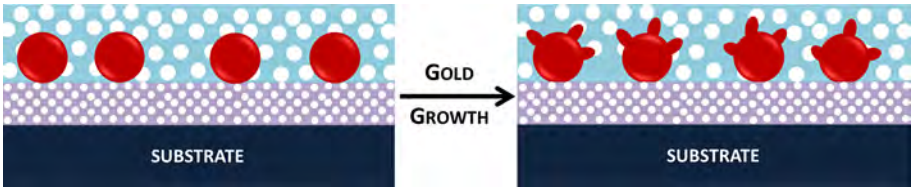

Figure 4.1. Scheme showing the expected structure of SBTF films before (left) and after (right) the growth of gold branches. A mesoporous film with small holes (SB, violet) covers the substrate; gold particles are then placed on top; and finally, a mesoporous film with big holes (TF, blue) covers the particles.

4.3 Results and Discussion

The aim of this work was the preparation of gold Janus nanoparticles using mesoporous thin films as planar masks. The approach was based on the work reported by Angelomé et al.,[280] on the growth kinetics of gold nanoparticles embedded between a substrate and a mesoporous thin silica film. Silica and titania films are labeled as SX and TX respectively, being X de corresponding surfactant: B represents Brij58, C corresponds to CTAB and F to F127. In the case of bilayers, the first two letters correspond to the inner film, and the next two letters to the upper film. Thus SBTF represents a sandwich composed of SiO_2 - Brij58 at the bottom and TiO_2 - F127 in the upper part. In Fig. 4.1 (left panel) a scheme is presented showing the expected structure of a SBTF sandwich. For the sake of clarity we focus on the SBTF system, with the bigger holes in the upper part. Notwithstanding, a wide variety of sandwich film configurations were prepared, with only silica and also with the bigger holes in the bottom (see types of bilayers in Table 4.1) Briefly, over a silicon wafer or a glass substrate a silica mesoporous thin film was prepared by spin coating. After thermal treatment, 60 nm gold spheres functionalized with PVP in ethanol were spin coated over this first film. The structure was subsequently completed by deposition of the second film, covering the gold particles. After the final thermal treatment, the organic templates were removed by inmmersing the films in ethanol for 3 days.

The as prepared SBTF sandwich was characterized by electron microscopy prior growing the gold branches. In Fig. 4.2 A we show a representative low magnification TEM image where the distribution of gold particles in between the films can be seen; no aggregation was found, and the pore structure (mainly of the

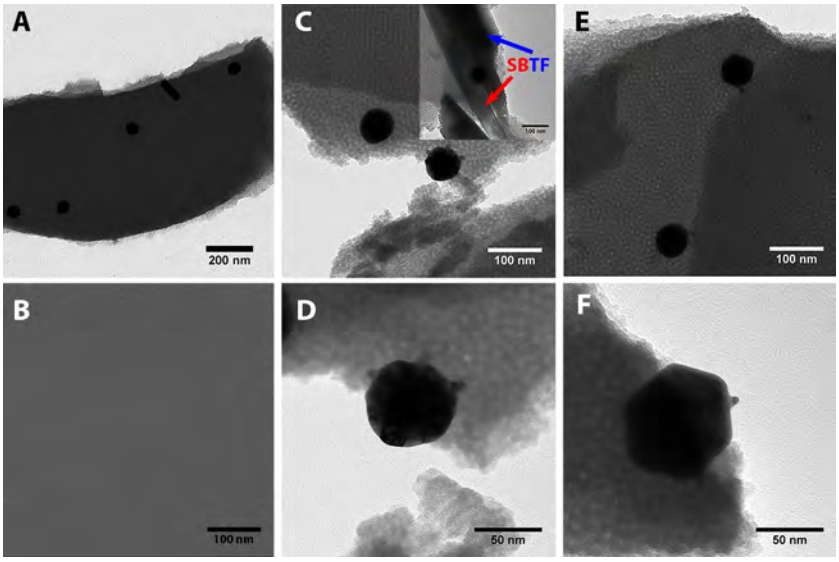

Figure 4.2. TEM (A, C - F) and SEM (B) images of SBTF films loaded with 60 nm gold spheres: (A) prior to the growth of gold; (B) region showing the order of TF pores; (C - D) Low and high magnification pictures after growing the gold particles with *R* method (inset, side view); (E - F) Low and high magnification images after metal growth using *P* method.

big TF pores) can be readily recognized. It is worth noting the presence of one rod like particle in image A, which is a byproduct of the synthesis of 60 nm gold particles.[282] These particles can also be removed by applying a purification step, but we omitted this step to simplify the process. Besides, this allows us to check in the same experiment if gold can grow over anisotropic particles, which is important for designing future experiments, but this is out of the scope of this chapter. In Fig. 4.2 B a SEM micrograph is shown from a region where the presence of pores (TF) in the structure is clearly visible. The side view of the films in the inset of Fig. 4.2 C confirms that particles are embedded in between them, and also the different nature of the films allows us to distinguish the SB from the TF film.

To determine the influence of the presence of the gold particles on the organization of the pores, small - angle X - ray scattering (SAXS) experiments were carried out. Shown in Fig. 4.3 are 2D - SAXS patterns obtained at 4° (upper panel) and 90° (lower panel) incidence, from thermally stabilized films at 200 °C. Due to the thermal treatment a certain uniaxial contraction of the films in the axis perpendicular to the substrate is observed (ellipsoidal pattern), in agreement with previous

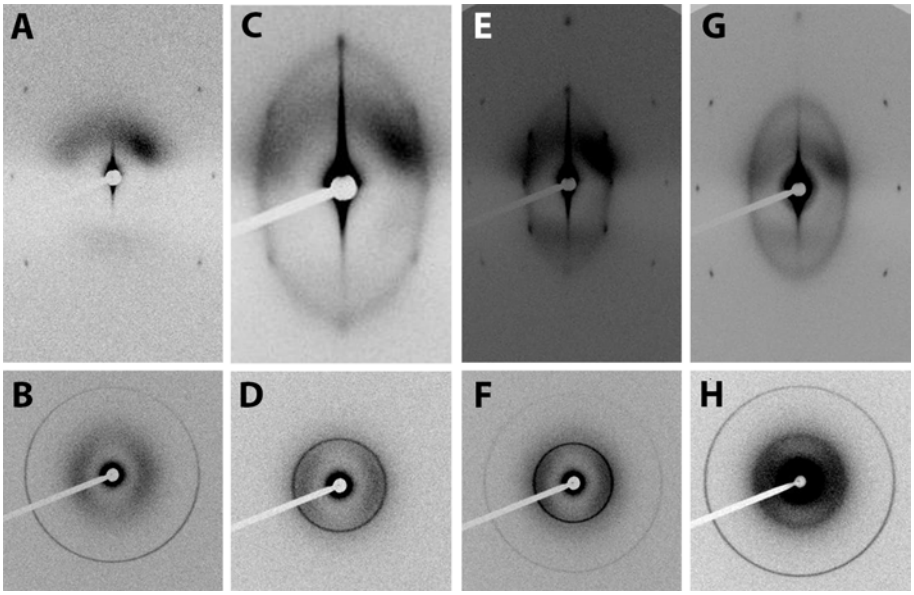

Figure 4.3. 2D - SAXS patterns of mesoporosus films obtained at 4° (upper panel) and 90° (lower panel): (A - B) SB monolayer; (C - D) TF monolayer; (E - F) SBTF bilayer; (G - H) SBTF bilayer loaded with 60 nm gold spheres.

reports.[286] Fig. 4.3 A - B and C - D shows the patterns for a SB and a TF monolayer, respectively. In both cases a cubic *Im3m* structure was determined, with the [110] plane oriented parallel to the substrate surface (a = 8.4 and 18.6 nm for the SB and TF network respectively).[287, 284] Fig. 4.3 E - F shows the SAXS pattern for a SBTF bilayer, where two distinct highly ordered and oriented structures are clearly visible. When 60 nm gold particles were deposited in between SBTF films a similar result was obtained (Fig. 4.3 G - H), meaning that bilayers preserve the order of the corresponding monolayers, with no loss of order due to the presence of the gold particles. The latter only produce an increase of the scattering intensity at the center of the image. As previously mentioned, different combinations of mesoporous film sandwiches were prepared, and they all yielded similar results, i.e. the particle loaded bilayers keep the mesoporous order of the corresponding monolayers (Table 4.1). Brij58 and F127 templated silica or titania films exhibit a cubic *Im3m* structure, whereas CTAB films are organized into 3D hexagonal *P63/mmc* structures.

A more complete characterization of the mesoporous thin films was carried out

by ellipsometric porosimetry (EP). Ellipsometry is a non - destructive optical technique based on the changes in the polarization of a polarized beam light when interacting with a material. This change is quantified in the reflected light through the ellipsometric angles Ψ and Δ, which can then be modeled to determine the film thickness and the refractive index of the material.[288] The EP set up includes a pressure control chamber coupled to a spectroscopic ellipsometer. This technique was first reported by Baklanov and co - workers in 2000 and is very powerful for the characterization of micro - and mesoporous thin films.[289] The procedure is based on plotting an adsorption - desorption isotherm from variations in the refractive index due to changes in the partial pressure of an organic solvent over a film. In our system an environmental ellipsometric porosimeter (EEP) was used, therefore water isotherms were plotted.[290] Two main problems limit the accuracy of the EP technique: first, the assumption that the adsorbate confined into the pores keeps its bulk properties; second, the models employed are not fully adapted to film characteristics. EEP measurements entail no experimental difficulty but the adjustment of the data remains challenging if realistic results are to be obtained. In the lower panel of Fig. 4.4 the isotherms are shown for SB and TF films forming a single monolayer over a silicon wafer. At $P/P^0 = 0$ the refractive index and the thickness of the corresponding film can be estimated (see the summary for all mesostructures on Table 4.1). Thickness values of 61 and 125 nm where obtained for SB and TF films respectively, so the as prepared films are relatively thin. The obtained thickness is related to the viscosity of the precursor solution containing the metal sol and to the spin speed employed during the film preparation. Therefore, low viscosity sols and high speeds lead to thinner films. From the same graph we can obtain the porosity, which results to be 39% and 34% for SB and TF, respectively. The highest porosity was achieved with SC films, where over 49% of the total volume is accessible. The adsorption plot can additionally be used to calculate the diameter of the pores and the desorption plot to estimate the diameter of the necks, i.e. the distance between pores. Similar pore sizes (around 3 nm) were determined for CTAB and Brij58, whereas for F127 bigger pores were obtained (6.6 nm). The smaller pore size of TB compared to SB could be attributed to the presence of some organic molecules from the template, avoiding the total saturation of the pores with water molecules, leading also to a lower porosity compared to the real value (saturation is reached faster). It is worth mentioning that two different neck diameters were obtained for SF films. A unique value around 2.6

nm was expected, so we postulate that the second diameter was determined when using a long time aged precursor metal sol. SF films exhibit a high porosity, but the gold growth step could be affected on these films.

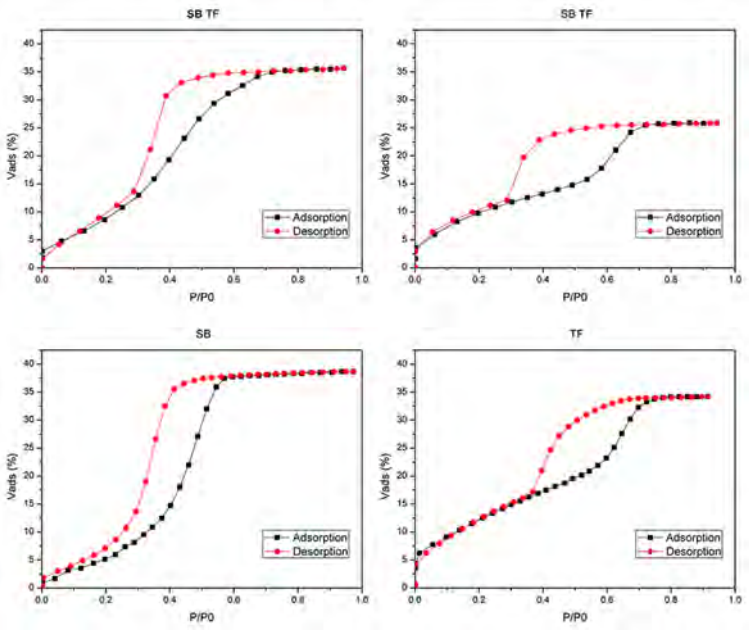

Figure 4.4. Water adsorption / desorption isotherms. The SB (left) and TF (right) components of the SBTF bilayer are shown in the upper panel. For comparison, we plotted in the lower panel the isotherms of the corresponding monolayers.

After characterization of the monolayers, the same analysis was applied to bilayers (without particles). Experimentally the process is exactly the same for bilayers, but the modeling is more challenging: each monolayer conforming the film's sandwich must be separately modeled, using data from the single monolayer as input, so that the most realistic result possible is achieved. In the upper panel of Fig. 4.4 are shown the isotherms for SBTF films: the SB monolayer is plotted on the left and the TF layer on the right. From these plots it can be first observed that the porosity is decreased in the bilayers, though still high, 36% and 26% for SB and TF, respectively. Nevertheless, a 128 nm film thickness was obtained for the SB layer, which is twice the value obtained when forming a single monolayer (closer to the value estimated on TEM), but all efforts made by decreasing the film thickness as an input gave worse results. Other bilayers yielded results that are closer to

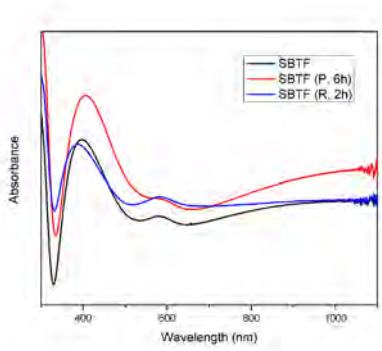

Figure 4.5. UV - vis - NIR spectra of the SBTF film loaded with 60 nm gold particles: before (black) and after growing gold under *P* (red) and *R* (blue) conditions.

those of single monolayers, except for SFSC, where the presence of two layers with very close refractive index values made the modeling rather difficult. Therefore, the main conclusion from EP on bilayers is that all thin films show accessible pores where gold growth can be expected to occur.

After confirming the preparation of a substrate with an accessible pore network, gold branches were grown over the 60 nm metallic spheres (Fig. 4.1 on the right). Two different growth conditions were employed: either three mild steps *(P)* or one step under more aggressive conditions *(R)*. *P* conditions were employed because this preocess was reported to yield good results with particles embedded between a substrate and a single mesoporous film,[280] whereas *R* conditions were used to test if similar results could be obtained faster, in one single step. Growth experiments were carried out in 10 mL plastic tubes. For *P* conditions, a mixture of gold salt and CTAB was aged for 1 h to ensure de formation of the organometallic complex $\left([\mathrm{Au}] = 6.25 \cdot 10^{-5}\,\mathrm{M},\, [\mathrm{CTAB}] = 30\,[\mathrm{Au}]\right)$. Then the mild reducing agent, ascorbic acid (AA), was added ($[\mathrm{AA}] = 16\,[\mathrm{Au}]$) to form a colorless Au^{+} - CTAB complex and the film sandwiches were finally introduced. After 2 h, a faint pink solution was obtained, indicating a certain degree of nucleation of gold particles, and the films were removed and washed with ethanol. The process was repeated twice to increase the size of the gold branches. In Fig. 4.5 are shown the UV - vis - NIR spectra of SBTF films, both before and after the growth process. When working with substrates, no attention to absorbance intensities can be taken into account due to small differences in the thicknesses of the substrate and the films,

making the comparison rather difficult. Additionally, titania films absorb in the UV - Vis region. These spectra show a small red - shift of ca. 3 nm (from 579 to 582 nm) after the growth of the spikes. As can be observed on Fig. 4.2 C - D, small spikes are indeed seen to protrude from the 60 nm gold particles. We expect these branches to grow only through the bigger pores of the F127 templated films, but not in CTAB or Brij58 pores, thereby leading to the desired Janus structures. The main goal is thus to demonstrate this asymmetric growth, but the small size of the spikes and the presence of two mesoporous films makes the characterization challenging. TEM micrographs suggest asymmetric growth, but as this is a 2D technique, it could also be an artifact. In the side view shown in the inset of Fig. 4.2 C we can only distinguish the gold particle in between the SBTF sandwich, but the film is too thick to focus the spikes, so it is not possible to show the asymmetry. The only way to demonstrate the Janus behaviour is by cutting a very thin slice of the film with a focused ion beam (FIB) at different particle positions, and analysing the structures with a TEM. For R conditions, the CTAB - gold ion mixture was aged for 30 min at 30 °C ([Au] = 0.5 mM, [CTAB] = 0.1 M). Then hydrochloric acid ([HCl] = 19 mM), silver nitrate ([$AgNO_3$] = 0.12 mM) and AA ([AA] = 0.8 mM) were subsequently added prior to introducing the mesoporous sandwiches. After 2 h, a faint pink solution was also obtained, and the films were removed and washed with ethanol. Shown in Fig. 4.2 E - F are characteristic TEM images, showing also a certain degree of growth of spikes like under P conditions.

Table 4.1. Summary of the parameters obtained by EEP for monolayers and bilayers (the corresponding monolayer in bold) without particles. N = refractive index, θ = contact angle

Film	Thickness (nm)	N	θ	Porosity (%)	d_{pore} (nm)	d_{neck} (nm)
SB	61	1.31	23	39	3.4	2.4
SC	124	1.26	36	49	2.8	2.0
SF	67	1.29	36	44	6.6	5.0 / 2.6
TB	97	1.67	50	30	2.0	1.6
TF	125	1.63	43	34	4.4	2.2
SBSF	63	1.36	-	28	-	-
SB***SF***	57	1.27	-	41	-	-
SBTF	128	1.35	-	36	-	-
SB***TF***	128	1.68	-	26	-	-
SCSF	114	1.32	-	30	-	-
SC***SF***	55	1.35	-	34	-	-
SCTF	119	1.36	-	32	-	-
SC***TF***	118	1.71	-	24	-	-
SFSC	97	1.32	-	32	-	-
SF***SC***	97	1.31	-	38	-	-
SFTB	65	1.22	-	58	-	-
SF***TB***	96	1.76	-	23	-	-

4.4 Conclusions

In summary, we have demonstrated the preparation of a wide variety of mesoporous thin film sandwiches made of silica and / or titania with 60 nm gold particles embedded at the interface. SAXS measurements confirm that the films show a high degree of organization in the pores and that the presence of the particles does not disturb the order. Environmental Ellipsometric Porosimetry has shown the high porosity of the as prepared sandwiches, allowing us to grow gold spikes over the em-

bedded gold spheres. Films were extensively characterized by electron microscopy, but the asymmetric growth cannot be confirmed with our current data (ongoing work is being carried out in this direction). These structures may have interesting applications as surface enhanced Raman scattering (SERS) detectors [278] or in catalysis, using the pore network as a molecular sieve.

Chapter 5

A Protecting Group Approach Toward Synthesis of Gold - Silica Janus nanostars

Abstract

Patchy and Janus particles offer new opportunities toward multifunctionality and directed self - assembly. Although colloid chemistry methods have been reported, these were mainly applied to sub - micron particles and not easily implemented for nanoparticles. We show here a synthetic approach based on the concept of protecting groups, widely used in organic chemistry, for the synthesis of gold - silica Janus nanostars, in which gold branches protrude from one half of gold - silica Janus spheres. This configuration opens up new possibilities to apply the plasmonic properties of gold nanostars, as well as a variety of chemical functionalizations on the silica component.

5.1 Introduction

Protecting groups are commonly used in organic chemistry to perform chemical reactions in the presence of other functional groups that can be affected by the process. The quest for new protecting groups with multiple properties has led synthetic protocols to a new level that allows the preparation of highly complex molecules.[291] Although protection and deprotection have been widely employed with great success at the molecular level and even with colloids larger than 100 nm, this strategy has been far less explored using small nanoparticles.[90, 7, 8, 292] Different molecular analogies have been proposed for the design of novel nanoscale materials, and in particular for plasmonic nanomaterials.[293] Nevertheless, whereas in organic chemistry these processes are mainly carried out in homogeneous solutions and the final products are obtained by routine techniques such as crystallization or chromatography and solvent evaporation, when working with colloids different parameters must be considered, e.g. to avoid aggregation during synthesis and recovery of the product, including the type of solvent, the nature of the nanoparticles or the stabilizing molecules, among others.

Nanostars are a special type of anisotropic nanoparticles comprising a core from which metallic branches grow, yielding star shape particles. It has been reported that these plasmonic structures, mainly of gold and silver, are able to largely enhance the electromagnetic field on their sharp tips, being optimal candidates for SERS detection (see Section 1.3).[294, 295]

Presented in this chapter is a protecting group - like strategy to synthesize Janus nanoparticles, exhibiting different materials on roughly each half of the particle. The aim was to achieve plasmonic nanoparticles that could hold different functionalities at opposite sides, while maintaining a strong optical (plasmonic) activity, for example gold nanostars in which the spikes protrude from only one half of the central sphere. Such a configuration may offer important advantages toward subsequent directed self - assembly processes or selective biofunctionalization. We thus devised a multistep procedure involving several strategies that have been previously used to synthesize patchy particles: self - assembly of ligands over a metallic surface, masking or protection and seeded growth.[296] First were prepared 40 nm gold nanoparticles, onto which two different ligands were self - assembled to guide the growth of a silica semishell, leading to the formation of gold - silica Janus particles. Besides providing colloidal stability due to a high negative charge, the silica

semishell can act as a mask to direct the subsequent seeded growth of gold spikes, exclusively on the part of the metal that remained exposed to the solution. This ultimately leads to a particle comprising a silica sphere with gold branches protruding from one side and therefore having highly anisotropic optical properties. Finally, the silica shell can also be removed, thus completely mimicking the behavior of protecting groups in organic chemistry.

5.2 Experimental Section

Chemicals

All chemicals were supplied by Sigma and used as received unless otherwise indicated. Tetrachloroauric acid ($HAuCl_4 \cdot 3H_2O$, 99%), sodium citrate tribasic dihydrate (98%), 4 - mercaptobenzoic acid (4 - MBA, 90%), polyacrylic acid solution (PAA $M_w = 250000$ g/mol, 35% H_2O), ammonium hydroxide (28 - 30%), tetraethylortosilicate (TEOS, 98%), silver nitrate (99%), L - Ascorbic acid (L - AA, 99%), hydrochloric acid (Panreac, 37%). 2 - propanol (Scharlab, 99.8%); absolute ethanol (Scharlab) and Milli - Q water were used as solvents. All glass material was washed with Aqua Regia (special care must be taken as it is a highly oxidizing agent) and rinsed gently with Milli - Q water prior to use.

Preparation of Gold - Silica Janus Particles

Twenty seven mL of 40 nm gold @ citrate spheres, prepared as previously reported, [297] were centrifuged at 2100 g for 20 min, washed with the same volume of water and dispersed again in water (10 mL). The seeds were added dropwise under vortex stirring to a mixture of 2 - propanol (38 mL) and H_2O (12 mL), containing 4 - MBA (400 μL, 5 mM in EtOH) and PAA (400 μL, $6.45 \cdot 10^{-5}$M in H_2O). After gentle stirring for 30 min to induce self - assembly of the ligands over the surface, ammonium hydroxide (1.8 mL) was added under fast stirring, followed by dropwise addition of TEOS (12 mL, 8.96 mM in 2 - propanol) and was stored for ~12 h under slow stirring. [Au] $\approx$ 0.3 mM; pH $\approx$ 11.

Preparation of Gold - Silica Janus Nanostars

First 6 - 10 mL, to yield longer or shorter tips respectively, of the as synthesized Janus particles were centrifuged at 2100 g for 30 min. The supernatant was centrifuged again under the same conditions and then the precipitates were collected, dispersed with half the volume of water and centrifuged again at 1900 g for 20 min and redispersed in 10 mL of water. To this solution we quickly added: $HAuCl_4$ (19.8 μL, 0.1265 M), HCl (10 μL, 1 M), $AgNO_3$ (100 μL, 3 mM) and L - AA (50 μL, 0.1 M) as previously reported for nanostars growth.[298] After 30 - 60 s the particles were collected by centrifugation at 1100 g for 5 min and washed with 5 mL of water (the maximum possible amount of supernatant was removed). The particles were transferred under sonication into a solution of 4 - MBA in ethanol (5 mL, 20 μM), and washed with ethanol (5 mL) to remove excess 4 - MBA.

Preparation of Gold Janus Nanostars

Gold - Silica Janus nanostars were dispersed in an aqueous solution of 4 - MBA (5 mL, 20 μM) and washed 3 - fold with water (5 mL) to remove 4 - MBA in excess. The process initially led to dissolution of the inner part of the silica semishell, which was completely removed after two days in water.

Instrumentation

Vis - NIR spectra were measured in 1 cm path length quartz cuvettes using an Agilent 8453 spectrophotometer. Conventional Transmission Electron Microscopy (TEM) analysis was performed with JEOL JEM 2100F and 1400F transmission electron microscopes operating at acceleration voltages of 200 and 100 kV, respectively. HAADF - STEM tomography series and high resolution HAADF - STEM images were acquired using an aberration corrected cubed FEI - Titan 60 - 300 electron microscope operated at 200 kV in colaboration with Sara Bals' group (University of Antwerp). The acquisition of all the tomography series was performed by using the Xplore 3D automatic acquisition software from FEI and the alignment of the series by using the Inspect 3D software from FEI. The reconstruction of all the series was performed by using the Simultaneous Iterative Reconstruction Technique (SIRT) as implemented in Inspect 3D.

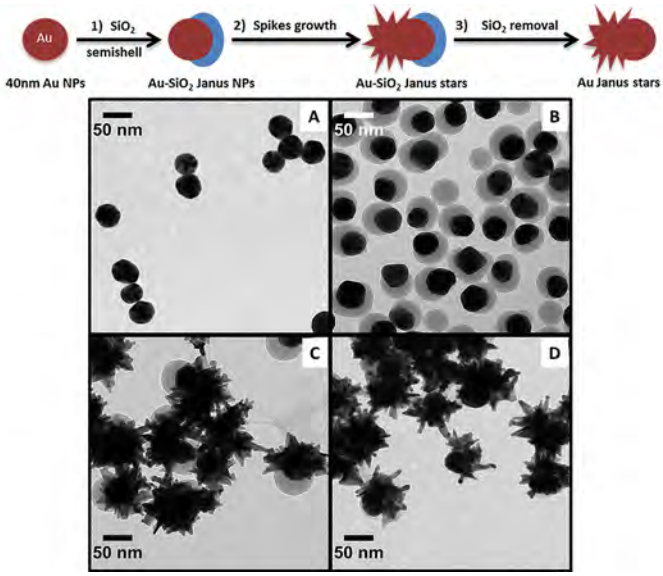

Figure 5.1. The top panel is a scheme of the synthesis. A-D: Representative TEM micrographs of: 40 nm Au@citrate (A); Janus gold - SiO_2 (B); gold - SiO_2 Janus nanostars (C); and gold Janus nanostars after SiO_2 removal (D).

5.3 Results and Discussion

A schematic representation of the steps followed for the production of gold Janus nanostars is shown in Fig. 5.1. First, ca. 40 nm citrate - capped gold spheres ($\lambda_{max} = 528\,nm$) were prepared using a variation of the well - known Turkevich method,[297] which could be easily transferred into alcoholic solution for growth of the silica semishells. Prior to formation of the oxide layer, in a 2 - propanol : water mixture (2 : 1) both ligands – 4 - mercaptobenzoic acid (4 - MBA) – poly-(acrylic acid) (PAA, $M_w = 250000\,g/mol$) – were allowed to self - assemble over the metallic surface, resulting in significant segregation as previously reported.[120] Silica was then grown by means of the well - known Stöber method [265] only on top of the 4 - MBA - capped area, while PAA acted as a stabilizer over the exposed gold surface (step 1, Fig. 5.1). These particles were stable in the synthesis solution, but could also be washed with 2 - propanol to remove the excess of reactants with no apparent aggregation or particle degradation. Typical TEM images and Vis - NIR spectra ($\lambda_{max} = 535\,nm$) are shown in Fig. 5.1 B and Fig. 5.2 respectively. The TEM micrographs nicely show the formation of silica semishells on the gold cores,

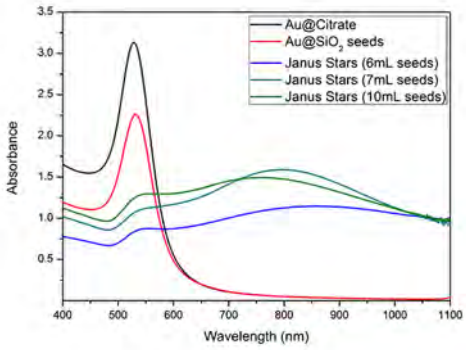

Figure 5.2. Vis - NIR spectra of 40 nm gold@citrate (black), gold - SiO_2 Janus seeds (red) and gold - SiO_2 Janus nanostars made from different amounts of seed solution as indicated in the labels.

with minor silica nucleation, which did not affect the subsequent synthesis steps, while the plasmon band shows a small redshift due to changes in the local refractive index around the gold nanoparticle cores.[299] Shown in Fig. 5.3 are the effects observed in the final geometry of the particles obtained during the silica growth when changing the amount of ligands. In the presence of 4 - MBA only, core - shell particles are obtained (more red - shifted spectrum). On the contrary, when only PAA was present in the reaction mixture, no silica encapsulation was obtained (more blue - shifted spectrum). The appropiate ratio of ligands is therefore crucial for obtaining the gold - SiO_2 Janus nanoparticles. These shifts are related to changes in the refractive index of the medium surrounding the metallic particles. Silica encapsulated particles are surrounded by a medium with a higher refractive index (1.46) in comparison to non - covered particles, which are in contact with ethanol (1.36). Janus particles are in an intermediate situation, explaining the appearance of their plasmon resonance in between.

The silica semishell was subsequently used as a hard mask to protect part of the surface against the further growth of gold spikes (step 2, Fig. 5.1). Upon centrifugation and washing with water, gold spikes were grown using a surfactant - free approach, where L - ascorbic acid acts as a weak reducing agent in the presence of silver nitrate and HCl (aq).[298] It has been observed that spikes can only be grown in the presence of silver ions, otherwise metal overgrowth takes place without branch formation (Fig. 5.4). Since this method avoids the use of surfactants and

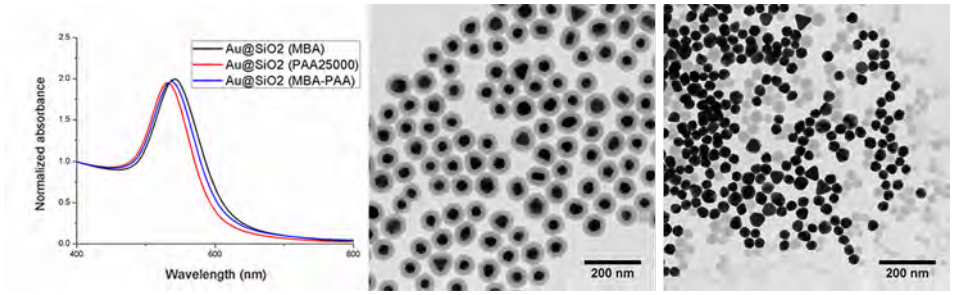

Figure 5.3. Spectra of the particles obtained when 4 - MBA and PAA 250000 were used alone or together during the silica growth. When only 4 - MBA was used (red - shifted spectrum), core - shell particles were obtained (left TEM picture). In contrast, when using only PAA (blue - shifted spectrum), silica nucleation was observed with no silica coating over the metal (right TEM picture). The appropriate mixture produces the segregation of ligands over the surface, yielding the Janus gold - SiO_2 particles.

polymers, exchange of the remaining PAA is not needed and the obtained branched structures display a rather clean surface, which makes them ideal candidates for self - assembly or surface enhanced Raman scattering (SERS), where subsequent functionalization is usually required.[300, 301, 302, 303, 304] Gold - SiO_2 Janus nanostars were obtained in less than one minute and collected by centrifugation. It has been reported that after several hours to days such nanostars may undergo a reshaping process, leading to less spiky structures, which is reflected in a plasmon band blue - shift.[305] In these surfactant - free stars this process was observed within a couple of days and additionally the silica semishell was found to dissolve if the particles were stored in aqueous solution after the synthesis (Fig. 5.5).[306] However, both processes can be prevented by transferring the particles into an ethanol solution containing 4 - MBA (20 μM) and washing several times with pure ethanol to remove unattached 4 - MBA molecules. As can be observed in Fig. 5.1 C, the silica shell and the spikes are still present in particles prepared in this way. The choice of 4 - MBA relies on the well - known adsorption of thiol molecules over metal surfaces, which prevents other surface phenomena from occurring, as reflected in the stability of the gold spikes, which remained unchanged for at least three months. Storage of gold - SiO_2 Janus nanostars in water without addition of 4 - MBA however leads to less spiky structures and silica dissolution within a few days (Fig. 5.5). In contrast, upon addition of 4 - MBA in water gold Janus nanostars were obtained, i.e. the gold branches were preserved while the silica protecting mask was removed (step 3, Fig. 5.1). A representative TEM image of these gold

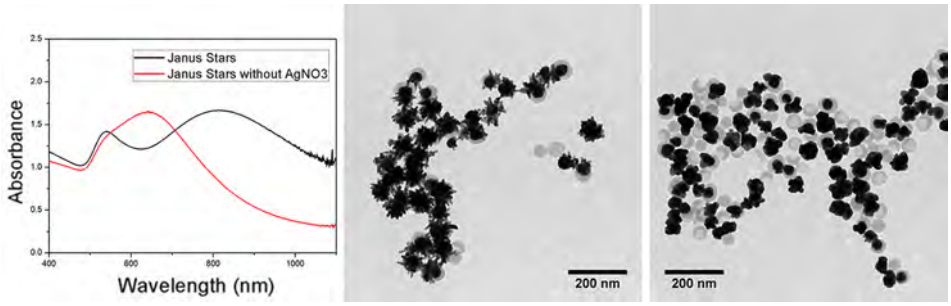

Figure 5.4. Effect of silver nitrate during gold spikes growth. When added, a strong red-shift is observed due to the presence of the tips as can be observed in the left TEM image. When no silver ions are added, a small red-shift appears due to overgrowth of gold over the Janus seeds, but no spikes are produced.

Janus nanostars is shown in Fig. 5.1 D, where the branches can be seen next to a smooth gold hemisphere.

Since conventional TEM images only provide 2D projections of 3D objects, more detailed characterization was carried out by high-angle annular dark-field scanning transmission electron microscopy (HAADF-STEM) tomography, and aberration corrected high resolution HAADF-STEM to clarify their morphology. Three examples are shown in Fig. 5.6 for gold-SiO_2 Janus nanostars with short and long branches and gold Janus nanostars, for which HAADF-STEM images obtained at different angles are displayed, together with the corresponding rendered 3D images. Silica is represented in blue and the metallic part in golden colour. These images clearly confirm that the gold spikes grow only from the exposed face of the metal, which is not covered by the silica hard mask (protecting group). Whereas for short spikes random orientation from the central core is observed, in the long branched nanoparticles, obtained when using a lower amount of seeds, the 3D structure suggests that secondary branching occurred on few spikes that were initially grown from the core. This cannot be observed in conventional TEM projection images, so HAADF-STEM tomography is an essential tool to understand this type of system. Tomography was also used to image the Janus nanostars after dissolution of the silica shell, again clearly showing a highly branched side, which is well differentiated from a quasi-spherical side.

A final piece of information regarding the ultrastructure of these unusual nanoparticles was provided by high resolution HAADF-STEM, as exemplified in Fig. 5.7.

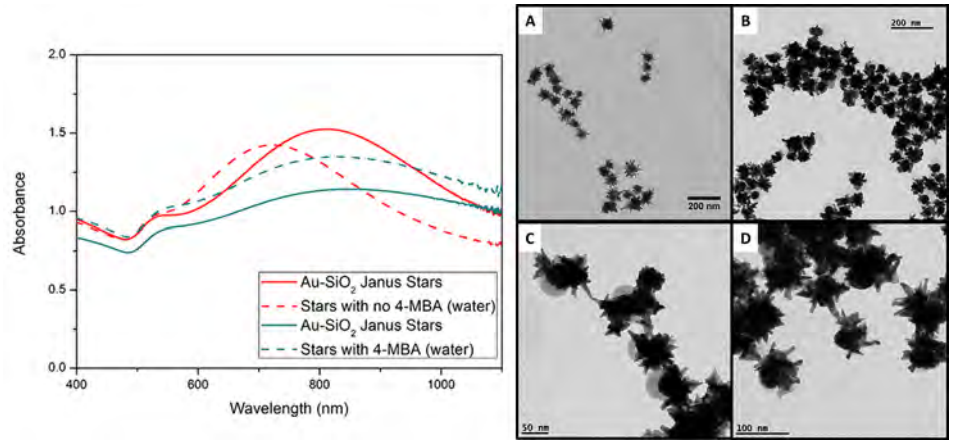

Figure 5.5. Evolution of Vis - NIR spectra of aqueous solutions of gold - SiO_2 Janus nanostars in the absence and presence of 4 - MBA, and the corresponding TEM micrographs. A 100 nm blue - shift is observed after two days when no 4 - MBA was added, indicating reshaping of the spikes and silica dissolution (red lines, A - B TEM images). Only a minor blue - shift can be seen when 4 - MBA was present in the aqueous Janus nanostars solution, indicating silica dissolution maintaining the spiky shape (blue lines, C - D TEM micrographs).

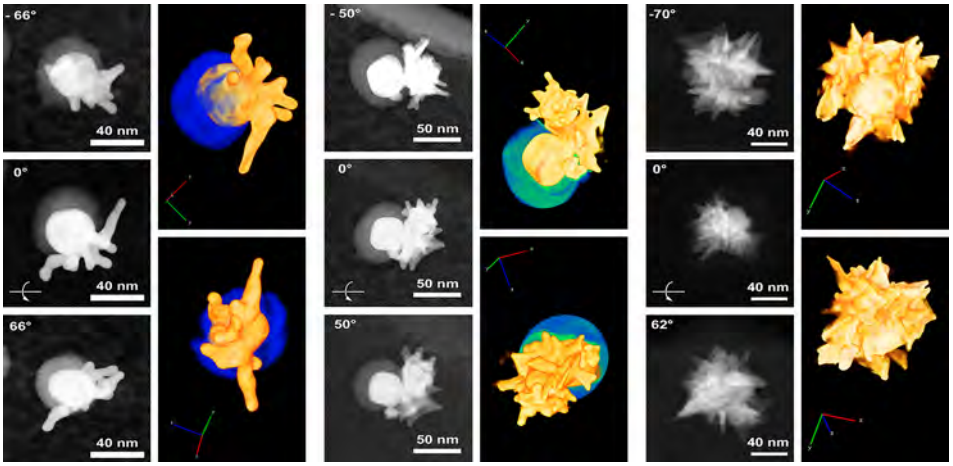

Figure 5.6. HAADF - STEM images used for tomographic reconstruction acquired at different angles and the corresponding rendered 3D reconstructions along different directions, showing the gold parts in yellow and the silica shells in blue, for two different gold - SiO_2 Janus nanostars (left: short branches; centre: large branches) and for gold Janus nanostars (right).

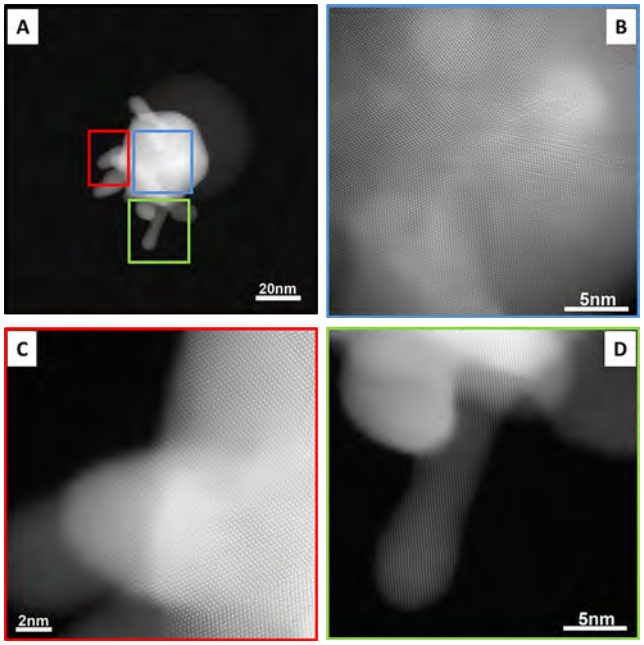

Figure 5.7. (A) HAADF - STEM image of a single gold - SiO_2 Janus nanostar with short spikes, revealing the presence of a gold core with branches (brighter features) and also a silica shell at one side of the particle (faint grey area). (B - D) HRSTEM images of the same particle showing that the gold core is multi - twinned, whereas the branches are single crystals.

A HAADF - STEM image of a single gold - SiO_2 Janus star with small branches is shown in Fig. 5.7 A, revealing the presence of a spherical gold core from which spikes protrude (bright areas) and a silica semishell (faint grey area). A more detailed image of the same particle in Fig. 5.7 B indicates that the gold core is multiply twinned, as expected for such large quasi - spherical particles, whereas the images in Fig. 5.7 C and D show the branching part from the core for several spikes, indicating that they are single crystalline. Paying more attention to the edge of the spike in Fig. 5.7 D, deviation from the zone axis orientation can be seen, so highly branched particles might exhibit different crystallographic orientations where secondary spikes grow over previous branches. A similar analysis was carried out on particles with larger branches (Fig. 5.8), but in this case the overlap between different parts of the particles makes it difficult to distinguish the corresponding crystallographic orientations.

Regarding the optical response of these anisotropic nanostructures, the Vis - NIR

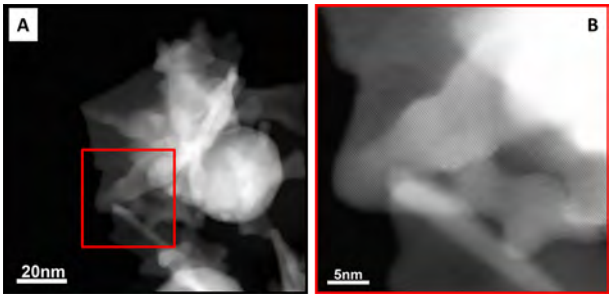

Figure 5.8. (A) HAADF - STEM image of a single gold Janus nanostar with long spikes, revealing the presence of a central core with branches. (B) HRSTEM image of the same particle showing the starting point of a monocrystalline spike.

spectra of colloids obtained with different amounts of seeds (Fig. 5.2) show that the main plasmon band is more red - shifted for lower amounts of seeds, which is in good correlation with the growth of longer branches, as previously reported.[304, 307, 308] It should be noted that the amount of seeds is also a critical parameter to optimize branched growth without secondary nucleation. Closer attention to the Vis - NIR spectra reveals that they comprise two localized surface plasmon resonance (LSPR) bands,[304] which is typical for star - like nanoparticles. The LSPR mode at around 540 nm depends on the core size, in this case determined by the original Janus seeds, whereas the second mode is localized at the tips and its position can be tuned between 700 and 850 nm by simply changing the amount of seeds (and in turn branch dimensions). Other parameters such as the addition of HCl or the amount of silver ions can also modify the morphology and affect the LSPR position, but it has been found that tuning the concentration of the seeds is a more reliable and reproducible strategy. When comparing these spectra with those of standard gold nanostars, it seems that the relative intensities between tip to core LSPR modes are lower in the Janus nanostars, which can be due to the smaller amount of branches per particle compared to standard nanostars. This agrees with theoretical modelling indicating that the intensity of the tip mode is proportional to the number of spikes.[304]

5.4 Conclusions

In summary, we have demonstrated the application of the protecting group concept for the synthesis of Janus nanoparticles comprising a spherical gold core half covered with a silica semishell and with gold tips branching out from the other half. Advances in the colloidal synthesis of Janus particles allowed to deposit silica half shells on metallic spheres, which were then used as hard masks to prevent the growth of gold spikes over the whole surface. The mask can be easily removed by dissolving silica in aqueous solution, thus completing the similarity with protecting groups in organic chemistry. These particles exhibit optical properties similar to those of gold nanostars in solution, but enhanced anisotropy can be expected for oriented assemblies by exploiting the Janus conformation. It has also been shown that aberration corrected HAADF - STEM imaging and tomography are essential tools to disclose the Janus morphology. Applications can be envisaged in e.g. surface enhanced spectroscopies due to the presence of metal branches or in the design of colloidal swimmers. The latter could be achieved by irradiating with an infrared lamp, absorbing the particles the light through the spikes, heating the surrounding media and therefore producing its movement by temperature gradient.

Chapter 6

Hybrid Au - SiO_2 Core - Satellite Colloids as Switchable SERS Tags

Abstract

Gold - silica self - assembled nanostructures are reported as multiplex surface enhanced Raman scattering (SERS) tags for imaging applications. These hybrid colloidal particles were obtained by hetero - assembly of Au - SiO_2 Janus particles with 15 nm Au spheres and two Raman active molecules that can be independently imaged by varying the excitation laser wavelength. The Janus structure of Au - SiO_2 not only directs the assembly but also provides physical separation of the Raman tags and colloidal stability thereby facilitating complete silica encapsulation. The bioimaging capabilities of this system are demonstrated through SERS mapping of single cells.

6.1 Introduction

Raman signals are intrinsically weak due to the low probability of the Raman scattering events, leading to very small cross sections. Notwithstanding, the local enhancement of the electromagnetic field (EM) close to plasmonic nanoparticles, when exposed to an external light source, can lead to the enhancement of Raman scattering cross sections by many orders of magnitude, which is known as surface enhanced Raman scattering (SERS). When plasmonic nanoparticles are in close proximity, the enhancement of the EM field is even higher due to the coupling of their localized surface plasmon resonances (LSPRs), generating so called hot spots and allowing high detection sensitivities, down to the single molecule limit.[309, 310, 44, 45, 47]

Apart from analytical detection, SERS has been proposed as a powerful imaging tool because high sensitivity and selectivity can be achieved even in complex media.[311, 312, 313] Special effort has been made to develop efficient SERS nanotags with non - invasive, in vivo multiplex imaging potential. Typical SERS multiplexing strategies involve the preparation of plasmonic nanoparticle batches individually encoded with different Raman active dyes (= "colors") which can be distinguished, localized and possibly quantified by their specific vibrational fingerprints.[314, 315, 316, 317] Using this approach, Zavaleta et al. demonstrated the in vivo detection of 10 different separately injected nanotags and the distinction of 5 synchronously injected nanotags to a nude mouse.[314] Complex multi - color (= multi - functional) nanotags were recently designed for the application of combined analytical (imaging) methods where each color selectively acts as a label for a specific technique, e.g. fluorescence, SERS, photo - thermal imaging, MRI, etc.[318, 319, 320, 321] We propose here a synthetic procedure to prepare hybrid core - satellite colloidal particles comprising 15 and 40 nm Au spheres in close contact. We loaded these particle clusters with two dye molecules, and finally covered them with silica to fix and protect the nanostructures for use as nanoantennas in SERS imaging applications using living cells.

Several examples of similar structures can be found in the literature, such as dimers and trimers of ~ 100 nm Au particles, for SERS purposes,[49, 322] or the more recently reported satellite particles prepared by a masking desilanization process.[323] Our strategy however exploits the Janus behavior of Au - SiO_2 particles to restrict the area where the assembly can be produced and therefore to achieve a bet-

ter control over the final geometry.[296] This configuration additionally allows the controlled introduction of two different dyes at specific locations within the composite particles, 4-mercaptobenzoic acid (4-MBA) under the silica shell of the Janus particle and rhodamine B isothiocyanate (RhB) within the hot spots generated during the assembly. Significant differences in the energy dependence of the molecular Raman scattering cross section permit the interference-free detection of the individual components by selecting the adequate excitation wavelength. As a result, both labels can be independently traced for SERS imaging purposes by simply varying the laser excitation color. We propose that our method is advantageous because it allows multiplex SERS imaging using a relatively simple colloid chemistry approach. The hybrid satellites described here serve as a proof of concept to demonstrate the capabilities of this type of assembled nanostructures and open the way to the development of new architectures with even higher complexity for future applications in sensing, diagnosis or drug delivery.

6.2 Experimental Section

Chemicals

All reactants were purchased from Sigma-Aldrich otherwise indicated, and were used as received. Tetrachloroauric acid ($HAuCl_4 \cdot 3\,H_2O$, 99%), poly(vinylpyrrolidone) (PVP, M_w = 10 kg / mol), sodium citrate tribasic dihydrate (98%), 4-mercaptobenzoic acid (4-MBA, 90%), polyacrylic acid solution (PAA M_w = 250 kg/mol, 35% H_2O), ammonium hydroxide (28-30%), tetraethylortosilicate (TEOS, 98%), Rhodamine B isothiocyanate (RhB, mixed isomers) and hydrochloric acid (Panreac, 37%). 2-propanol (Scharlab, 99.8%); absolute ethanol (Scharlab) and Milli-Q water were used as solvents.

Synthesis of 15 nm gold spheres

Au nanospheres of 15 nm average diameter were prepared according to the well-known Turkevich method.[281] The as prepared particles were transferred to ethanol upon exchanging the capping agent to poly(vinylpyrrolidone) (PVP, M_w = 10 kg / mol). The particles were incubated for 24 h with the polymer (60 mole-

cules / nm^2) at room temperature, then centrifuged at 6000 rpm and transferred to ethanol adjusting the final concentration of gold to 0.42 mM.[283]

Synthesis of 40 nm Au - SiO_2 Janus particles

The synthesis of gold - SiO_2 Janus nanoparticles was done following the process described in Chapter 5. First, 27 mL of Au @ citrate spheres (40 nm av. diameter) were prepared, centrifuged at 2100 g for 20 min, washed and dispersed in Milli - Q water (10 mL). The seeds ([Au] ~ 0.3 mM in the final mixture) were then added dropwise under vortex stirring to a mixture of 2 - propanol (38 mL) and H_2O (12 mL), containing 4 - MBA (400 μL, 5 mM in EtOH) and PAA (400 μL, M_w = 250 kg / mol, 6.45 $\cdot$ 10^{-5} M in H_2O). After stirring for 30 min to induce self - assembly of the ligands over the surface, ammonium hydroxide (1.8 mL, pH ~ 11) was added under fast stirring, followed by dropwise addition of TEOS (12 mL, 8.96 mM in 2 - propanol) and was stored for ~ 12 h under slow stirring. Afterwards the particles were washed and transferred to ethanol as follows: 10 mL of the as synthesized particles were centrifuged at 2100 g for 30 min. The supernatant was centrifuged again under the same conditions and precipitates were collected and washed with 5 mL of water at 1900 g for 20 min. The supernatant was removed and then the particles were added drop - wise to 10 mL of absolute ethanol under sonication ([Au] = 0.247 mM).

Synthesis of the hybrid Au - SiO_2 Core - Satellites

The assembly experiments were carried out in quartz UV cells of 1 cm length path at room temperature. To 2.5 mL of absolute ethanol were added 32 μL of Rhodamine B isothiocyanate 10^{-5} M $\left([RhB]_{Final} = 9.6 \cdot 10^{-8}\, M\right)$, 172 μL of Au_{15nm} @ PVP 0.42 mM in gold ($2.4 \cdot 10^{12}$particles / mL) and 490 μL of Janus Au_{40nm} (PAA − MBA @ SiO_2) 0.247 mM in Au ($7.5 \cdot 10^{10}$ particles / mL). The amount of RhB added taking into account the total gold surface available, considering half of the Janus particle and the Au_{15nm} spheres, is estimated to be 0.5 molecules / nm^2. After each addition the cell was shaked manually. The mixture was incubated for 2 h in the dark with no apparent aggregation, and then 140 μL of HCl_{aq} 1 mM were added to start the assembly (pH from ~ 8.5 to 5) (NOTE: the amount of HCl_{aq} 1 mM may vary when using different stock solutions of Au_{40nm} (PAA − MBA @ SiO_2) particles due to slight differences during

the washing steps and subsequent transfer to ethanol). After a few minutes, controlling spectrum evolution in the visible, the process was stopped by adding 90 μL of ammonia. The solution was then transferred to a vial and 800 μL of Milli Q water and 133 μL of TEOS (0.15 M in EtOH) were added while magnetically vortexing the mixture. After 30 seconds the solution was stirred slowly for 2 h to complete the encapsulation. The assembled structures were washed 4 times with 1 mL of EtOH to remove silica nucleation, recovering them by centrifugation at 2100 g for 30 min, and finally were dispersed in 1 mL of EtOH, storing them in the dark to minimize dyes photodegradation.

Cell culture

J774 macrophages were purchased from ATCC (LGC Standards, Barcelona) and were cultured in DMEM media supplemented with 5% fetal bovine serum (FBS) and 1% penicillin - streptomycicn (PS). Cells were maintained in a humidified atmosphere at 37 °C, 5% CO_2 and passaged using pipetting. All reagents were purchased from Invitrogen.

SERS of particles in cells

Cells were detached from growth flasks, counted and plated in a specially made cell slide formed of a normal microscopy glass slide or Suprasil Quartz glass to which a micro - chamber made of PDMS was glued. The surface area of each microchamber was approximately 0.5 cm^2, to which 8000 cells were added in a volume of 200 μL. Once attached, (no functionalization of the glass was needed), media was replaced with PBS (10 mM, pH 7.4) and the sample was ready for viewing background levels. For SERS imaging of particles within cells, culture medium was removed and 15 - 30 μL of particle solution, suspended in PBS, was added to the well and left for 1 h at 37 °C. After 1 h the samples were washed using PBS and SERS maps were taken. For experiments in which SERS signal measurements at 785 nm were involved, a special Suprasil Quartz glass was used (thereby minimizing background fluorescence).

Raman / SERS spectroscopy

Raman / SERS spectra and the corresponding maps were performed using a Renishaw InVia confocal Raman spectrometer coupled to a Leica DM - LM microscope and equipped with three different excitation lasers with wavelengths λ_{exc} of 532 nm, 633 nm and 785 nm as well as two CCD cameras as detectors. SERS spectra of the Janus particles with and without satellites were recorded within 1 mm quartz UV cells using a 1800 (532 and 633 nm) or 1200 lines / mm grating (785 nm) and a long - distance 50x objective with a numerical aperture (NA) of 0.45. The integration time tint was set to 10 s. The laser powers measured at the focus distance through the objective were 1.1 mW for 532 nm, 6.0 mW for 633 nm and 11.0 mW for 785 nm. SERS spectra of Janus particle encoded J774 macrophage cells were collected with a 40x immersion objective (NA = 0.85) in combination with a 600 lines / mm grating by measuring with an integration time of 0.5 s over the selected x -, y - range at each point of the grid (spacing of $\Delta x = \Delta y = 2\,\mu m$) using a motorized microscope stage. For these measurements, laser powers of 2.0 mW (532 nm), 0.5 mW (633 nm) and 16.1 mW (785 nm) were applied. The 2D SERS map was created by plotting the baseline corrected intensity of characteristic vibrations at each point as function of grid position. The normalized SERS intensities were displayed on a rainbow - colored code from black (low intensity, I = 0 - 5) via violet (I = 5 - 15), blue (I = 15 - 30), lila - white (I = 30 - 40), green (I = 40 - 60), yellow (I = 60 - 65), orange (I = 65 - 70) and red (I > 70).

Instrumentation

Visible - NIR spectra were measured in 1 cm path length quartz cuvettes using an Agilent 8453 spectrophotometer. Conventional Transmission Electron Microscopy (TEM) analysis was performed with a JEOL JEM 1400F microscope operating at an acceleration voltage of 120 kV.

6.3 Results and Discussion

Fig. 6.1 summarizes the synthetic procedure for the production of Au - SiO_2 hybrid satellites. For this purpose, gold spheres of 15 nm (Au_{15}) uniformly covered with poly (vinylpyrrolidone) (PVP, M_w = 10 kg / mol) and Au - SiO_2 Janus particles with a 40 nm Au core and a silica semishell, both dispersed in ethanol, were employed as building blocks. The Janus nanoparticles were prepared following the process described in Chapter 5, by self - assembling a mixture of the ligands 4 - mercaptobenzoic acid (4 - MBA) and polyacrylic acid (PAA, M_w = 250 kg/mol), to grow a silica semishell over the surface covered with 4 - MBA (Fig. 6.3 A). Both types of particles were first incubated with Rhodamine B isothiocyanate (RhB, $9.6 \cdot 10^{-8}$ M) in ethanol for 2 h. This Raman reporter was selected because it features a high Raman cross section, as well as an isothiocyanate group that facilitates adsorption to gold particles, even when covered by a polymer shell, and high stability in both acidic and basic media within the pH range between 5 and 11. We thus expect that RhB adsorbs on both the small Au_{15} spheres and the exposed Au surface of the Janus particles (0.5 molecules / nm^2).[324]

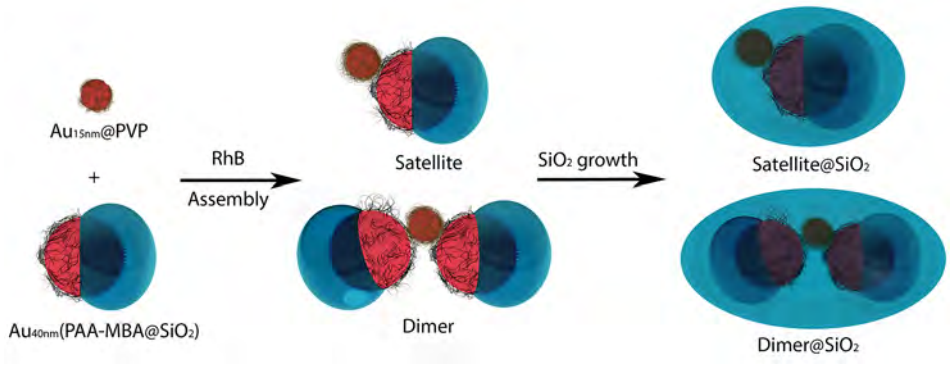

Figure 6.1. Rhodamine B isothiocyanate (RhB) is incubated for 2 h with Au_{15nm} @ PVP spheres and Janus Au_{40nm} (PAA − MBA @ SiO_2) particles. Self - assembly occurs when the pH is set to 5 and can be stopped by increasing the solution pH. Finally a silica shell is grown to stabilize the hybrid nanostructures.

Therefore, two Raman active species are incorporated within the final nanostructures: RhB in the hot spots generated at the gaps between assembled Au particles, and 4 - MBA at the Au - silica interface of the Janus nanoparticles. Importantly, addition of the dye did not trigger aggregation of the particles, as indicated by

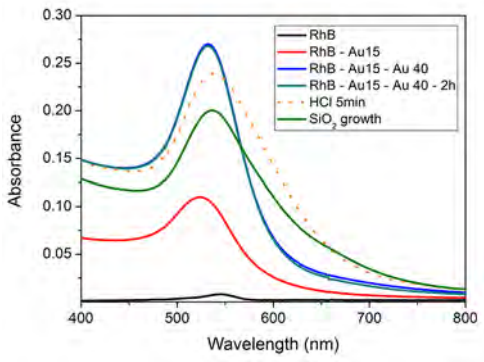

Figure 6.2. Spectral evolution during assembly and silica encapsulation.

UV - vis spectroscopy (Fig. 6.2). Aggregation was prevented due to the basic pH of the mixture (pH ~ 8.5), where the PAA is mainly deprotonated, thereby providing electrostatic stability. However when the pH was decreased to 5 via addition of 1 mM HCl_{aq}, aggregation started through van der Waals and electrostatic attractions between PVP and PAA due to the protonation of PAA ($pK_a \sim 4.8$).[325] The assembly is indicated by the redshift and broadening of the plasmon band, due to plasmon coupling (Fig. 6.2).[326] Although a sufficient amount of Au_{15} spheres were added to cover ~ 80% of the available Au surface at the Janus particles, the assembly process was stopped after 5 minutes (by adding ammonia, increasing the pH of the mixture to ~ 11) to avoid the formation of bigger clusters comprising three or more Janus particles. It is worth noting that no clusters comprising Au_{15} @ PVP only were observed in TEM images, but instead they are always found to adsorb on Janus particles, either forming hybrid satellites or acting as bridges to produce dimers or bigger clusters. The low particle concentration in the TEM image in Fig. 6.3 B is due to the process used to avoid excessive particle aggregation during drying on the carbon - coated grid. As the assembly is a fast and dynamic process, five drops (8.5μL each) were casted on the grid, which was placed over paper. The paper support absorbed the excess of solution thereby providing more separated particles as well as a more realistic idea of what was present in solution.

Since the assembled nanoparticles are dispersed at high pH, silica shells can be grown using the well - known Stöber method,[265] so as to fix and protect the obtained structures (Fig. 6.3 C - D). Growing the silica layer immediately after completing the assembly helps to avoid the dissolution of the silica semishell from

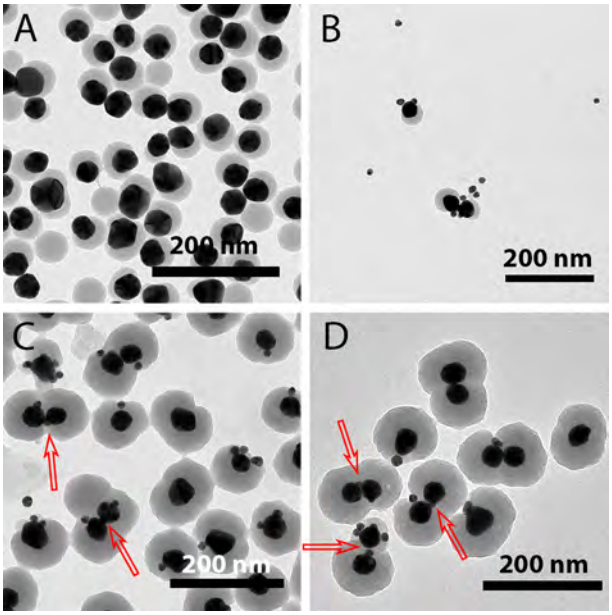

Figure 6.3. Representative TEM images of: (A) the Au_{40nm} (PAA − MBA@SiO_2) Janus particles; (B) Intermediate structures formed after 5 min of assembly; (C - D) Au - SiO_2 hybrid satellites. Red arrows indicate the position of Au_{15nm} acting as linkers for the Janus particles.

the Janus nanoparticles. The final outer shell is stable in ethanol for long periods of time and at least for one month in water, with no apparent dissolution as seen by TEM. Fig. 6.3 C - D shows representative TEM images of the final hybrid satellites after one washing step to remove excess organic molecules. Various types of particles can be clearly seen including satellites made of one Janus particle and a few small spheres, dimers comprising two Janus particles linked by small Au_{15} spheres and some silica nucleation. The latter and the non - assembled Au_{15} spheres can be easily removed by 4 - fold centrifugation and washing with ethanol. Analysis of ~500 particles revealed that ca. 49% hybrid satellites comprise one Au_{40} core with at least one Au_{15} particle, whereas 23% are Au_{40} dimers, 24% non - assembled Au_{40} particles, and some 4% are larger clusters, all of them covered with silica.

SERS measurements were carried out in water (upon transfer from ethanol) so as to minimize interference from the solvent and because it is a more realistic medium toward experiments with cells. The concentrations of particles were estimated as $6.1 \cdot 10^{-11}$ M of Janus and $7.1 \cdot 10^{-9}$ M of Au_{15}, considering that no loses occurred

during assembly, subsequent silica growth, and washing. In reality, non-adsorbed Au_{15} particles were removed during washing due to their smaller weight as compared to the hybrid satellites. 4-MBA was added during the synthesis of Au-SiO_2 Janus particles, at a concentration of $2.7 \cdot 10^{-5}$ M (35 molecules / nm^2), while RhB was incorporated during the assembly process, at a concentration of $9.6 \cdot 10^{-8}$ M (0.5 molecules / nm^2).

The SERS spectra of the hybrid satellites in water upon excitation with three different laser wavelengths (532, 633 and 785 nm) are shown in Fig. 6.4 A. Upon 532 nm excitation (green spectrum), only scattered frequencies were detected that are related to the excitation of characteristic RhB vibrations (1620, 1580, 1560, 1340, 1280 and 1210 cm^{-1}). The peak positions are in good agreement with the modes reported for RhB adsorbed on micron sized silver powder or on Ag nanoshells upon excitation with 514 and 633 nm.[327, 328] In contrast, totally different frequencies were scattered upon 785 nm excitation. The signals correspond to the vibrationally excited states of the second Raman label, 4-MBA (1585, 1075, 1180 and 700 cm^{-1}, black curve), which do not overlap with the vibrations of the RhB label. Using the 633 nm excitation wavelength, a more complex spectrum was recorded in which the scattered 4-MBA frequencies dominate (black dots over the red curve in Fig. 6.4 A) and less intense contributions from scattered RhB frequencies (marked by green dots). A control experiment using Janus particles without satellites was carried out to study the relation between the hybrid structure and the observed color-selective SERS behavior of the incorporated Raman tags. Strong SERS was observed with 633 nm excitation whereas much lower signal was detected in the 785 nm channel originating from 4-MBA. In the 532 nm channel only background fluorescence was detected, arising from unbound RhB molecules (Fig 6.4 B). This clearly indicates that the assembly of satellites is required for RhB detection and that the SERS signal originates exclusively from molecules located within the hot spots between the central Janus particles and the small satellites. The strong SERS signal can be explained by the enhanced Raman cross section at 532 nm due to the electronic RhB resonance state around 550 nm.[327] These results demonstrate the ability of this system to act as a SERS switcher in water, allowing us to turn on or off the dye molecules at will by using different laser excitation colors. This offers the possibility for multiplex particle tracking via SERS using the excitation wavelength as an additional channel.

We next show that the molecular fingerprints of both RhB and 4-MBA can also

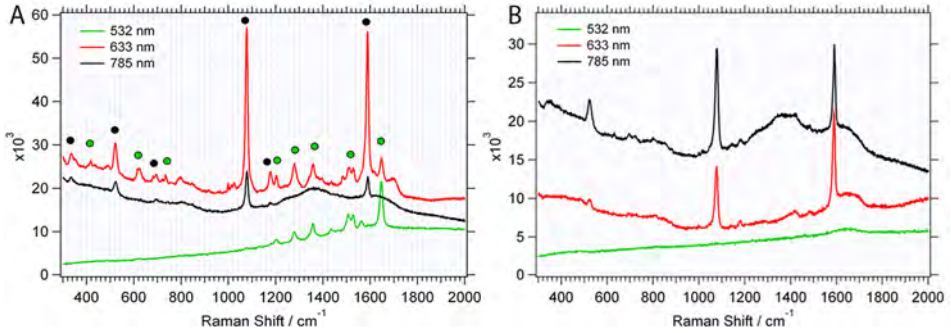

Figure 6.4. SERS spectra using 3 different laser wavelength lines: 532 nm (green line), 785 nm (black line) and 633 nm, (red line) of: (A) hybrid satellites in water, indicating with green dots the RhB vibrations and with black dots the 4-MBA signature; (B) a control experiment in water, using Janus Au_{40nm} (PAA − MBA@SiO_2) particles incubated for 2 h with RhB at 10^{-7} M at pH 8.5 (without aggregation) and fully covered with an outer silica shell, where the peaks from 4-MBA are clearly visible in both cases.

be detected when the hybrid particles are internalized by cells in vitro. We selected the continuous macrophage cell line J774 because it is quickly adherent and actively phagocytoses (uptakes) particles. Both factors were important because of the small working volume of the sample and therefore long term incubation times of the cells with the particles were not possible, due to risk of evaporation of the entire media solution. Therefore, cells do not have an elongated form but are instead round (Fig. 6.5 A). Hybrid satellites were added to cells and SERS spectra at excitation wavelengths of 532, 633 and 785 nm were collected after 1 h incubation from a single cell (Fig. 6.5 B-D). As the cell did not move noticeably over the measurement period, the same cell could be used for all excitation wavelengths. For each wavelength one individual SERS spectrum (green curve for 532 nm in B, black curve for 785 nm in C, and red curve for 633 nm in D) recorded at a single point within the cell was chosen and compared with the corresponding color-dependent reference from the hybrid satellites measured in solution without cells (grey lines in Fig. 6.5 B-D). The SERS spectra obtained in cells perfectly reflect the fingerprints of the RhB label at 532 nm, of the 4-MBA label at 785 nm and of both labels at 633 nm. No additional peaks were observed from the cell or the buffer solution under the present experimental conditions. As the reference spectra of hybrid satellites in solution were measured using 1800 or 1200 lines / mm gratings, whereas the cell maps were recorded with a 600 lines / mm grating (all wavelengths), a slight broadening of the SERS features in the cell compared to the reference sample was

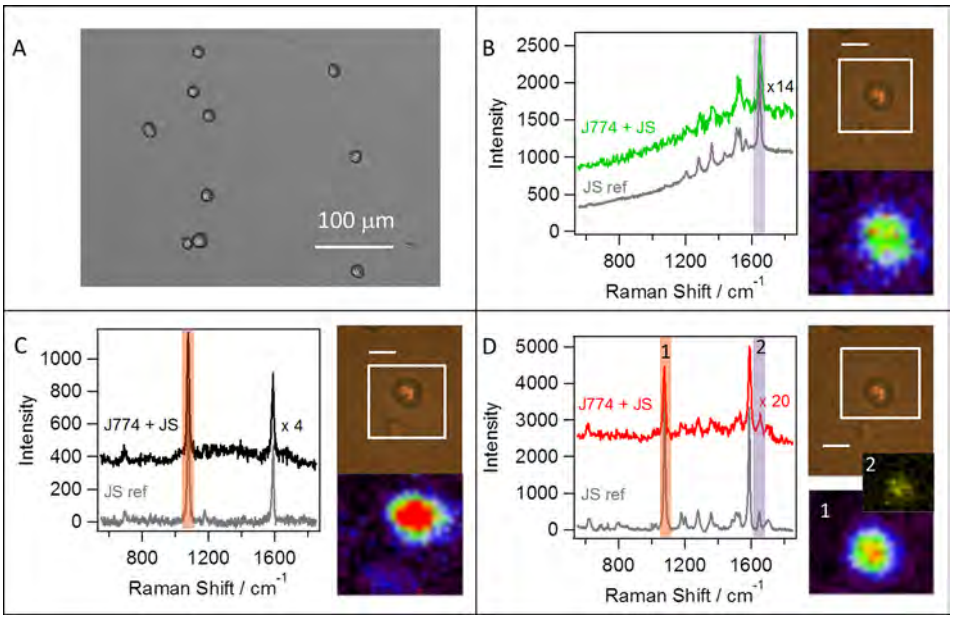

Figure 6.5. (A): Representative transmitted light image of the macrophage cell line J744 before incubation with hybrid satellites; (B - D): color - dependent SERS spectra of J744 (left), white - light image and SERS maps (right) recorded 1 h after incubation with hybrid satellites from the same single cell, at 532 nm (B), 785 nm (C) and 633 nm (D). To facilitate comparison of the cell spectra (J774 + JS, green, black and red curves) with the corresponding reference spectra from hybrid satellites in water at the same wavelengths (JS ref, grey curves), the SERS intensities were multiplied by: 14 (B), 4 (C) and 20 (D). SERS maps for each excitation color were created by plotting the intensity of the selected mode (marked in the SERS spectrum with an orange bar for 4 - MBA at 1078 cm^{-1} and a purple bar for RhB at 1617 cm^{-1}) within the selected area (marked by the white frame in the white - light image) using a color code from black (low intensity) to red (highest intensity); the color code in the SERS map 2 (RhB / 1617 cm^{-1}) in D ranged from black (low) to bright yellow (high intensity). The white scale bar corresponds to 20 μm.

observed. The reference spectra were collected with long integration times of 10 s instead of the 0.5 s applied for the cell. Indeed, the signal - to - noise ratio of hybrid satellites in the cell strongly decreases but is still high enough to record the less intense vibrations.

The intensity distribution of the characteristic vibrations at 1620 cm^{-1} (RhB) and 1080 cm^{-1} (4 - MBA) in the SERS maps appear to show that the hybrid satellites filled the interior of the macrophage (Fig. 6.5 B - D). By conducting SERS mapping in either the streamline mode (line focus) or the mapping mode using short step sizes (≤ 1 μm), a higher level of lateral resolution for the hybrid satellites could

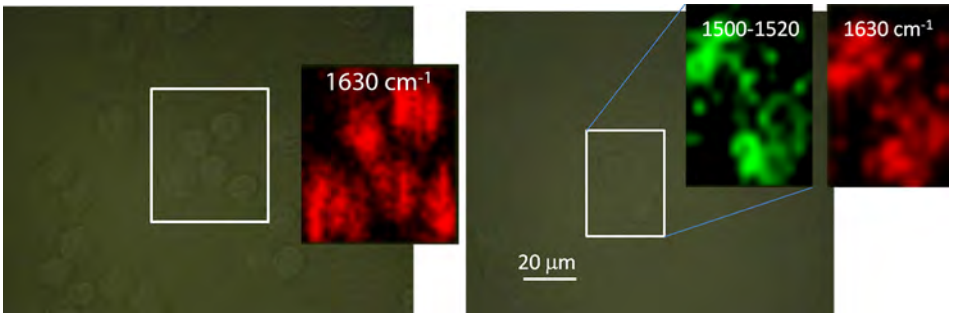

Figure 6.6. SERS maps of the 1630 cm^{-1} and 1520 cm^{-1} vibrations of the RhB label in hybrid satellites incubated in J774 macrophages measured at 532 nm. The SERS signal appeared only in presence of the cells and cell boundaries within the group were clearly resolved. On the left, the map was measured in streamline mode (line focus), integration time 7 s with laser power of 2.0 mW, and on the right point mapping mode with an integration time of 1 s at laser power of 0.14 mW.

be obtained (Fig. 6.6). Importantly, although the cells were not fully adhered and the incubation times between cells and particles were short (1 h), endocytosis of particles was noted at high levels and was not affected by washing. It is possible that part of the SERS signal came from particles associated to the cell membrane, however bearing in mind the phagocytic nature of J774's, such levels should be negligible.

6.4 Conclusions

In conclusion, we have shown that hybrid satellites composed of silica and gold nanoparticles can be codified with two different dyes and applied for multiplex applications in aqueous solutions and in multiplex color-sensitive SERS bioimaging. This concept should be interesting for applications where the independent detection of two different components using the same analytical technique is of advantage. Such a scenario is potentially interesting, e.g. in drug delivery – drug release schemes. Through replacement of RhB by a drug molecule and introduction of a disassembly step of the hybrid satellites, drug tracking and release could be directly controlled via SERS signal intensity using the green laser excitation. Additionally, tracking and fate of the delivery medium, i.e. the Au nanoparticles, can be independently monitored by the SERS fingerprint of the fixed residue molecule just by switching to another excitation line. These assemblies are thus a proof of

concept showing the capabilities of these structures, but the design can be varied to extend their possible applications. For example, the outer silica layer could be modified to make these structures specifically bind to cancer cells.

Conclusions

Altogether this thesis represents a significant advancement in the preparation of new types of metallic Janus nanoparticles. A variety of methods were developed for this purpose, mainly in solution but also using solid substrates. The optical characterization of the prepared nanoparticles and nanostructures derived from them, together with electromagnetic simulations, envisage interesting SERS applications. We demonstrate such applications with the hybrid satellites system, in which multiplexing can be achieved as a result of their unique self-assembled structure. Applications in other fields such as catalysis, colloidal swimmers or the formation of new superstructures can also be expected in the future. Even though specific conclusions have been included at the end of each chapter, the most relevant, overall conclusions of the research described in this thesis are presented herein.

1. A masking process in solution based on wax in water Pickering emulsions was developed to synthesize gold semishells and semicapsules using Janus colloidal silica particles of 495 nm diameter as templates.

   (a) This process allows us to produce large quantities of Janus metal particles with a certain degree of morphology control by adjusting the amount of cationic surfactant DDAB, which is responsible for inmersion of the particles in the wax droplets.

   (b) Simulations of the optical properties of gold semishells were carried out using the boundary element method, indicating that the main optical features are located beyond the NIR region, showing a blue-shifted axial and a red-shifted transverse dipolar modes, therefore giving an anisotropic optical response.

(c) Additional simulations indicated that the optical properties of semishells with core sizes around 100 nm would be located within the vis - NIR spectral region, which is more interesting for biological applications. Unfortunately, our method was not suitable to obtain high quality semishells with such small core sizes.

(d) Self - assembly of gold semishells using the Langmuir - Blodgett technique was attempted taking advantage of their Janus behaviour. However, problems arose when transfering the monolayer to solid substrates.

2. Gold nanowire forests were successfully grown for the first time over 3D objects, using 260 nm silica particles as seeding substrates, so that a radial configuration was obtained and the length of the nanowires could be controlled (40 - 200 nm) by simply tuning the gold ions to seeds molar ratio.

   (a) The radial configuration and high nanowire density lead to strong plasmon coupling, which is reflected in a significant blue - shift of the plasmon band due to side - to - side interactions. However, when dettaching the nanowires from the silica surface their random distribution produces a red - shift, except for the shortest nanowires, which continue assembled side by side in solution.

   (b) A recently developed numerical approach (SIE - MoM) for the resolution of Maxwell's equations was employed to simulate the optical response of this complex structure, showing great accuracy and agreement with experimental measurements, both in radial configuration and in solution, opening the way for the study of more complex systems.

   (c) A rather simple adjustment of the synthesis conditions used for the preparation of gold semishells is expected to lead to the production of Janus silica particles half - covered with gold nanowires, which would enhance their possible applications in self - assembly and sensing.

3. Mesoporous thin films were employed to direct the growth of small gold branches on 60 nm gold spheres embedded in between two films with different pore sizes.

   (a) The pore network structure of the films in the bilayers keeps the order of the monolayers even in the presence of the gold particles, as confirmed by SAXS measurements.

(b) Elipsometric characterization confirmed the high porosity of the film sandwiches, thus envisaging enhanced catalytic properties when compared to composite materials comprising a mesoporous thin film covering a layer of particles directly attached to the substrate.

(c) Electron microscopy analysis indicated asymmetric growth of the gold spikes, but confirmation would require cutting film sections with a FIB and analysing the lamelas with a HRTEM.

4. A colloid chemistry approach based on the concept of protecting groups used in organic chemistry has been devised and implemented to synthesize gold - silica Janus nanostars.

(a) HAADF - STEM and HRTEM studies have shown the single crystallinity of short branches, which however become polycrystalline when second branches protrude from the shorter ones.

(b) The labile behaviour of the silica mask in water solution leads to Janus gold nanostars by gradual dissolution, so that the previously protected metal surface becomes accesible for further functionalization.

(c) We demonstrated that silver ions are needed to induce formation of gold branches, with length determined by the ratio between seeds and gold ions in solution.

(d) The Janus behavior of these spiky particles could lead to oriented assemblies with interesting SERS applications, but we chose a simpler system for the initial experiments, as described in the last chapter.

5. A pH triggered self - assembly process was used to prepare gold - silica core - satellite hybrid particles.

(a) Outer silica shells were grown to fix the self - assembled nanostructures, which could allow the functionalization of the exposed oxide layer to provide selectivity for biological applications.

(b) A multiplex color - sensitive SERS (bio)imaging system was demonstrated by the presence of two different dyes that are physically separated within the heterostructures.

(c) This promising structure could be interesting in drug delivery systems, by simply replacing RhB with a drug molecule and introducing a disassembly step of the hybrid satellites. By using the same technique the drug and the particles could be tracked independently by swithching the excitation wavelength.

Resumen

Ensamblaje Dirigido de Nanopartículas Tipo Janus para Aplicaciones en Detección por SERS

Con este resumen se pretende ofrecer una visión global del trabajo presentado en los diferentes capítulos de esta tesis. El objeto de estudio de este trabajo han sido las nanopartículas tipo Janus formadas por oro y sílice. Se han desarrollado diferentes rutas sintéticas con el fin de controlar el tamaño, geometría y propiedades ópticas de este sistema en distintas configuraciones. Las cambios en la morfología de las partículas han sido caracterizados por microscopía electrónica, y en algunos casos se han realizado simulaciones de sus propiedades ópticas para relacionar los resultados experimentales con las predicciones teóricas. Finalmente se ha llevado a cabo el ensamblaje dirigido de estas partículas y se han demostrado algunas de sus potenciales aplicaciones basadas en detección por dispersión Raman aumentada por superficie.

7.1 Objetivos

El trabajo que se presenta en esta tesis consiste principalmente en la preparación de nuevos tipos de nanopartículas de oro tipo Janus, para lo cual se han usado distintas aproximaciones. Los cambios inducidos en la geometría de las partículas han sido determinados por microscopía electrónica de transmisión y de barrido, de forma que se pudiesen correlacionar con sus propiedades ópticas. Se han realizado también simulaciones de sus propiedades ópticas para confirmar los resultados experimentales con la teoría. Se muestra adicionalmente el ensamblaje dirigido de partículas Janus, con el objetivo final de demostrar su potencial de cara a aplicaciones como sustratos para detección por dispersión Raman aumentada por superficie (SERS). El contenido de cada capítulo se justifica brevemente a continuación.

La primera mitad de la investigación realizada durante esta tesis fue realizada en el grupo de investigación de Química Coloidal, en el Departamento de Química Física de la Universidad de Vigo, mientras que la segunda se llevó a cabo en el Laboratorio de Bionanoplasmónica del Centro de Investigación Cooperativa en Biomateriales (CIC biomaGUNE, San Sebastián). Dado que ambos grupos de investigación están liderados por la misma persona, este cambio de localización no ha supuesto una ruptura en el desarrollo de la tesis. En ambos grupos, el principal tema de investigación se centra en la síntesis y ensamblaje de nanopartículas metálicas (oro y plata principalmente) para aplicaciones en la detección, con un enfoque importante en la técnica de SERS. Existe por tanto amplia experiencia en la preparación de partículas con formas y tamaños determinados, lo cual permite un control fino de las propiedades ópticas que estos coloides exhiben en las regiones ultravioleta - visible - infrarrojo cercano del espectro electromagnético. Una revisión bibliográfica realizada al comienzo de esta tesis puso de manifiesto el reciente interés en las nanopartículas tipo Janus (su nombre hace referencia a un dios romano con dos caras), las cuales presentan diferentes propiedades a ambos lados. Este tipo de partículas tiene un gran potencial de cara al ensamblaje dirigido a la formación de nuevas nanoestructuras o bien para su uso en catálisis, detección, etc. Por tanto, empleando la experiencia del grupo, durante esta tesis se han preparado nanopartículas tipo Janus formadas por oro y sílice, mediante el uso de métodos coloidales en disolución. Se ha escogido trabajar con oro debido a que es químicamente inerte en comparación con la plata, por lo que sus propiedades ópticas se mantienen durante largos períodos de tiempo, mientras que la sílice proporciona

estabilidad electrostática al sistema coloidal. Por consiguiente, el objetivo de esta tesis ha sido la preparación de nuevos tipos de nanopartículas Janus y el control de su ensamblaje para mejorar su capacidad en aplicaciones de detección por SERS.

El el Capítulo 2 se muestra la preparación de semiconchas de oro usando esferas de sílice de 495 nm de diámetro como moldes. El proceso se basa en la funcionalización parcial de la superficie de las esferas de sílice, usando emulsiones Pickering de agua y cera para enmascarar parte de la superficie. El posterior crecimiento de esferas pequeñas (1 - 3 nm) de oro adheridas sobre la parte funcionalizada conduce a la obtención de las semiconchas. Se han crecido también nanohilos de oro sobre esferas de sílice (Capítulo 3), como primer paso para obtener este tipo de partículas con geometría Janus en un futuro próximo. Para ambos sistemas se realizaron simulaciones de sus propiedades ópticas, estableciendo una relación directa entre los resultados experimentales y la teoría.

La preparación de partículas tipo Janus usando películas mesoporososas delgadas con diferente tamaño de poro como plantillas para el crecimiento de puntas de oro se muestra en el Capítulo 4. Se aporta una amplia caracterización de los films mediante microscopía electrónica de transmisión y de barrido, TEM y SEM respectivamente, porosimetría elipsométrica medioambiental (EEP) y dispersión de rayos X de bajo ángulo (SAXS).

Se han sintetizado nanoestrellas de oro y sílice empleando diferentes aproximaciones para la preparación de partículas tipo Janus en solución, tales como: el ensamblaje de una mezcla de ligandos mutuamente incompatibles sobre la superficie de un metal; la formación de una máscara de óxido de silicio y el posterior crecimiento de puntas de oro sobre la cara expuesta del metal (Capítulo 5). La estructura de las partículas obtenidas ha sido estudiada en profundidad mediante microscopía electrónica de transmisión de alta resolución y de barrido por transmisión, HRTEM y STEM respectivamente. En el Capítulo 6 se muestra el ensamblaje dirigido de partículas Janus de oro y sílice con esferas pequeñas de oro para formar nuevas nanoestructuras híbridas. También se demuestra la aplicación de estos ensamblajes como agentes de contraste para imagen por SERS.

Como resumen, se espera que esta tesis represente un avance significativo en la preparación de nuevas nanopartículas metálicas tipo Janus, considerando los métodos sintéticos empleados, la caracterización óptica junto a las simulaciones y las posibles aplicaciones de estos sistemas como herramientas de imagen para SERS

derivadas de su comportamiento único para el ensamblaje dirigido. Los resultados presentados podrían tener importantes aplicaciones en campos tan diversos como la catálisis, la biodetección o la formación de nuevas estructuras mediante auto - ensamblaje.

7.2 Introducción

En las últimas dos décadas se ha producido un gran desarrollo en el campo de la Química Coloidal para la obtención de nanopartículas con composición, tamaño y geometría determinadas. Si bien estos avances han permitido su utilización en diferentes campos como la catálisis, la detección de moléculas o en la liberación de fármacos, hoy en día el interés radica en combinar diferentes propiedades dentro de un mismo sistema para ampliar sus posibles aplicaciones.

Una primera aproximación para conseguir dicha combinación de propiedades consiste en el llamado ensamblaje dirigido de nanopartículas, basado en la unión controlada de estas unidades de construcción para formar estructuras de orden superior, que pueden ir desde pequeños clústeres a grandes estructuras tridimensionales. El proceso se puede modular químicamente, es decir, controlando las fuerzas intermoleculares entre los ligandos que se encuentran sobre las partículas, o bien aplicando campos externos (eléctricos y / o magnéticos). También es posible combinar propiedades dentro de una misma nanopartícula produciendo las llamadas partículas tipo Janus, las cuales presentan diferentes propiedades a ambos lados.

En el caso de las partículas metálicas, especialmente aquellas formadas por oro, plata y cobre, la reducción de su tamaño a la escala nanométrica tiene importantes implicaciones en sus propiedades ópticas, las cuales se encuentran entre las regiones visible e infrarrojo cercano del espectro electromagnético. Cuando estas partículas interaccionan con una radiación electromagnética se produce la oscilación coherente de los electrones de la banda de conducción del metal, produciendo resonancias de plasmones superficiales altamente confinados. Estos plasmones dependen del metal, del tamaño de partícula, de su geometría, de las moléculas que se encuentren en su superficie y de las propiedades dieléctricas del medio. Una consecuencia del ensamblaje de partículas metálicas es el acoplamiento de estos plasmones, produciendo incrementos importantes en la intensiadad del campo eléctrico generada en la zona intermedia entre dos o más partículas, lo cual ha aumentando en los úl-

timos años el interés por la espectroscopía por dispersión Raman aumentada por superficie (SERS), como técnica de ultradetección de moléculas. Las partículas tipo Janus presentan la ventaja de poder delimitar la región a través de la cual se pueden ensamblar con otras partículas, permitiendo un mayor grado de control sobre la estructura final (incluso dando lugar a geometrías inaccesibles con partículas simétricas), y por tanto de sus propiedades ópticas de cara a su aplicación en SERS.

7.3 Síntesis Coloidal de Semiconchas de Oro

En el Capítulo 2 se describe la preparación de semiconchas de oro sobre núcleos de sílice de 495 nm. El proceso se divide en dos partes: primero se obtienen partículas Janus de sílice funcionalizadas parcialmente con un aminosilano, y en una segunda parte se pegan y se crecen semillas de oro (1 - 3 nm) para formar una semiconcha homogénea. Las partículas Janus se han obtenido por un método basado en la formación de emulsiones *Pickering* de parafina fundida en agua y estabilizadas con partículas de sílice, dando lugar a coloidosomas que se pueden solidificar por disminución de la temperatura (Fig. 7.1 A).[89] La inmersión de las partículas de sílice en los coloidosomas se puede ajustar variando la concentración de un surfactante catiónico, bromuro de didodecildimetilamonio (DDAB), dando lugar a partículas Janus usando una concentración de 60 mg / L. Empleando la cera como máscara se puede funcionalizar la superficie expuesta de la sílice con un aminosilano, y tras disolver la cera se obtienen partículas Janus de sílice.[108] La presencia de grupos amino permite la adhesión de nanopartículas de oro selectivamente en un lado de las partículas de sílice, para posteriormente crecerlas mediante un método desarrollado por Halas y colaboradores para formar conchas completas de oro (Fig. 7.1 B).[243] Finalmente, la sílice se puede disolver para obtener semicápsulas huecas de oro (Fig. 7.1 C)).

Las propiedades ópticas de las semiconchas preparadas se encuentran principalmente en el infrarrojo, como se puede ver en las simulaciones de la Fig. 7.1 D. Los cálculos se han realizado mediante el método de elementos de contorno (BEM), utilizando como variables el grado de recubrimiento, el espesor y el tamaño de partícula (también se realizaron cálculos para núcleos de 100 nm). Es de destacar el desplazamiento a mayores longitudes de onda a medida que la partícula pierde simetría (de concha a semiconcha) para un mismo espesor.

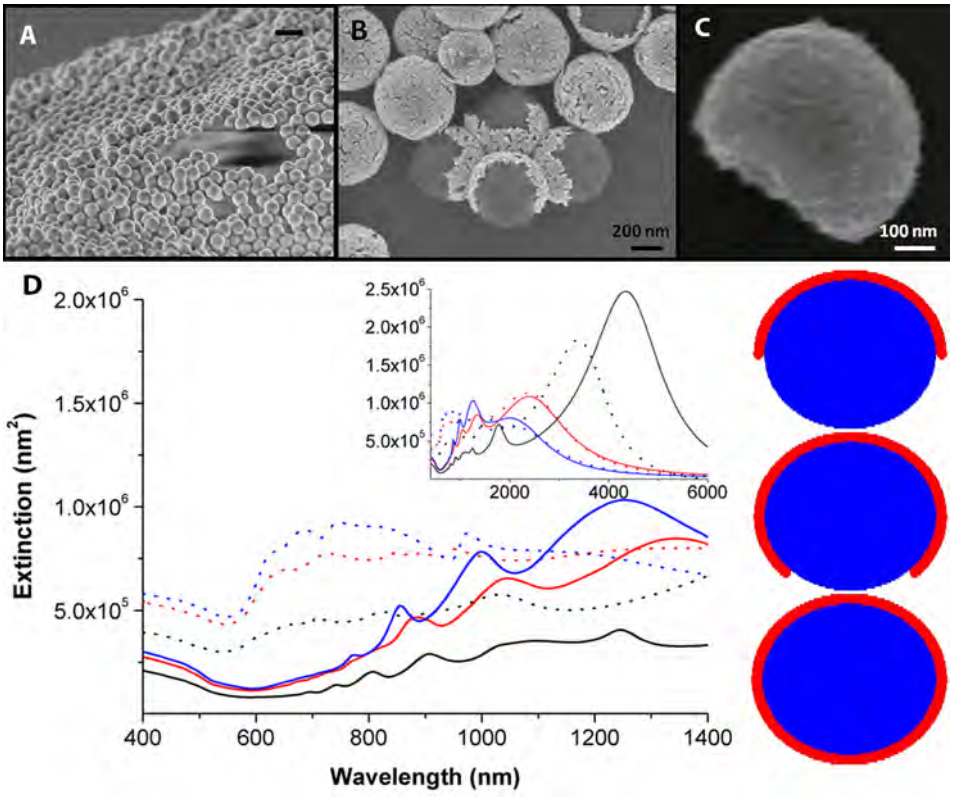

Figura 7.1. En la parte superior se muestran imágenes de SEM de partículas de sílice de 495 nm obtenidas usando [DDAB] = 60 mg / L: (A) Superficie de un coloidosoma (barra de escala 1 μm), (B) Semiconchas de oro y sílice, (C) Semicápsula de oro. En la parte inferior se muestran los espectros de extinción calculados para semiconchas de oro con núcleos de sílice de 495 nm y con 50 % (línea negra) y 75 % (línea roja) de recubrimiento metálico, y nanoconchas (totalmente cubiertas, línea azul). Se han usado dos grosores para las conchas de oro: 10 nm (líneas sólidas) y 30 nm (líneas punteadas). En el recuadro se muestran los mismos espectros para un intervalo de longitudes de onda hasta 6000 nm. A la derecha se representan los modelos geométricos empleados en las simulaciones.

7.4 Crecimiento Radial de Nanohilos de Oro con Plasmones Acoplados sobre Moldes Coloidales

Mediante una aproximación similar a la descrita anteriormente para la síntesis de semiconchas, en el Capítulo 3 se muestra el crecimiento de nanohilos de oro sobre esferas de sílice. Nanopartículas de sílice de 264 nm se han usado como moldes sobre los que se han adherido nanoesferas de oro de 4.3 nm. Empleando estas nanoesferas como semillas, a continuación se ha realizado el crecimiento de nanohilos de oro en disolución, dirigido por el ácido 4-mercaptobenzoico (4-MBA), mediante la adaptación de un método previamente descrito por He y colaboradores para crecer nanohilos sobre sustratos planos de sílice.[262] La longitud final de los nanohilos, hasta 200 nm, viene determinada por la relación entre la cantidad de sal de oro añadida y el número de partículas de sílice cubiertas de semillas, es decir, a menor número de semillas, la longitud de los hilos obtenidos será mayor, siempre y cuando el resto de condiciones se mantengan constantes. En la parte superior de la Fig. 7.2 B se puede observar una típica imagen de TEM de la mitad de una partícula recubierta con nanohilos.

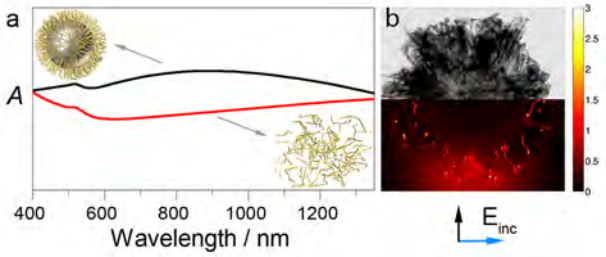

Figura 7.2. Simulaciones ópticas de nanohilos de oro. (A) Espectros de extinción simulados de nanohilos de oro radialmente distribuidos sobre la superficie de una esfera de sílice (negro) y aleatoriamente distribuidos en agua (rojo). Se muestran los modelos tridimensionales usados para las simulaciones, ambos compuestos por aproximadamente 1000 hilos. (B) Imagen de TEM acoplada al mapa del campo eléctrico calculado ($\lambda = 785$ nm) de los nanohilos distribuidos radialmente, mostrando la presencia de múltiples puntos calientes (más brillantes).

Se ha empleado un novedoso método numérico basado en ecuaciones integrales superficiales-formulación del método de los momentos (SIE-MoM, M3 solver), en colaboración con el Departamento de Teoría de la Señal y Comunicaciones (Univ. de Vigo), para determinar las propiedades ópticas del sistema completo en disolución, y también para el caso de nanohilos separados de la sílice, experimentalmente

realizado mediante la irradiación con ultrasonidos (Fig. 7.2 A). Cuando los nanohilos se encuentran sobre la sílice éstos están ensamblados de forma paralela entre sí, lo cual se refleja en que su banda plasmónica se encuentra desplazada hacia menores longitudes de onda. Por el contrario, al separarlos de la sílice se distribuyen de forma aleatoria en solución y la banda se desplaza a mayores longitudes de onda. Esto se observa con los nanohilos más largos (207 nm) y los de longitud intermedia (114 nm), mientras que los más cortos (38 nm) se mantienen ensamblados una vez despegados de la sílice, probablemente debido a la fuerte interacción entre los nanohilos y la molécula estabilizante (4 - MBA). Se muesra además en la parte inferior de la Fig. 7.2 C una simulación del campo eléctrico alrededor de la partícula, en donde se pueden ver en rojo los llamados puntos calientes, zonas cuya intensidad es muy elevada (importante para su uso en ultradetección por SERS).

7.5 Películas Mesoporosas Delgadas como Plantillas para el Crecimiento de Puntas de Oro sobre Nanopartículas de Oro

En el capítulo 4 se describe la preparación de un material compuesto de dos películas delgadas mesoporosas, con esferas de oro de 60 nm integradas en la zona de contacto entre ambas. Este trabajo se ha realizado en colaboración con la Dra. Paula Angelomé (Comisión Nacional de Energía Atómica, Buenos Aires). Esta configuración permite crecer puntas de oro sobre las esferas usando los poros de las películas delgadas como plantillas.[280] En la Fig. 7.3 A se muestra una imagen de TEM tras el crecimiento del sistema SBTF, formado por una película inferior de sílice y otra superior de óxido de titanio usando respectivamente Brij58 y F127 como plantillas de los poros. En este sistema se pueden distinguir las puntas de oro sobre las esferas y los poros de la mesoestructura. Adicionalmente se muestra una imagen de perfil, en la cual se puede apreciar que las nanopartículas se encuentran localizadas entre dos películas de óxido bien definidas. Se espera que el crecimiento de las puntas de oro solo se produzca a través de los poros más grandes, dando lugar a partículas tipo Janus. Aunque las imágenes de TEM sugieren un crecimiento asimétrico, esto podría ser un artificio derivado del carácter bidimensional de esta técnica. Por tanto, la única manera de asegurarse de la asimetría sería mediante la realización de cortes delgados de las películas en diferentes posiciones mediante un haz de iones focalizado (FIB en inglés), y examinar las lamelas resultantes

mediante TEM (este trabajo está en proceso).

Se ha estudiado el orden de los mesoporos con y sin partículas mediante dispersión de rayos X de bajo ángulo (SAXS). En la figura 7.3 B - C se pueden ver sendas imágenes tomadas a 4° y 90° respectivamente para el sistema SBTF con partículas de oro. Con esta técnica se puede concluir que el orden de los poros no se ve afectado significativamente por la presencia de las partículas de oro. Se ha comprobado mediante porosimetría elipsométrica medioambiental (EEP) que se han obtenido estructuras porosas con poros accesibles. En la Fig. 7.3 D - E se muestran las isotermas de adsorción de vapor de agua en los poros de la bicapa SBTF. Para comparar, se han incluido las respectivas isotermas de cada película cuando forman una monocapa. Se puede ver que en la bicapa disminuye la porosidad para ambas películas, aunque ésta sigue siendo altamente accesible a las moléculas de agua.

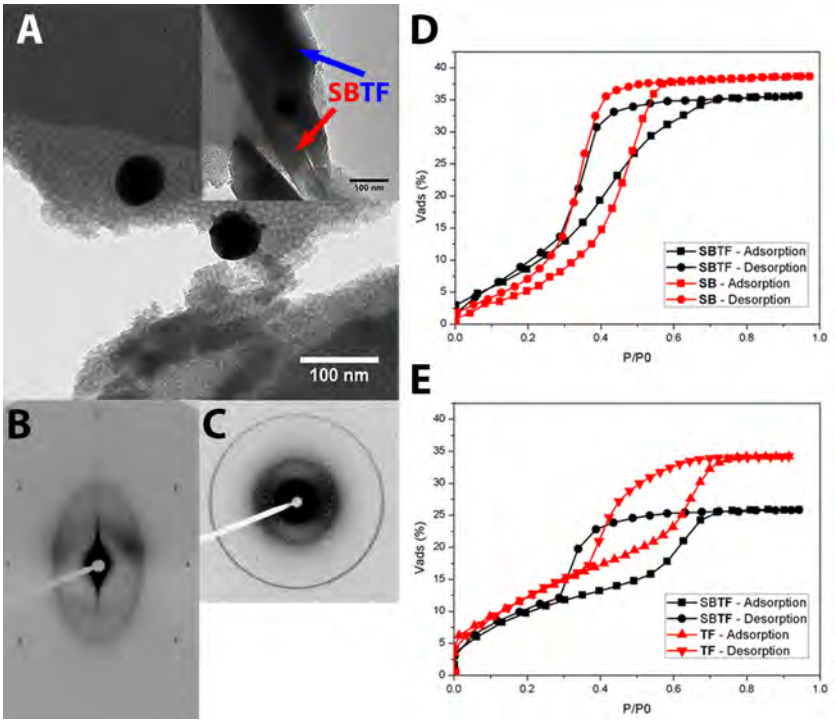

Figura 7.3. (A) Imagen de TEM de una bicapa SBTF con puntas de oro crecidas sobre esferas de oro de 60 nm (en el cuadro interior se muestra una vista de perfil); (B - C) Imágenes de SAXS a 4° y 90°, respectivamente, de una bicapa SBTF con esferas de oro; (D - E) Isotermas de adsorción - desorción de agua para el film SB formando una monocapa y en la bicapa SBTF (D), y para el film TF formando una monocapa y en la bicapa SBTF (E).

7.6 Una Aproximación Basada en Grupos Protectores hacia la Síntesis de Nanoestrellas Janus de Oro y Sílice

En el capítulo 5 se describe la aplicación de una aproximación ampliamente utilizada en síntesis orgánica, el uso de grupos protectores, para la obtención de nanoestrellas Janus de oro y sílice. En este caso, una semicápsula de sílice se ha crecido primero sobre una esfera de oro, para actuar como protección para dirigir el posterior crecimiento de puntas de oro sobre la superficie de metal no protegida (Fig. 7.4 A). Como todo grupo protector, se puede eliminar a posteriori mediante la dispersión de las partículas en agua. La longitud de las puntas de las semiestrellas se puede ajustar variando la cantidad de partículas semilla adicionadas durante el crecimiento de las puntas. En la Fig. 7.4 D se muestran los espectros de absorción de nanoestrellas Janus con diferente tamaño de puntas. Se observa asimismo que la banda plasmónica localizada a mayores longitudes de onda está determinada por las puntas, de forma que se desplaza más hacia el rojo según aumenta el tamaño de las puntas.

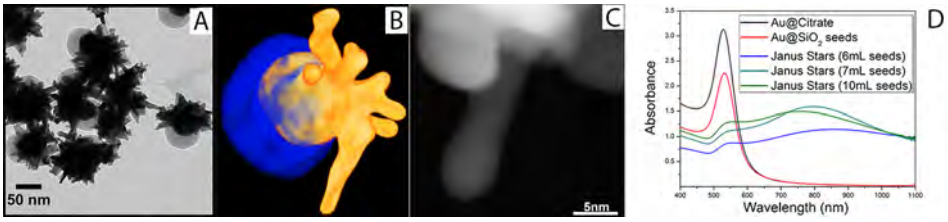

Figura 7.4. (A) Imagen de TEM de las nanoestrellas Janus de oro y sílice; (B) reconstrucción tridimensional de una nanoestrella Janus a partir de imágenes de HAADF - STEM, representando en azul la sílice y en amarillo el núcleo y las puntas de oro; (C) imagen de HRSTEM mostrando la monocristalinidad de las puntas de oro; (D) Espectro UV - visible de esferas de oro de 40 nm (negro), semillas Janus de oro y sílice (rojo), y nanoestrellas Janus usando diferentes cantidades de semillas, como se indica en la leyenda.

Estas partículas han sido caracterizadas por microscopía electrónica, tanto de transmisión como de barrido, para estudiar la asimetría del sistema. En la Fig. 7.4 B se muestra la reconstrucción tridimensional de una nanoestrella con puntas cortas, a partir de imágenes de microscopía electrónica de barrido por transmisión acoplado a un detector de campo oscuro anular de alto ángulo (HAADF - STEM). En esta imagen se ha coloreado en azul la sílice y en amarillo el núcleo y las puntas de oro. Mediante STEM de alta resolución (HRSTEM) se puede observar el carácter monocristalino de las puntas cuando éstas son cortas (Fig. 7.4 C), volviéndose

policristalinas cuando su longitud aumenta.

Estas partículas presentan puntas metálicas, en donde es bien sabido que se producen grandes incrementos en la intensidad del campo eléctrico al ser irradiadas con un haz luminoso, dando lugar a *puntos calientes* intrínsecos, lo cual unido a la posibilidad de realizar ensamblajes dirigidos por su geometría Janus, hace prever interesantes aplicaciones en SERS.

7.7 Satélites Híbridos como Etiquetas Modulables para SERS

Se ha mencionado repetidamente durante esta tesis la capacidad de las partículas Janus de ensamblarse para formar superestructuras que no se pueden obtener con partículas simétricas, así como de sus posibilidades en la detección por espectroscopía Raman aumentada por superficie (SERS). En el capítulo 6 se muestran los resultados del ensamblaje de las partículas Janus preparadas en el capítulo 5, junto con esferas de oro de 15 nm por modulación de pH. Este sistema permite la introducción de dos moléculas diferentes para su detección independiente por SERS: ácido 4 - mercaptobenzoico (4 - MBA) colocado bajo la semicapa de sílice en la partícula Janus, e isotiocianato de rodamina B (RhB) situado entre las partículas Janus y las esferas pequeñas de oro, en los llamado *puntos calientes*. Durante el proceso se forman partículas satelitales, con las esferas pequeñas adhiriéndose exclusivamente sobre la parte expuesta de las partículas Janus. Adicionalmente se forman dímeros de partículas Janus unidas por esferas pequeñas. Se trata de un proceso dinámico, pero se puede detener aumentando el pH de nuevo, lo que permite a su vez crecer una capa de sílice alrededor de las esferas mediante el conocido método de Stöber,[265] fijando y protegiendo la estructura (Fig. 7.5 A).

En la Fig. 7.5 B se muestran las capacidades del sistema en la detección por SERS en medio acuoso. Básicamente, dependiendo de la longitud de onda de excitación se pueden observar los picos derivados de las vibraciones de enlaces en la RhB (532 nm) y el 4 - MBA (785 nm) independientemente o ambos a la vez (633 nm). Además, las vibraciones correspondientes a cada molécula no se superponen, pudiendo así asignar cada vibración a la molécula correspondiente.

Finalmente, se han empleado estos satélites híbridos para tomar imágenes de células *in vitro* usando SERS (Fig. 7.5 C). Se ha conseguido detectar las partículas en medio biológico usando diferentes longitudes de onda de excitación, de forma que

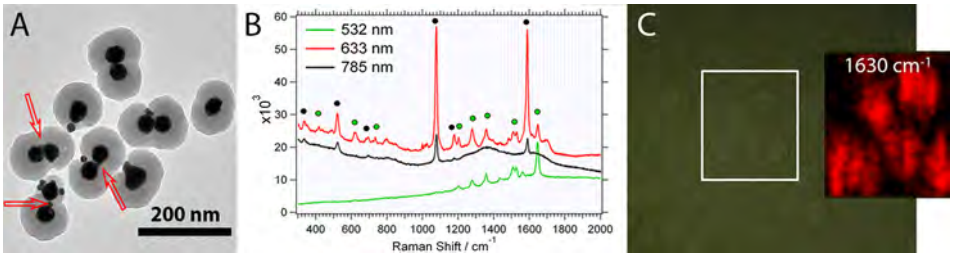

Figura 7.5. (A) Imagen TEM de los satélites híbridos y de los dímeros, indicando con flechas las esferas de oro de 15 nm que actúan como puentes de unión entre las partículas más grandes; (B) Espectros SERS de los satélites híbridos en dispersión, usando 3 longitudes de onda de excitación diferentes: 532 nm (verde), 785 nm (negro) y 633 nm (rojo), indicando con puntos verdes las vibraciones de la RhB y con puntos negros las del 4-MBA; (C) mapa SERS de la vibracion a 1630 cm^{-1} de la RhB de satélites híbridos incubados con macrófagos J774, medidos con iluminación a 532 nm.

se podría observar cada molécula por separado (iluminando a 532 nm y 785 nm) o ambas a la vez, por irradiación a 633 nm. Esto sirve como prueba de concepto de la aplicación de estos sistemas a la liberación controlada de fármacos, es decir, cambiando la RhB por un fármaco se podría seguir la liberación de éste a 532 nm y a su vez localizar las partículas a 785 nm.

7.8 Conclusiones

En conjunto esta tesis representa un avance significativo en la preparación de nuevos tipos de partículas Janus metálicas. Una gran variedad de métodos de síntesis han sido desarrollados con este fin, principalmente en solución pero también usando substratos sólidos. La caracterización óptica de las nanopartículas y de las nanoestructuras derivadas de ellas, junto con las simulaciones realizadas, prevén interesantes aplicaciones en SERS. Hemos mostrado este tipo de aplicaciones con los satélites híbridos, cuyo uso en análisis múltiple es el resultado de su estructura única como consecuencia de su autoensamblaje. Se esperan aplicaciones de estos sistemas en otros campos como la catálisis, nanomotores coloidales o la formación de nuevas estructuras. A continuación se indican las conclusiones más relevantes que se pueden extraer de la investigación llevada a cabo durante esta tesis.

1. Se ha desarrollado un proceso basado en emulsiones *Pickering* para sintetizar semiconchas y semicápsulas de oro con un núcleo de sílice de 495 nm.

(a) Este proceso permite la producción de grandes cantidades de partículas Janus, permitiendo el control de la geometría final mediante el ajuste de la cantidad de surfactante catiónico DDAB, el cual es responsable del grado de inmersión de las partículas en la cera.

(b) Simulaciones realizadas con BEM confirman que las principales propiedades ópticas están localizadas en el infrarrojo, mostrando un modo dipolar axial y otro transversal desplazados hacia el azul y el rojo respectivamente. Por lo tanto, muestran una respuesta anisotrópica.

(c) En cambio, las simulaciones para semiconchas con un núcleo de 100 nm indican que las propiedades ópticas estarían localizadas en la región visible - infrarrojo cercano, sin embargo no ha sido posible aplicar el mismo método para obtener semiconchas de alta calidad con tamaños tan reducidos.

(d) Se ha intentado ensamblar estas partículas usando una balanza de Langmuir - Blodgett aprovechando la geometría Janus, sin embargo surgieron problemas durante la transferencia de la monocapa al sustrato.

2. Por primera vez se han crecido bosques de nanohilos de oro sobre objetos tridimensionales (esferas de sílice de 260 nm), con una configuración radial y una longitud comprendida entre 40 y 200 nm.

(a) La configuración radial de los nanohilos da lugar a un acoplamiento de los plasmones por estar lateralmente próximos, reflejándose en un desplazamiento al azul de su banda plasmónica. La separación de los nanohilos de sus esferas soporte conlleva un desplazamiento del plasmón hacia mayores longitudes de onda, excepto en los más cortos, cuya fuerte interacción con el 4 - MBA hace que los nanohilos se mantengan ensamblados tras la separación de la sílice.

(b) Se ha empleado el método (SIE - MoM) para la resolución de las ecuaciones de Maxwell con el fin de simular las propiedades ópticas de esta estructura compleja. Los resultados muestran una gran concordancia entre la teoría y los resultados experimentales, abriendo así el camino al diseño de estructuras más complejas.

(c) Un simple ajuste de las condiciones para preparar las semiconchas de oro podría ser usado para producir partículas Janus de sílice recubiertas

parcialmente de nanohilos de oro, ampliando así sus posibilidades para el ensamblaje y la detección por SERS.

3. Se han usado películas finas mesoporosas como plantillas para dirigir el crecimiento de puntas de oro sobre esferas de oro de 60 nm embebidas entre dos películas con diferente tamaño de poro.

   (a) Las medidas de SAXS indican que la organización de los poros en las bicapas con partículas de oro mantienen el orden de las monocapas.

   (b) La caracterización por EEP ha confirmado la alta porosidad de las bicapas preparadas, lo cual permite prever una mayor actividad catalítica, en comparación con los materiales compuestos de una película recubriendo una monocapa de partículas directamente adheridas sobre el sustrato.

   (c) Las imágenes tomadas por microscopía electrónica sugieren que el crecimiento de puntas ha sido asimétrico, sin embargo para confirmarlo es necesario cortar secciones con un FIB y analizar las correspondientes lamelas por TEM.

4. Se ha empleado una sencilla aproximación coloidal basada en los grupos protectores usados en química orgánica para la preparación de nanoestrellas Janus de oro y sílice.

   (a) La presencia de iones de plata es necesaria para inducir el crecimiento de puntas de oro, estando su longitud determinada por la relación entre la concentración de iones de oro en disolución y la cantidad de partículas empleadas.

   (b) Se ha demostrado mediante imágenes de HAADF - STEM y HRTEM el carácter monocristalino de las puntas cuando son cortas, volviéndose policristalinas a medida que aumenta su longitud debido a que puntas secundarias crecen a partir de las primarias.

   (c) La capa protectora de sílice se puede eliminar fácilmente exponiendo las partículas a un medio acuoso, permitiendo así la funcionalización de la nueva superficie metálica expuesta.

   (d) El carácter Janus de las nanoestrellas presentadas podría dar lugar a ensamblajes orientados para aplicaciones en detección por SERS, sin embargo, ha sido elegido un sistema más sencillo para realizar la primera aproximación, como se discute en el último capítulo.

5. Se han preparado satélites híbridos mediante el ensamblaje dirigido por pH de partículas Janus de oro y sílice con esferas de 15 nm de oro.

   (a) Los ensamblajes se han recubierto de sílice para proteger la estructura, lo cual podría permitir su posterior funcionalización para proporcionar selectividad al sistema en posibles aplicaciones biológicas.

   (b) Se ha demostrado la aplicación de estas partículas, precargadas con dos moléculas sensibles a Raman, como sistema de imagen múltiple para SERS en células.

   (c) Esta estructura presenta interesantes aplicaciones como sistema de liberación de fármacos, cambiando la RhB por un fármaco e implementando un paso de desensamblaje de los satélites híbridos. Entonces, con la misma técnica (SERS), la droga y las partículas se podrían monitorizar independientemente cambiando la longitud de onda de excitación.

Bibliography

[1] U. Kreibig, L. Genzel, *Surface Science* **1985**, *156, Part 2*, 678 – 700.

[2] P. Zhao, N. Li, D. Astruc, *Coordination Chemistry Reviews* **2013**, *257*, 638–665.

[3] N. Li, P. Zhao, D. Astruc, *Angewandte Chemie International Edition* **2014**, *53*, 1756–1789.

[4] A. Bitar, N. M. Ahmad, H. Fessi, A. Elaissari, *Drug Discovery Today* **2012**, *17*, 1147 – 1154.

[5] B. A. Grzybowski, C. E. Wilmer, J. Kim, K. P. Browne, K. J. M. Bishop, *Soft Matter* **2009**, *5*, 1110–1128.

[6] M. Grzelczak, J. Vermant, E. M. Furst, L. M. Liz-Marzan, *ACS Nano* **2010**, *4*, 3591–3605.

[7] X. Xu, N. L. Rosi, Y. Wang, F. Huo, C. A. Mirkin, *Journal of the American Chemical Society* **2006**, *128*, 9286–9287.

[8] M. M. Maye, D. Nykypanchuk, M. Cuisinier, D. van der Lelie, O. Gang, *Nature Materials* **2009**, *8*, 388–391.

[9] W. Cheng, M. J. Campolongo, J. J. Cha, S. J. Tan, C. C. Umbach, D. A. Muller, D. Luo, *Nat Mater* **2009**, *8*, 519–525.

[10] R. Klajn, K. J. M. Bishop, B. A. Grzybowski, *Proceedings of the National Academy of Sciences* **2007**, *104*, 10305–10309.

[11] M. Grzelczak, A. Sanchez-Iglesias, H. H. Mezerji, S. Bals, J. Perez-Juste, L. M. Liz-Marzan, *Nano Letters* **2012**, *12*, 4380–4384.

[12] Z. Nie, D. Fava, E. Kumacheva, S. Zou, G. C. Walker, M. Rubinstein, *Nat Mater* **2007**, *6*, 609–614.

[13] M. Quintana, M. Prato, *Chem. Commun.* **2009**, 6005–6007.

[14] M. A. Olson, A. Coskun, R. Klajn, L. Fang, S. K. Dey, K. P. Browne, B. A. Grzybowski, J. F. Stoddart, *Nano Letters* **2009**, *9*, 3185–3190.

[15] M. A. Correa-Duarte, L. M. Liz-Marzan, *J. Mater. Chem.* **2006**, *16*, 22–25.

[16] Y. Zhao, K. Thorkelsson, A. J. Mastroianni, T. Schilling, J. M. Luther, B. J. Rancatore, K. Matsunaga, H. Jinnai, Y. Wu, D. Poulsen, J. M. J. Frechet, A. Paul Alivisatos, T. Xu, *Nat Mater* **2009**, *8*, 979–985.

[17] M. Mittal, E. M. Furst, *Advanced Functional Materials* **2009**, *19*, 3271–3278.

[18] T. Ding, K. Song, K. Clays, C.-H. Tung, *Advanced Materials* **2009**, *21*, 1936–1940.

[19] L. Hu, M. Chen, X. Fang, L. Wu, *Chem. Soc. Rev.* **2012**, *41*, 1350–1362.

[20] Q. Chen, S. C. Bae, S. Granick, *Nature* **2011**, *469*, 381–384.

[21] A. Klinkova, R. M. Choueiri, E. Kumacheva, *Chem. Soc. Rev.* **2014**, *43*, 3976–3991.

[22] J. B. Edel, A. A. Kornyshev, M. Urbakh, *ACS Nano* **2013**, *7*, 9526–9532.

[23] M. Faraday, *Philosophical Transactions of the Royal Society of London* **1857**, *147*, 145–181.

[24] S. Link, M. A. El-Sayed, *The Journal of Physical Chemistry B* **1999**, *103*, 8410–8426.

[25] P. Mulvaney, *Langmuir* **1996**, *12*, 788–800.

[26] T. Ung, L. M. Liz-Marzan, P. Mulvaney, *The Journal of Physical Chemistry B* **2001**, *105*, 3441–3452.

[27] F. Sala, S. D'Agostino, *Handbook of Molecular Plasmonics*, Taylor & Francis, **2013**.

[28] Y. Zhao, H. Pan, Y. Lou, X. Qiu, J. Zhu, C. Burda, *Journal of the American Chemical Society* **2009**, *131*, 4253–4261.

[29] J. M. Luther, P. K. Jain, T. Ewers, A. P. Alivisatos, *Nat Mater* **2011**, *10*, 361–366.

[30] I. Kriegel, J. Rodriguez-Fernandez, A. Wisnet, H. Zhang, C. Waurisch, A. Eychmüller, A. Dubavik, A. O. Govorov, J. Feldmann, *ACS Nano* **2013**, *7*, 4367–4377.

[31] G. Mie, *Annalen der Physik* **1908**, *330*, 377–445.

[32] C. F. Bohren, D. R. Huffman, *Absorption and Scattering of Light by Small Particles*, Wiley, New York, **1983**.

[33] R. Gans, *Ann. Phys.* **1912**, *37*, 881–900.

[34] V. Myroshnychenko, J. Rodriguez-Fernandez, I. Pastoriza-Santos, A. M. Funston, C. Novo, P. Mulvaney, L. M. Liz-Marzan, F. J. Garcia de Abajo, *Chem. Soc. Rev.* **2008**, *37*, 1792–1805.

[35] D. M. Solis, J. M. Taboada, F. Obelleiro, L. M. Liz-Marzan, F. J. Garcia de Abajo, *ACS Nano* **2014**, *8*, 7559–7570.

[36] E. M. Purcell, C. R. Pennypacker, *Astrophys. J.* **1973**, *186*, 705–714.

[37] B. T. Draine, P. J. Flatau, *J. Opt. Soc. Am. A* **1994**, *11*, 1491–1499.

[38] F. J. García de Abajo, A. Howie, *Phys. Rev. B* **2002**, *65*, 115418.

[39] M. Fleischmann, P. Hendra, A. McQuillan, *Chemical Physics Letters* **1974**, *26*, 163–166.

[40] D. L. Jeanmaire, R. P. Van Duyne, *Journal of Electroanalytical Chemistry and Interfacial Electrochemistry* **1977**, *84*, 1–20.

[41] M. G. Albrecht, J. A. Creighton, *Journal of the American Chemical Society* **1977**, *99*, 5215–5217.

[42] A. Otto in *Light Scattering in Solids IV*, *Vol. 54* (Eds.: M. Cardona, G. Guntherodt), Springer Berlin Heidelberg, **1984**, pp. 289–418.

[43] M. Moskovits, *Rev. Mod. Phys.* **1985**, *57*, 783–826.

[44] S. Nie, S. R. Emory, *Science* **1997**, *275*, 1102–1106.

[45] K. Kneipp, Y. Wang, H. Kneipp, L. T. Perelman, I. Itzkan, R. R. Dasari, M. S. Feld, *Phys. Rev. Lett.* **1997**, *78*, 1667–1670.

[46] S. Schlücker, *Angewandte Chemie International Edition* **2014**, *53*, 4756–4795.

[47] M. D. Sonntag, J. M. Klingsporn, A. B. Zrimsek, B. Sharma, L. K. Ruvuna, R. P. Van Duyne, *Chem. Soc. Rev.* **2014**, *43*, 1230–1247.

[48] T. Xiao, Q. Ye, L. Sun, *The Journal of Physical Chemistry B* **1997**, *101*, 632–638.

[49] K. L. Wustholz, A.-I. Henry, J. M. McMahon, R. G. Freeman, N. Valley, M. E. Piotti, M. J. Natan, G. C. Schatz, R. P. V. Duyne, *Journal of the American Chemical Society* **2010**, *132*, 10903–10910.

[50] C. J. Brinker, G. W. Scherer, *Sol-gel science*, San Diego, CA (USA); Academic Press Inc., **1990**.

[51] A. C. Pierre, *Introduction to Sol-Gel Processing*, Kluwer Publishers, **1998**.

[52] V. Chiola, J. E. Ritsko, C. D. Vanderpool, **1971**.

[53] C. T. Kresge, M. E. Leonowicz, W. J. Roth, J. C. Vartuli, J. S. Beck, *Nature* **1992**, *359*, 710–712.

[54] J. S. Beck, J. C. Vartuli, W. J. Roth, M. E. Leonowicz, C. T. Kresge, K. D. Schmitt, C. T. W. Chu, D. H. Olson, E. W. a. Sheppard, *Journal of the American Chemical Society* **1992**, *114*, 10834–10843.

[55] C.-Y. Chen, S. L. Burkett, H.-X. Li, M. E. Davis, *Microporous Materials* **1993**, *2*, 27–34.

[56] A. Monnier, F. Schüth, Q. Huo, D. Kumar, D. Margolese, R. S. Maxwell, G. D. Stucky, M. Krishnamurty, P. Petroff, A. Firouzi, M. Janicke, B. F. Chmelka, *Science* **1993**, *261*, 1299–1303.

[57] J. S. Beck, J. C. Vartuli, G. J. Kennedy, C. T. Kresge, W. J. Roth, S. E. Schramm, *Chemistry of Materials* **1994**, *6*, 1816–1821.

[58] Q. Huo, D. I. Margolese, U. Ciesla, P. Feng, T. E. Gier, P. Sieger, R. Leon, P. M. Petroff, F. Schuth, G. D. Stucky, *Nature* **1994**, *368*, 317–321.

[59] Q. Huo, D. I. Margolese, U. Ciesla, D. G. Demuth, P. Feng, T. E. Gier, P. Sieger, A. Firouzi, B. F. a. Chmelka, *Chemistry of Materials* **1994**, *6*, 1176–1191.

[60] D. M. Antonelli, J. Y. Ying, *Angew. Chem. Int. Ed. Engl.* **1995**, *34*, 2014–2017.

[61] N. Ulagappan, C. N. R. Rao, *Chem. Commun.* **1996**, 1685–1686.

[62] U. Ciesla, S. Schacht, G. D. Stucky, K. K. Unger, F. Schüth, *Angewandte Chemie International Edition in English* **1996**, *35*, 541–543.

[63] D. Feng, J. Wei, M. Wang, Q. Yue, Y. Deng, A. M. Asiri, D. Zhao, *Advanced Porous Materials* **2013**, *1*, 164–186.

[64] P. Innocenzi, L. Malfatti, *Chem. Soc. Rev.* **2013**, *42*, 4198–4216.

[65] M. Ogawa, *Journal of the American Chemical Society* **1994**, *116*, 7941–7942.

[66] M. Ogawa, *Chem. Commun.* **1996**, 1149–1150.

[67] H. Yang, A. Kuperman, N. Coombs, S. Mamiche-Afara, G. A. Ozin, *Nature* **1996**, *379*, 703–705.

[68] H. Yang, N. Coombs, I. Sokolov, G. A. Ozin, *Nature* **1996**, *381*, 589–592.

[69] Y. Lu, R. Ganguli, C. A. Drewien, M. T. Anderson, C. J. Brinker, W. Gong, Y. Guo, H. Soyez, B. Dunn, M. H. Huang, J. I. Zink, *Nature* **1997**, *389*, 364–368.

[70] D. Zhao, P. Yang, N. Melosh, J. Feng, B. F. Chmelka, G. D. Stucky, *Advanced Materials* **1998**, *10*, 1380–1385.

[71] C. J. Brinker, Y. Lu, A. Sellinger, H. Fan, *Advanced Materials* **1999**, *11*, 579–585.

[72] C. Casagrande, P. Fabre, E. Raphaël, M. Veyssié, *EPL (Europhysics Letters)* **1989**, *9*, 251.

[73] P. De Gennes, *Angewandte Chemie International Edition* **1992**, *31*, 842–845.

[74] Z. Zhang, S. Glotzer, *Nano Letters* **2004**, *4*, 1407–1413.

[75] S. Jiang, Q. Chen, M. Tripathy, E. Luijten, K. S. Schweizer, S. Granick, *Advanced Materials* **2010**, *22*, 1060–1071.

[76] Q. Chen, J. K. Whitmer, S. Jiang, S. C. Bae, E. Luijten, S. Granick, *Science* **2011**, *331*, 199–202.

[77] M. Lattuada, T. A. Hatton, *Nano Today* **2011**, *6*, 286–308.

[78] J. Hu, S. Zhou, Y. Sun, X. Fang, L. Wu, *Chemical Society Reviews* **2012**, *41*, 4356–4378.

[79] G. Loget, A. Kuhn, *Journal of Materials Chemistry* **2012**, *22*, 15457–15474.

[80] A. Walther, A. H. E. Müller, *Chemical Reviews* **2013**, *113*, 5194–5261.

[81] M. Feyen, C. Weidenthaler, F. Schueth, A.-H. Lu, *Journal of the American Chemical Society* **2010**, *132*, 6791–6799.

[82] J.-W. Kim, D. Lee, H. C. Shum, D. A. Weitz, *Advanced Materials* **2008**, *20*, 3239+.

[83] E. B. Mock, C. F. Zukoski, *Langmuir* **2010**, *26*, 13747–13750.

[84] N. Pazos-Perez, Y. Gao, M. Hilgendorff, S. Irsen, J. Pereez-Juste, M. Spasova, M. Farle, L. M. Liz-Marzan, M. Giersig, *Chemistry of Materials* **2007**, *19*, 4415–4422.

[85] A. Ohnuma, E. C. Cho, P. H. C. Camargo, L. Au, B. Ohtani, Y. Xia, *Journal of the American Chemical Society* **2009**, *131*, 1352+.

[86] C. Wang, H. Yin, S. Dai, S. Sun, *Chemistry of Materials* **2010**, *22*, 3277–3282.

[87] H. Takei, N. Shimizu, *Langmuir* **1997**, *13*, 1865–1868.

[88] Z. Bao, L. Chen, M. Weldon, E. Chandross, O. Cherniavskaya, Y. Dai, J. Tok, *Chemistry of Materials* **2002**, *14*, 24+.

[89] S. Jiang, S. Granick, *Langmuir* **2008**, *24*, 2438–2445.

[90] A. Perro, S. Reculusa, F. Pereira, M.-H. Delville, C. Mingotaud, E. Duguet, E. Bourgeat-Lami, S. Ravaine, *Chem. Commun.* **2005**, *44*, 5542–5543.

[91] A. Wolf, A. Walther, A. H. E. Mueller, *Macromolecules* **2011**, *44*, 9221–9229.

[92] D. M. Andala, S. H. R. Shin, H.-Y. Lee, K. J. M. Bishop, *ACS Nano* **2012**, *6*, 1044–1050.

[93] B. M. Teo, S. K. Suh, T. A. Hatton, M. Ashokkumar, F. Grieser, *Langmuir* **2011**, *27*, 30–33.

[94] C. Tang, C. Zhang, J. Liu, X. Qu, J. Li, Z. Yang, *Macromolecules* **2010**, *43*, 5114–5120.

[95] Z. Nie, W. Li, M. Seo, S. Xu, E. Kumacheva, *Journal of the American Chemical Society* **2006**, *128*, 9408–9412.

[96] T. Nisisako, T. Torii, T. Takahashi, Y. Takizawa, *Advanced Materials* **2006**, *18*, 1152–1156.

[97] C.-H. Chen, R. K. Shah, A. R. Abate, D. A. Weitz, *Langmuir* **2009**, *25*, 4320–4323.

[98] S. Seiffert, M. B. Romanowsky, D. A. Weitz, *Langmuir* **2010**, *26*, 14842–14847.

[99] S.-H. Kim, S.-J. Jeon, W. C. Jeong, H. S. Park, S.-M. Yang, *Advanced Materials* **2008**, *20*, 4129–4134.

[100] S. Lone, S. H. Kim, S. W. Nam, S. Park, I. W. Cheong, *Langmuir* **2010**, *26*, 17975–17980.

[101] S. Lone, S. H. Kim, S. W. Nam, S. Park, J. Joo, I. W. Cheong, *Chemical Communications* **2011**, *47*, 2634–2636.

[102] K.-H. Roh, D. C. Martin, J. Lahann, *Nat Mater* **2005**, *4*, 759–763.

[103] K.-H. Roh, M. Yoshida, J. Lahann, *Langmuir* **2007**, *23*, 5683–5688.

[104] A. C. Misra, S. Bhaskar, N. Clay, J. Lahann, *Advanced Materials* **2012**, *24*, 3850–3856.

[105] K. Eriksson, L. Johansson, E. Gothelid, L. Nyholm, S. Oscarsson, *Journal of Materials Chemistry* **2012**, *22*, 7681–7683.

[106] S. Zhang, Z. Li, S. Samarajeewa, G. Sun, C. Yang, K. L. Wooley, *Journal of the American Chemical Society* **2011**, *133*, 11046–11049.

[107] O. Cayre, V. Paunov, O. Velev, *Journal of Materials Chemistry* **2003**, *13*, 2445–2450.

[108] S. Jiang, M. J. Schultz, Q. Chen, J. S. Moore, S. Granick, *Langmuir* **2008**, *24*, 10073–10077.

[109] A. Jackson, J. Myerson, F. Stellacci, *Nature Materials* **2004**, *3*, 330–336.

[110] A. Centrone, Y. Hu, A. M. Jackson, G. Zerbi, F. Stellacci, *Small* **2007**, *3*, 814–817.

[111] C. Gentilini, L. Pasquato, *Journal of Materials Chemistry* **2010**, *20*, 1403–1412.

[112] C. Vilain, F. Goettmann, A. Moores, P. Le Floch, C. Sanchez, *Journal of Materials Chemistry* **2007**, *17*, 3509–3514.

[113] H. Kim, R. P. Carney, J. Reguera, Q. K. Ong, X. Liu, F. Stellacci, *Advanced Materials* **2012**, *24*, 3857–3863.

[114] J. van Herrikhuyzen, G. Portale, J. C. Gielen, P. C. M. Christianen, N. A. J. M. Sommerdijk, S. C. J. Meskers, A. P. H. J. Schenning, *Chemical Communications* **2008**, 697–699.

[115] R. T. M. Jakobs, J. van Herrikhuyzen, J. C. Gielen, P. C. M. Christianen, S. C. J. Meskers, A. P. H. J. Schenning, *Journal of Materials Chemistry* **2008**, *18*, 3438–3441.

[116] V. Sashuk, R. Holyst, T. Wojciechowski, M. Fialkowski, *Journal of Colloid and Interface Science* **2012**, *375*, 180–186.

[117] S. Pradhan, L.-P. Xu, S. Chen, *Advanced Functional Materials* **2007**, *17*, 2385–2392.

[118] S. Pradhan, L. E. Brown, J. P. Konopelski, S. Chen, *Journal of Nanoparticle Research* **2009**, *11*, 1895–1903.

[119] Y. Song, L. M. Klivansky, Y. Liu, S. Chen, *Langmuir* **2011**, *27*, 14581–14588.

[120] T. Chen, G. Chen, S. Xing, T. Wu, H. Chen, *Chemistry of Materials* **2010**, *22*, 3826–3828.

[121] F. Huo, A. K. R. Lytton-Jean, C. A. Mirkin, *Advanced Materials* **2006**, *18*, 2304+.

[122] S. Ye, R. L. Carroll, *ACS Applied Materials and Interfaces* **2010**, *2*, 616–620.

[123] R. Sardar, J. S. Shumaker-Parry, *Nano Letters* **2008**, *8*, 731–736.

[124] B. Wang, B. Li, B. Zhao, C. Y. Li, *Journal of the American Chemical Society* **2008**, *130*, 11594–11595.

[125] B. Wang, B. Dong, B. Li, B. Zhao, C. Y. Li, *Polymer* **2010**, *51*, 4814–4822.

[126] B. Dong, B. Li, C. Y. Li, *Journal of Materials Chemistry* **2011**, *21*, 13155–13158.

[127] L. Carbone, P. D. Cozzoli, *Nano Today* **2010**, *5*, 449–493.

[128] S. Xing, Y. Feng, Y. Y. Tay, T. Chen, J. Xu, M. Pan, J. He, H. H. Hng, Q. Yan, H. Chen, *Journal of the American Chemical Society* **2010**, *132*, 9537–9539.

[129] T. Pellegrino, A. Fiore, E. Carlino, C. Giannini, P. D. Cozzoli, G. Ciccarella, M. Respaud, L. Palmirotta, R. Cingolani, L. Manna, *Journal of the American Chemical Society* **2006**, *128*, 6690–6698.

[130] M. Grzelczak, J. Perez-Juste, P. Mulvaney, L. M. Liz-Marzan, *Chemical Society Reviews* **2008**, *37*, 1783–1791.

[131] Y.-H. Xu, J.-P. Wang, *Advanced Materials* **2008**, *20*, 994.

[132] Y. Feng, J. He, H. Wang, Y. Y. Tay, H. Sun, L. Zhu, H. Chen, *Journal of the American Chemical Society* **2012**, *134*, 2004–2007.

[133] J.-H. Lee, G.-H. Kim, J.-M. Nam, *Journal of the American Chemical Society* **2012**, *134*, 5456–5459.

[134] J. Love, B. Gates, D. Wolfe, K. Paul, G. Whitesides, *Nano Letters* **2002**, *2*, 891–894.

[135] Y. Lu, H. Xiong, X. Jiang, Y. Xia, M. Prentiss, G. M. Whitesides, *Journal of the American Chemical Society* **2003**, *125*, 12724–12725.

[136] D. Suzuki, H. Kawaguchi, *Colloid and Polymer Science* **2006**, *284*, 1471–1476.

[137] V. Paunov, O. Cayre, *Advanced Materials* **2004**, *16*, 788+.

[138] S. G. Jang, S.-H. Kim, S. Y. Lee, W. C. Jeong, S.-M. Yang, *Journal of Colloid and Interface Science* **2010**, *350*, 387–395.

[139] Z. Zhao, Z. Shi, Y. Yu, G. Zhang, *langmuir* **2012**, *28*, 2382–2386.

[140] S. Yang, J. Xu, Z. Wang, H. Zeng, Y. Lei, *Journal of Materials Chemistry* **2011**, *21*, 11930–11935.

[141] M. Correa-Duarte, V. Salgueirino-Maceira, B. Rodriguez-Gonzalez, L. Liz-Marzan, A. Kosiorek, W. Kandulski, M. Giersig, *Advanced Materials* **2005**, *17*, 2014.

[142] T. Brugarolas, B. J. Park, M. H. Lee, D. Lee, *Advanced Functional Materials* **2011**, *21*, 3924–3931.

[143] S. Jiang, S. Granick, *Langmuir* **2009**, *25*, 8915–8918.

[144] S. Pradhan, D. Ghosh, S. Chen, *ACS Applied Materials and Interfaces* **2009**, *1*, 2060–2065.

[145] L. Hong, S. Jiang, S. Granick, *Langmuir* **2006**, *22*, 9495–9499.

[146] A. Perro, F. Meunier, V. Schmitt, S. Ravaine, *Colloids and Surfaces A: Physicochemical and Engineering Aspects* **2009**, *332*, 57 – 62.

[147] H. Gu, Z. Yang, J. Gao, C. Chang, B. Xu, *Journal of the American Chemical Society* **2005**, *127*, 34–35.

[148] Y. Pan, J. Gao, B. Zhang, X. Zhang, B. Xu, *Langmuir* **2010**, *26*, 4184–4187.

[149] B. Liu, W. Wei, X. Qu, Z. Yang, *Angew. Chem. Int. Ed.* **2008**, *47*, 3973–3975.

[150] D. Suzuki, S. Tsuji, H. Kawaguchi, *Journal of the American Chemical Society* **2007**, *129*, 8088.

[151] F. Wang, N. Phonthammachai, K. Y. Mya, W. W. Tjiu, C. He, *Chem. Commun.* **2011**, *47*, 767–769.

[152] C.-C. Ho, W.-S. Chen, T.-Y. Shie, J.-N. Lin, C. Kuo, *Langmuir* **2008**, *24*, 5663–5666.

[153] C.-C. Lin, C.-W. Liao, Y.-C. Chao, C. Kuo, *ACS Applied Materials and Interfaces* **2010**, *2*, 3185–3191.

[154] M. D. McConnell, M. J. Kraeutler, S. Yang, R. J. Composto, *Nano Letters* **2010**, *10*, 603–609.

[155] T. Chen, M. Yang, X. Wang, L. H. Tan, H. Chen, *Journal of the American Chemical Society* **2008**, *130*, 11858–11859.

[156] L. H. Tan, S. Xing, T. Chen, G. Chen, X. Huang, H. Zhang, H. Chen, *ACS Nano* **2009**, *3*, 3469–3474.

[157] J. He, M. T. Perez, P. Zhang, Y. Liu, T. Babu, J. Gong, Z. Nie, *Journal of the American Chemical Society* **2012**, *134*, 3639–3642.

[158] J. He, P. Zhang, J. Gong, Z. Nie, *Chemical Communications* **2012**, *48*, 7344–7346.

[159] D. W. Lim, S. Hwang, O. Uzun, F. Stellacci, J. Lahann, *Macromolecular Rapid Communications* **2010**, *31*, 176–182.

[160] A. Ohnuma, E. C. Cho, M. Jiang, B. Ohtani, Y. Xia, *Langmuir* **2009**, *25*, 13880–13887.

[161] H. Yabu, K. Koike, K. Motoyoshi, T. Higuchi, M. Shimomura, *Macromolecular Rapid Communications* **2010**, *31*, 1267–1271.

[162] T. Rao, X.-H. Dong, B. C. Katzenmeyer, C. Wesdemiotis, S. Z. D. Cheng, M. L. Becker, *Soft Matter* **2012**, *8*, 2965–2971.

[163] M. R. Rasch, E. Rossinyol, J. L. Hueso, B. W. Goodfellow, J. Arbiol, B. A. Korgel, *Nano Letters* **2010**, *10*, 3733–3739.

[164] E. Jeong, K. Kim, I. Choi, S. Jeong, Y. Park, H. Lee, S. H. Kim, L. P. Lee, Y. Choi, T. Kang, *Nano Letters* **2012**, *12*, 2436–2440.

[165] H. Yu, M. Chen, P. Rice, S. Wang, R. White, S. Sun, *Nano Letters* **2005**, *5*, 379–382.

[166] L. Zhang, Y. Dou, H. Gu, *Journal of Colloid and Interface Science* **2006**, *297*, 660–664.

[167] J. Jiang, H. Gu, H. Shao, E. Devlin, G. C. Papaefthymiou, J. Y. Ying, *Advanced Materials* **2008**, *20*, 4403–4407.

[168] X. Gao, L. Yu, R. MacCuspie, H. Matsui, *Advanced Materials* **2005**, *17*, 426.

[169] J. Yang, H. I. Elim, Q. Zhang, J. Y. Lee, W. Ji, *Journal of the American Chemical Society* **2006**, *128*, 11921–11926.

[170] A. E. Saunders, I. Popov, U. Banin, *Zeitschrift fuer Anorganische und Allgemeine Chemie* **2007**, *633*, 2414–2419.

[171] H. Bao, W. Peukert, R. K. Taylor, *Advanced Materials* **2011**, *23*, 2644–2649.

[172] Z. W. Seh, S. Liu, S.-Y. Zhang, M. S. Bharathi, H. Ramanarayan, M. Low, K. W. Shah, Y.-W. Zhang, M.-Y. Han, *Angew. Chem. Int. Ed.* **2011**, *50*, 10140–10143.

[173] W. Shi, H. Zeng, Y. Sahoo, T. Ohulchanskyy, Y. Ding, Z. Wang, M. Swihart, P. Prasad, *Nano Letters* **2006**, *6*, 875–881.

[174] M. R. Buck, J. F. Bondi, R. E. Schaak, *Nature Chemistry* **2012**, *4*, 37–44.

[175] J. Yang, J. Y. Ying, *Journal of the American Chemical Society* **2010**, *132*, 2114.

[176] J. Zeng, J. Huang, C. Liu, C. H. Wu, Y. Lin, X. Wang, S. Zhang, J. Hou, Y. Xia, *Advanced Materials* **2010**, *22*, 1936.

[177] G. A. Sotiriou, A. M. Hirt, P.-Y. Lozach, A. Teleki, F. Krumeich, S. E. Pratsinis, *Chemistry of Materials* **2011**, *23*, 1985–1992.

[178] G. Menagen, J. E. Macdonald, Y. Shemesh, I. Popov, U. Banin, *Journal of the American Chemical Society* **2009**, *131*, 17406–17411.

[179] L. Carbone, A. Jakab, Y. Khalavka, C. Soennichsen, *Nano Letters* **2009**, *9*, 3710–3714.

[180] S. Chakrabortty, J. A. Yang, Y. M. Tan, N. Mishra, Y. Chan, *Angewandte Chemie International Edition* **2010**, *49*, 2888–2892.

[181] S. Deka, A. Falqui, G. Bertoni, C. Sangregorio, G. Poneti, G. Morello, M. De Giorgi, C. Giannini, R. Cingolani, L. Manna, P. D. Cozzoli, *Journal of the American Chemical Society* **2009**, *131*, 12817–12828.

[182] T. Mokari, C. Sztrum, A. Salant, E. Rabani, U. Banin, *Nature Materials* **2005**, *4*, 855–863.

[183] J. Maynadie, A. Salant, A. Falqui, M. Respaud, E. Shaviv, U. Banin, K. Soulantica, B. Chaudret, *Angewandte Chemie International Edition* **2009**, *48*, 1814–1817.

[184] T. Wetz, K. Soulantica, A. Talqui, M. Respaud, E. Snoeck, B. Chaudret, *Angewandte Chemie International Edition* **2007**, *46*, 7079–7081.

[185] Z.-H. Lin, Y.-W. Lin, K.-H. Lee, H.-T. Chang, *Journal of Materials Chemistry* **2008**, *18*, 2569–2572.

[186] T. P. Vinod, M. Yang, J. Kim, N. A. Kotov, *Langmuir* **2009**, *25*, 13545–13550.

[187] P. H. C. Camargo, Y. Xiong, L. Ji, J. M. Zuo, Y. Xia, *Journal of the American Chemical Society* **2007**, *129*, 15452.

[188] C. Pacholski, A. Kornowski, H. Weller, *Angewandte Chemie International Edition* **2004**, *43*, 4774–4777.

[189] M. Casavola, V. Grillo, E. Carlino, C. Giannini, F. Gozzo, E. Fernandez Pinel, M. Angel Garcia, L. Manna, R. Cingolani, P. Davide Cozzoli, *Nano Letters* **2007**, *7*, 1386–1395.

[190] L. O. Mair, B. Evans, A. R. Hall, J. Carpenter, A. Shields, K. Ford, M. Millard, R. Superfine, *Journal of Physics D: Applied Physics* **2011**, *44*, 125001.

[191] K. Chaudhary, Q. Chen, J. J. Juarez, S. Granick, J. A. Lewis, *Journal of the American Chemical Society* **2012**, *134*, 12901–12903.

[192] S. Choi, E. Kim, T. Hyeon, *Journal of the American Chemical Society* **2006**, *128*, 2520–2521.

[193] M. Casavola, A. Falqui, M. Angel Garcia, M. Garcia-Hernandez, C. Giannini, R. Cingolani, P. D. Cozzoli, *Nano Letters* **2009**, *9*, 366–376.

[194] C. Wang, W. Tian, Y. Ding, Y.-q. Ma, Z. L. Wang, N. M. Markovic, V. R. Stamenkovic, H. Daimon, S. Sun, *Journal of the American Chemical Society* **2010**, *132*, 6524–6529.

[195] L. De Trizio, A. Figuerola, L. Manna, A. Genovese, C. George, R. Brescia, Z. Saghi, R. Simonutti, M. Van Huis, A. Falqui, *ACS Nano* **2012**, *6*, 32–41.

[196] M. Pang, J. Hu, H. C. Zeng, *Journal of the American Chemical Society* **2010**, *132*, 10771–10785.

[197] G. Loget, V. Lapeyre, P. Garrigue, C. Warakulwit, J. Limtrakul, M.-H. Delville, A. Kuhn, *Chemistry of Materials* **2011**, *23*, 2595–2599.

[198] C. M. Sweeney, W. Hasan, C. L. Nehl, T. W. Odom, *Journal of Physical Chemistry A* **2009**, *113*, 4265–4268.

[199] J. Zeng, C. Zhu, J. Tao, M. Jin, H. Zhang, Z.-Y. Li, Y. Zhu, Y. Xia, *Angewandte Chemie International Edition* **2012**, *51*, 2354–2358.

[200] C. Xu, B. Wang, S. Sun, *Journal of the American Chemical Society* **2009**, *131*, 4216.

[201] N. Glaser, D. J. Adams, A. Boeker, G. Krausch, *Langmuir* **2006**, *22*, 5227–5229.

[202] B. J. Park, T. Brugarolas, D. Lee, *Soft Matter* **2011**, *7*, 6413–6417.

[203] H. Wang, G. Goodrich, F. Tam, C. Oubre, P. Nordlander, N. Halas, *Journal of Physical Chemistry B* **2005**, *109*, 11083–11087.

[204] N. A. Mirin, N. J. Halas, *Nano Letters* **2009**, *9*, 1255–1259.

[205] N. S. King, Y. Li, C. Ayala-Orozco, T. Brannan, P. Nordlander, N. J. Halas, *ACS Nano* **2011**, *5*, 7254–7262.

[206] J. Ye, P. Van Dorpe, W. Van Roy, K. Lodewijks, I. De Vlaminck, G. Maes, G. Borghs, *The Journal of Physical Chemistry C* **2009**, *113*, 3110–3115.

[207] E. Prodan, C. Radloff, N. Halas, P. Nordlander, *Science* **2003**, *302*, 419–422.

[208] R. M. Cole, J. J. Baumberg, F. J. Garcia de Abajo, S. Mahajan, M. Abdelsalam, P. N. Bartlett, *Nano Letters* **2007**, *7*, 2094–2100.

[209] J. Ye, N. Verellen, W. Van Roy, L. Lagae, G. Maes, G. Borghs, P. Van Dorpe, *ACS Nano* **2010**, *4*, 1457–1464.

[210] M. Cortie, M. Ford, *Nanotechnology* **2007**, *18*, 235704.

[211] O. Peña-Rodríguez, U. Pal, *The Journal of Physical Chemistry C* **2011**, *115*, 22271–22275.

[212] E. Shaviv, O. Schubert, M. Alves-Santos, G. Goldoni, R. Di Felice, F. Vallee, N. Del Fatti, U. Banin, C. Soennichsen, *ACS Nano* **2011**, *5*, 4712–4719.

[213] H.-R. Jiang, N. Yoshinaga, M. Sano, *Physical Review Letters* **2010**, *105*, 268302.

[214] G. Rosenthal, K. E. Gubbins, S. H. L. Klapp, *Journal of Chemical Physics* **2012**, *136*, year.

[215] Y. Liu, W. Li, T. Perez, J. D. Gunton, G. Brett, *Langmuir* **2012**, *28*, 3–9.

[216] S. Gangwal, O. J. Cayre, O. D. Velev, *Langmuir* **2008**, *24*, 13312–13320.

[217] S. K. Smoukov, S. Gangwal, M. Marquez, O. D. Velev, *Soft Matter* **2009**, *5*, 1285–1292.

[218] H. Xing, Z. Wang, Z. Xu, N. Y. Wong, Y. Xiang, G. L. Liu, Y. Lu, *ACS Nano* **2012**, *6*, 802–809.

[219] Z. Li, E. Cheng, W. Huang, T. Zhang, Z. Yang, D. Liu, Z. Tang, *Journal of the American Chemical Society* **2011**, *133*, 15284–15287.

[220] E. R. Zubarev, J. Xu, A. Sayyad, J. D. Gibson, *Journal of the American Chemical Society* **2006**, *128*, 15098–15099.

[221] B. Wang, B. Li, B. Dong, B. Zhao, C. Y. Li, *Macromolecules* **2010**, *43*, 9234–9238.

[222] J. K. Sahoo, M. N. Tahir, F. Hoshyargar, B. Nakhjavan, R. Branscheid, U. Kolb, W. Tremel, *Angewandte Chemie International Edition* **2011**, *50*, 12271–12275.

[223] R. A. Alvarez-Puebla, L. M. Liz-Marzan, *Small* **2010**, *6*, 604–610.

[224] J. M. Romo-Herrera, R. A. Alvarez-Puebla, L. M. Liz-Marzan, *Nanoscale* **2011**, *3*, 1304–1315.

[225] Z. W. Seh, S. Liu, M. Low, S.-Y. Zhang, Z. Liu, A. Mlayah, M.-Y. Han, *Advanced Materials* **2012**, *24*, 2310–2314.

[226] J. Wang, W. Gao, *ACS Nano* **2012**, *6*, 5745–5751.

[227] J. R. Howse, R. A. L. Jones, A. J. Ryan, T. Gough, R. Vafabakhsh, R. Golestanian, *Physical Review Letters* **2007**, *99*, 048102.

[228] P. M. Wheat, N. A. Marine, J. L. Moran, J. D. Posner, *langmuir* **2010**, *26*, 13052–13055.

[229] N. Chaturvedi, Y. Hong, A. Sen, D. Velegol, *langmuir* **2010**, *26*, 6308–6313.

[230] R. A. Pavlick, S. Sengupta, T. McFadden, H. Zhang, A. Sen, *Angewandte Chemie International Edition* **2011**, *50*, 9374–9377.

[231] S. J. Ebbens, J. R. Howse, *Langmuir* **2011**, *27*, 12293–12296.

[232] H. Wang, G. Zhao, M. Pumera, *Journal of the American Chemical Society* **2014**, *136*, 2719–2722.

[233] W. Wang, L. A. Castro, M. Hoyos, T. E. Mallouk, *ACS Nano* **2012**, *6*, 6122–6132.

[234] V. Garcia-Gradilla, J. Orozco, S. Sattayasamitsathit, F. Soto, F. Kuralay, A. Pourazary, A. Katzenberg, W. Gao, Y. Shen, J. Wang, *ACS Nano* **2013**, *7*, 9232–9240.

[235] L. Baraban, M. Tasinkevych, M. N. Popescu, S. Sanchez, S. Dietrich, O. G. Schmidt, *Soft Matter* **2012**, *8*, 48–52.

[236] F. Lugli, E. Brini, F. Zerbetto, *Journal of Physical Chemistry C* **2012**, *116*, 592–598.

[237] P. de Gennes, *Angew. Chem. Int. Ed.* **1992**, *31*, 842–845.

[238] T. Isojima, M. Lattuada, J. B. Vander Sande, T. A. Hatton, *ACS Nano* **2008**, *2*, 1799–1806.

[239] R. N. Klupp Taylor, H. Bao, C. Tian, S. Vasylyev, W. Peukert, *Langmuir* **2010**, *26*, 13564–13571.

[240] P. Van Dorpe, J. Ye, *ACS Nano* **2011**, *5*, 6774–6778.

[241] C. M. Soukoulis, S. Linden, M. Wegener, *Science* **2007**, *315*, 47–49.

[242] Y. Lu, G. L. Liu, J. Kim, Y. X. Mejia, L. P. Lee, *Nano Letters* **2005**, *5*, 119–124.

[243] B. E. Brinson, J. B. Lassiter, C. S. Levin, R. Bardhan, N. Mirin, N. J. Halas, *Langmuir* **2008**, *24*, 14166–14171.

[244] F. García de Abajo, A. Howie, *Physical review letters* **1998**, *80*, 5180–5183.

[245] G. Bogush, M. Tracy, C. Z. IV, *Journal of Non-Crystalline Solids* **1988**, *104*, 95 – 106.

[246] D. G. Duff, A. Baiker, P. P. Edwards, *Langmuir* **1993**, *9*, 2301–2309.

[247] P. B. Johnson, R. W. Christy, *Phys. Rev. B* **1972**, *6*, 4370–4379.

[248] E. Palik, *Handbook of Optical Constants of Solids*, Academic Press, **1985**.

[249] L. White, C. Tripp, *Journal of Colloid and Interface Science* **2000**, *232*, 400 – 407.

[250] S. Oldenburg, R. Averitt, S. Westcott, N. Halas, *Chemical Physics Letters* **1998**, *288*, 243 – 247.

[251] D. V. Leff, L. Brandt, J. R. Heath, *Langmuir* **1996**, *12*, 4723–4730.

[252] F. Tam, A. L. Chen, J. Kundu, H. Wang, N. J. Halas, *The Journal of Chemical Physics* **2007**, *127*, year.

[253] N. J. Halas, S. Lal, W.-S. Chang, S. Link, P. Nordlander, *Chemical Reviews* **2011**, *111*, 3913–3961.

[254] Z. Nie, A. Petukhova, E. Kumacheva, *Nat Nano* **2010**, *5*, 15–25.

[255] A. Polman, *Science* **2008**, *322*, 868–869.

[256] A. M. Funston, C. Novo, T. J. Davis, P. Mulvaney, *Nano Letters* **2009**, *9*, 1651–1658.

[257] L. Polavarapu, J. Perez-Juste, Q.-H. Xu, L. M. Liz-Marzan, *J. Mater. Chem. C* **2014**, *2*, 7460–7476.

[258] R. A. Alvarez-Puebla, A. Agarwal, P. Manna, B. P. Khanal, P. Aldeanueva-Potel, E. Carbó-Argibay, N. Pazos-Pérez, L. Vigderman, E. R. Zubarev, N. A. Kotov, L. M. Liz-Marzán, *Proceedings of the National Academy of Sciences* **2011**, *108*, 8157–8161.

[259] S. Gomez-Graña, J. Perez-Juste, R. A. Alvarez-Puebla, A. Guerrero-Martinez, L. M. Liz-Marzan, *Advanced Optical Materials* **2013**, *1*, 477–481.

[260] H. Ko, S. Singamaneni, V. V. Tsukruk, *Small* **2008**, *4*, 1576–1599.

[261] L. Guerrini, D. Graham, *Chemical Society Reviews* **2012**, *41*, 7085–7107.

[262] J. He, Y. Wang, Y. Feng, X. Qi, Z. Zeng, Q. Liu, W. S. Teo, C. L. Gan, H. Zhang, H. Chen, *ACS Nano* **2013**, *7*, 2733–2740.

[263] A. La Porta, M. Grzelczak, L. M. Liz-Marzan, *ChemistryOpen* **2014**, *3*, 146–151.

[264] J. Perez-Juste, L. M. Liz-Marzan, S. Carnie, D. Y. C. Chan, P. Mulvaney, *Advanced Functional Materials* **2004**, *14*, 571–579.

[265] E. B. Werner Stöber, Arthur Fink, *Journal of Colloid and Interface Science* **1968**, *26*, 62–69.

[266] J. Taboada, M. Araújo, F. Basteiro, J. Rodriguez, L. Landesa, *Proceedings of the IEEE* **2013**, *101*, 350–363.

[267] Y. Xia, Y. Xiong, B. Lim, S. E. Skrabalak, *Angewandte Chemie International Edition* **2009**, *48*, 60–103.

[268] Liu, P. Guyot-Sionnest, *The Journal of Physical Chemistry B* **2005**, *109*, 22192–22200.

[269] H. Feng, Y. Yang, Y. You, G. Li, J. Guo, T. Yu, Z. Shen, T. Wu, B. Xing, *Chem. Commun.* **2009**, 1984–1986.

[270] A. Sanchez-Iglesias, B. Rivas-Murias, M. Grzelczak, J. Perez-Juste, L. M. Liz-Marzan, F. Rivadulla, M. A. Correa-Duarte, *Nano Letters* **2012**, *12*, 6066–6070.

[271] J. Xu, Y. Wang, X. Qi, C. Liu, J. He, H. Zhang, H. Chen, *Angewandte Chemie International Edition* **2013**, *52*, 6019–6023.

[272] J. He, W. Ji, L. Yao, Y. Wang, B. Khezri, R. D. Webster, H. Chen, *Advanced Materials* **2014**, *26*, 4151–4155.

[273] R. Schreiber, J. Do, E.-M. Roller, T. Zhang, V. J. Schuller, P. C. Nickels, J. Feldmann, T. Liedl, *Nat Nano* **2014**, *9*, 74–78.

[274] D. Tarn, C. E. Ashley, M. Xue, E. C. Carnes, J. I. Zink, C. J. Brinker, *Accounts of chemical research* **2013**, *46*, 792–801.

[275] G. Dong, S. Ferdi, *Chemical Society Reviews* **2014**, *43*, 313.

[276] G. Soler-Illia, P. Angelome, M. Fuertes, A. Calvo, A. Wolosiuk, A. Zelcer, M. Bellino, E. Martinez, *Journal of Sol-Gel Science and Technology* **2011**, *57*, 299–312.

[277] L. Malfatti, P. Falcaro, B. Marmiroli, H. Amenitsch, M. Piccinini, A. Falqui, P. Innocenzi, *Nanoscale* **2011**, *3*, 3760–3766.

[278] V. Lopez-Puente, S. Abalde-Cela, P. C. Angelome, R. A. Alvarez-Puebla, L. M. Liz-Marzan, *The Journal of Physical Chemistry Letters* **2013**, *4*, 2715–2720.

[279] P. C. Angelome, L. M. Liz-Marzan, *The Journal of Physical Chemistry C* **2010**, *114*, 18379–18383.

[280] P. C. Angelome, I. Pastoriza-Santos, J. Perez-Juste, B. Rodriguez-Gonzalez, A. Zelcer, G. J. A. A. Soler-Illia, L. M. Liz-Marzan, *Nanoscale* **2012**, *4*, 931–939.

[281] J. Turkevich, P. C. Stevenson, J. Hillier, *Discuss. Faraday Soc.* **1951**, *11*, 55–75.

[282] J. Rodriguez-Fernandez, J. Perez-Juste, F. J. Garcia de Abajo, L. M. Liz-Marzan, *Langmuir* **2006**, *22*, 7007–7010.

[283] C. Graf, D. L. J. Vossen, A. Imhof, A. van Blaaderen, *Langmuir* **2003**, *19*, 6693–6700.

[284] P. C. Angelomé, M. C. Fuertes, G. J. A. A. Soler-Illia, *Advanced Materials* **2006**, *18*, 2397–2402.

[285] M. C. Fuertes, M. P. Barrera, J. Pla, *Thin Solid Films* **2012**, *520*, 4853 – 4862.

[286] D. Grosso, A. R. Balkenende, P. A. Albouy, A. Ayral, H. Amenitsch, F. Babonneau, *Chemistry of Materials* **2001**, *13*, 1848–1856.

[287] E. L. Crepaldi, G. J. d. A. A. Soler-Illia, D. Grosso, F. Cagnol, F. Ribot, C. Sanchez, *Journal of the American Chemical Society* **2003**, *125*, 9770–9786.

[288] R. M. A. Azzam, N. M. Bashara, *Ellipsometry and Polarized Light*, North Holland, **1987**.

[289] M. R. Baklanov, K. P. Mogilnikov, V. G. Polovinkin, F. N. Dultsev, *Journal of Vacuum Science & Technology B* **2000**, *18*, 1385–1391.

[290] C. Boissiere, D. Grosso, S. Lepoutre, L. Nicole, A. B. Bruneau, C. Sanchez, *Langmuir* **2005**, *21*, 12362–12371.

[291] G. M. Wuts, T. W. Greene, *Protective Groups in Organic Synthesis*, John Wiley & Sons Inc., Hoboken, New Jersey, 4th ed., **2007**.

[292] F. Wang, S. Cheng, Z. Bao, J. Wang, *Angewandte Chemie International Edition* **2013**, *52*, 10344–10348.

[293] A. Guerrero-Martínez, M. Grzelczak, L. M. Liz-Marzán, *ACS Nano* **2012**, *6*, 3655–3662.

[294] A. Guerrero-Martínez, S. Barbosa, I. Pastoriza-Santos, L. M. Liz-Marzan, *Current Opinion in Colloid & Interface Science* **2011**, *16*, 118 – 127.

[295] L. Rodriguez-Lorenzo, R. A. Alvarez-Puebla, I. Pastoriza-Santos, S. Mazzucco, O. Stephan, M. Kociak, L. M. Liz-Marzan, F. J. Garcia de Abajo, *Journal of the American Chemical Society* **2009**, *131*, 4616–4618.

[296] D. Rodríguez-Fernández, L. M. Liz-Marzán, *Particle & Particle Systems Characterization* **2013**, *30*, 46–60.

[297] N. G. Bastús, J. Comenge, V. Puntes, *Langmuir* **2011**, *27*, 11098–11105.

[298] H. Yuan, C. G. Khoury, H. Hwang, C. M. Wilson, G. A. Grant, T. Vo-Dinh, *Nanotechnology* **2012**, *23*, 075102.

[299] L. M. Liz-Marzán, M. Giersig, P. Mulvaney, *Langmuir* **1996**, *12*, 4329–4335.

[300] S. Chen, Z. L. Wang, J. Ballato, S. H. Foulger, D. L. Carroll, *Journal of the American Chemical Society* **2003**, *125*, 16186–16187.

[301] E. Hao, R. C. Bailey, G. C. Schatz, J. T. Hupp, S. Li, *Nano Letters* **2004**, *4*, 327–330.

[302] T. K. Sau, C. J. Murphy, *Journal of the American Chemical Society* **2004**, *126*, 8648–8649.

[303] J. Xie, J. Y. Lee, D. I. C. Wang, *Chemistry of Materials* **2007**, *19*, 2823–2830.

[304] P. S. Kumar, I. Pastoriza-Santos, B. Rodriguez-Gonzalez, F. J. G. de Abajo, L. M. Liz-Marzan, *Nanotechnology* **2008**, *19*, 015606.

[305] L. Rodriguez-Lorenzo, J. M. Romo-Herrera, J. Perez-Juste, R. A. Alvarez-Puebla, L. M. Liz-Marzan, *J. Mater. Chem.* **2011**, *21*, 11544–11549.

[306] Y. J. Wong, L. Zhu, W. S. Teo, Y. W. Tan, Y. Yang, C. Wang, H. Chen, *Journal of the American Chemical Society* **2011**, *133*, 11422–11425.

[307] F. Hao, C. L. Nehl, J. H. Hafner, P. Nordlander, *Nano Letters* **2007**, *7*, 729–732.

[308] W. Y. Ma, H. Yang, J. P. Hilton, Q. Lin, J. Y. Liu, L. X. Huang, J. Yao, *Opt. Express* **2010**, *18*, 843–853.

[309] P. Nordlander, C. Oubre, E. Prodan, K. Li, M. I. Stockman, *Nano Letters* **2004**, *4*, 899–903.

[310] G. W. Bryant, F. J. Garcia de Abajo, J. Aizpurua, *Nano Letters* **2008**, *8*, 631–636.

[311] J. F. Li, Y. F. Huang, Y. Ding, Z. L. Yang, S. B. Li, X. S. Zhou, F. R. Fan, W. Zhang, Z. Y. Zhou, W. Yin, B. Ren, Z. L. Wang, Z. Q. Tian, *Nature* **2010**, *464*, 392–395.

[312] A. Pallaoro, G. B. Braun, N. O. Reich, M. Moskovits, *Small* **2010**, *6*, 618–622.

[313] Y. Wang, J. L. Seebald, D. P. Szeto, J. Irudayaraj, *ACS Nano* **2010**, *4*, 4039–4053.

[314] C. L. Zavaleta, B. R. Smith, I. Walton, W. Doering, G. Davis, B. Shojaei, M. J. Natan, S. S. Gambhir, *Proceedings of the National Academy of Sciences* **2009**, *106*, 13511–13516.

[315] M. Gellner, K. Kömpe, S. Schlücker, *Analytical and Bioanalytical Chemistry* **2009**, *394*, 1839–1844.

[316] D. C. Kennedy, K. A. Hoop, L.-L. Tay, J. P. Pezacki, *Nanoscale* **2010**, *2*, 1413–1416.

[317] K. K. Maiti, U. Dinish, A. Samanta, M. Vendrell, K.-S. Soh, S.-J. Park, M. Olivo, Y.-T. Chang, *Nano Today* **2012**, *7*, 85–93.

[318] G. von Maltzahn, A. Centrone, J.-H. Park, R. Ramanathan, M. J. Sailor, T. A. Hatton, S. N. Bhatia, *Advanced Materials* **2009**, *21*, 3175–3180.

[319] M. Xiao, J. Nyagilo, V. Arora, P. Kulkarni, D. Xu, X. Sun, D. P. Davé, *Nanotechnology* **2010**, *21*, 035101.

[320] M. F. Kircher, A. de la Zerda, J. V. Jokerst, C. L. Zavaleta, P. J. Kempen, E. Mittra, K. Pitter, R. Huang, C. Campos, F. Habte, R. Sinclair, C. W. Brennan, I. K. Mellinghoff, E. C. Holland, S. S. Gambhir, *Nature medicine* **2012**, *18*, 829–834.

[321] Z. A. Nima, M. Mahmood, Y. Xu, T. Mustafa, F. Watanabe, D. A. Nedosekin, M. A. Juratli, T. Fahmi, E. I. Galanzha, J. P. Nolan, A. G. Basnakian, V. P. Zharov, A. S. Biris, *Sci. Rep.* **2014**, *4*, year.

[322] S. L. Kleinman, B. Sharma, M. G. Blaber, A.-I. Henry, N. Valley, R. G. Freeman, M. J. Natan, G. C. Schatz, R. P. Van Duyne, *Journal of the American Chemical Society* **2013**, *135*, 301–308.

[323] H. Cha, J. H. Yoon, S. Yoon, *ACS Nano* **2014**, *8*, 8554–8563.

[324] X. Qian, S. R. Emory, S. Nie, *Journal of the American Chemical Society* **2012**, *134*, 2000–2003.

[325] A. S. Michaels, O. Morelos, *Industrial & Engineering Chemistry* **1955**, *47*, 1801–1809.

[326] L. Liz-Marzan, *Langmuir* **2006**, *22*, 32–41.

[327] K. Kim, Y. M. Lee, J. W. Lee, K. S. Shin, *Langmuir* **2009**, *25*, 2641–2645.

[328] K. Kim, H. B. Lee, Y. M. Lee, K. S. Shin, *Biosensors and Bioelectronics* **2009**, *24*, 1864 – 1869.

List of Publications

- D. Rodríguez-Fernández, L. M. Liz-Marzán, *Metallic Janus and Patchy Particles*, Part. Part. Sist. Charact. **2013**, *30*, 46-60.
- D. Rodríguez-Fernández, J. Pérez-Juste, I. Pastoriza Santos, L. M. Liz-Marzán, *Colloidal Synthesis of Gold Semishells*, Chemistry Open **2012**, *1*, 90-95.
- E. Farrokhtakin, D. Rodríguez-Fernández, V. Mattoli, D. M. Solís, J. M. Taboada, F. Obelleiro, M. Grzelczak, and L. M. Liz-Marzán, *Radial Growth of Plasmon Coupled Gold Nanowires on Colloidal Templates*, J. Colloid Interface Sci. **2014**, accepted.
- D. Rodríguez-Fernández, P. C. Angelomé, G. Soler-Illia, L. M. Liz-Marzán, in preparation.
- D. Rodríguez-Fernández, T. Altantzis, H. Heidari, S. Bals, L. M. Liz-Marzán, *A Protecting Group Approach toward Au-Silica Janus Nanostars,* Chem. Commun. **2014**, *50*, 79-81.
- D. Rodríguez-Fernández, J. Langer, M. Henriksen-Lacey, L. M. Liz-Marzán, *Hybrid Au-SiO_2 Core-Satellite Colloids as Switchable SERS Tags,* submitted.

Acknowledgments

First of all I would like to thank my PhD supervisors, Prof. Luis M. Liz Marzán and Dr. Jorge Pérez Juste, for welcoming me to the Colloid Chemistry Group first and, not having enough, to the Bio Nanoplasmonics Lab later, and also for their support and assistance all over this period.

I wish also to thank Dr. Isabel Pastoriza Santos for being a pillar during the first half of this PhD thesis period, with whom many discussions have taught me how to deal with lab issues and have made me a better scientist.

I would like to especially acknowledge Prof. Jan Vermant for allowing me to work in his group, and for introducing me into Langmuir - Blodgett's trough self - assembly and rheology during my stay in Leuven, the latter with no great success, but he tried. I am also thankful to Dr. Luna Imperialli Dafflito for her help with the measurements.

I thank Prof. Galo Soler Illia for work stuff and also for his great sense of humor during my stays in Buenos Aires. I would like to thank especially Dr. Paula C. Angelomé not only for helping me in the lab, being a great supervisor, mainly for showing me the real Buenos Aires in company of her husband Diego. I miss *asado*s and also *dulce de leche*. Oh! *La operación engorde*...

Now, the hardest part. Regarding people from the lab I wish to thank first Ana Sánchez and Marek, the only ones bearing me during the whole PhD, who almost became my supervisors at BNP Lab. It is impossible for me to thank everyone, we are too many guys, so for sure I will forget some important persons (*do not get angry please*). I would like to mention especially some great people I met during my last period in Donostia as: *Adita y su carrito* who really helped me during the few bad moments I had there; *la siempre contenta Marta Sanz* and Pablo for *basketpote*

times, and for taking me to the hospital, just before announcing my retirement; *La Ibi y sus bolas de carne del Amalur* (I am biting my tongue to do not extend this); *Margarita de Corrupción en Mañami*; Andrea and my *exapañera de piso* Ana Belén for long party times; *Leo* for teaching me what *carbonara* really is; Juanjo and the countless hours at *Minuto y medio...* and cheap ones! The crazy German Judith for the long funny chats during Raman measurements. María, Dorleta, Susana, *La Perce* y su *osho ondo,* thank you all! We have had such great moments guys like our trip to Navarra and Huesca, being the best our unforgettable hiking trip to Jaizkibel... we should write a book, it is a great story for a film! I do not forget my last flatmates, Cyrille and Ana. Thank you both! Apart from people from the lab, also mention *Manolo*, to whom I really wish the best. Thank you *Manu!* Also an especial acknowledge to Nina, Rūta and Silvia, too much fun together. The last 2 years have been the best of my life, that would be impossible without all of you, THANKS!

Going back to the beginning, I want to thank all my friends I left at UVigo. Was hard at the beginning, but now, when coming back I feel like you are my second family, I am really proud of all of you: *Da,* it has taken some time but after many years you have become a great friend *(I am waiting for THE TRIP), Sansán, grazas polo teu apoio chuliña*; *Noe* for innumerable party nights, *Martita* and her incredible sweets, *Isma* for terrible bad movie sessions, and *Nico me falte dios!* Apologies but I prefer to do not extend more, you already know how especial you are. I do not want to forget Berto. What to say, I will never forget the countless hours playing cards or my speech at *Historia de la Química,* among many other funny moments. Thank you *Berto!*

Antes de acabar quiero agradecer a mis amigos de infancia, que aunque cada vez nos vemos menos, siempre estáis ahí. Gracias a Dani, Ra, Pablo y todos los demás.

Finalmente, y ya acabo, quería agradecer el apoyo de mi familia sobre todo estos últimos años, especialmente de mis padres y de mi hermana. Jessica, la más grande, que aún estando lejos sé que siempre estás cerca para lo que haga falta. Tú también cuñao!

¡¡¡Eskerrik asko!!!